

Towards Versatile and Robust Spectrum Sensing in Cognitive Radio

von der Fakultät für Elektrotechnik und Informatik
der Gottfried Wilhelm Leibniz Universität Hannover
zur Erlangung des akademischen Grades

DOKTOR DER INGENIEURWISSENSCHAFTEN
Dr.-Ing.

genehmigte Dissertation
von

M.Sc. Hanwen Cao
geboren am 20.02.1983, in Sichuan in China
2012

Referent: Prof. Dr.-Ing. Thomas Kaiser
Koreferent: Prof. Dr. Jürgen Peissig
Vorsitzender: Prof. Dr.-Ing. Jörn Ostermann
Tag der Promotion: 24. Oktober 2012

ZUSAMMENFASSUNG

Eine der wichtigsten Herausforderungen für die Innovation in der drahtlosen Industrie und Markt ist der scheinbare Mangel an Funkfrequenzspektrum durch die traditionelle „command-and-control“ Frequenzregulierungspolitik, die auf ausschließlich zugewiesenen Lizenzen zur Vermeidung von Störungen setzt verursacht. Das Konzept der „Cognitive Radio (CR)“ und damit verbundene „Dynamic Spectrum Access (DSA)“ ist eine vielversprechende Lösung für dieses Problem. Es ermöglicht sekundären Benutzern die nicht ausgelasteten Ressourcen in das Spektrum lizenzfrei zu nutzen und gleichzeitig mit Hilfe der Spectrum Sensing zu vermeiden, dass schädliche Interferenzen auf das hinterlassene lizenzierte primäre Benutzer. Außerdem wird aufgrund der laufenden Entwicklung neuer Technologien und neuer Geschäftsmodelle erwartet, dass zahlreiche heterogene Systeme die gleichen Funkfrequenzen in der Zukunft zu teilen. Daher müssen die Koordination und die Koexistenz dieser Systeme für die Gewährleistung ihrer jeweiligen Qualität der Dienstleistung optimiert werden. Zu diesem Zweck sollen nicht nur die Anwesenheit von Signalen der primären Benutzer erkannt werden, sondern auch die umfassende Kenntnisse über die Koexistenz verschiedener Systeme muss über Spectrum Sensing, das ein schwieriges Thema wird bezogen werden. In diesem Hintergrund wird die Doktorarbeit an die Erkundung der vielseitigen Spectrum Sensing Techniken für den Erwerb umfassender Informationen aus anderen Netzen oder Geräten in der gemeinsam genutzten Funkfrequenzen sollen.

Diese Doktorarbeit leistet einen Beitrag auf dem Gebiet der CR in drei Aspekten. Erstens wurden die wichtigsten Signaldetektionstechniken zusammengefasst und weitere vorgeschlagene „Power Spectrum based Whiteness Detection (PSWD)“ sowie die „Dimension Cancellation (DIC)“-Verfahren zur Beseitigung des „Noise Uncertainty (NU)“ Problems vorgeschlagen. Zweitens wurde ein auf der Signaldetektion basierendes Signalklassifikationsframework mit dem Ziel, eine robuste Erkennung der wichtigsten Primär- und Sekundärnutzerstandards, die im TV-Band betrieben werden können vorgeschlagen. Drittens, wurden neue Verfahren vorgestellt, welche die hohe Flexibilität der „Embedded Cyclostationary Signature (ECS)“ der Mehrträgersignale ausnutzen und dadurch sowohl die Signalklassifizierung als auch den Austausch beliebiger erweiterter Informationen zwischen heterogenen Systemen ermöglichen, was die Erkenntnisse, welche das Spectrum Sensing zur Verfügung stellt, deutlich erweitern kann.

Durch die Diskussion der Spectrum Sensing Techniken in der vorliegenden Doktorarbeit wird ein besonderes Augenmerk auf die Robustheit in der praktischen Implementierung gerichtet. Die Unvollkommenheiten und Beschränkungen in Sensing Hardware wie zum Beispiel, NU, Taktfrequenzfehlanspassung, nicht-weißer Rauschteppich, Spurious und Mehrwegeausbreitung werden dabei berücksichtigt. Weiterhin wird zusätzlich zur Simulationsanalyse ein Testbed zur Durchführung von experimentellen Studien mit realen Funkfrequenzsignalen verwendet. Durch den Vergleich der experimentellen und simulierten Ergebnisse sind die Machbarkeit und die erreichbare Leistung der vorgeschlagenen Spectrum Sensing Techniken in realen Implementierungen gut validiert.

Schlagwörter - Cognitive Radio, Spectrum Sensing, Messungen

ABSTRACT

One of the major challenges to the innovation in wireless industry and market is the seeming scarcity of Radio Frequency (RF) electromagnetic spectrum caused by the traditional “*command-and-control*” spectrum regulation policy which relies upon exclusively assigned licenses for avoiding interferences. Cognitive Radio (CR) and the Dynamic Spectrum Access (DSA) enabled by it offer a promising solution to this problem by allowing unlicensed Secondary User (SU) to exploit the underutilized spectrum resources while using spectrum sensing to avoid causing harmful interference to the legacy licensed Primary User (PU). Besides, due to the continuing development of new technologies and new business models, it is expected that numerous heterogeneous systems will share the same spectrum resources in the future. Therefore, the coordination and coexistence of these systems need to be optimized for guaranteeing their respective Quality of Service (QoS). For this purpose, not only the presence of PU’s signal should be detected, but also the comprehensive knowledge of multiple coexisting wireless systems needs to be obtained via spectrum sensing, which becomes a challenging issue. In this background, the thesis is aimed at exploring the versatile spectrum sensing techniques for acquiring comprehensive information from other networks or devices in the shared RF spectrum.

This thesis contributes to the field of CR in three aspects. First, we summarize the major signal detection techniques and present our proposed Power Spectrum based Whiteness Detection (PSWD) algorithms as well as the Dimension Cancellation (DIC) method for mitigating the Noise Uncertainty (NU) problem, which is applicable to nearly all the signal detection methods. Second, based on the investigation on signal detection, we propose a signal classification framework with the robust implementation aiming at the major primary and secondary standards which coexist in TV band. Third, it is proposed in this thesis the novel schemes of utilizing the highly flexible Embedded Cyclostationary Signature (ECS) in multicarrier signal for achieving signal classification and exchange of arbitrary extended information among heterogeneous systems, which can greatly enrich the knowledge acquired via spectrum sensing.

When discussing the spectrum sensing techniques in this thesis, special focus is addressed to the robustness in practical implementation. The constraints and imperfections in sensing hardware, such as NU, clock mismatch, nonwhite noise floor, spurs and multipath fading are taken into account. Further more, in addition to simulation analysis, a testbed is built for performing experimental studies with real-world RF signals. By comparing the experimented results with simulated results, the feasibility and achievable performances of the proposed versatile sensing techniques in real-world implementations are well validated.

Keywords - Cognitive Radio, Spectrum Sensing, Measurements

CONTENTS

List of Figures	iii
List of Tables	viii
Acronyms	ix
1 INTRODUCTION	1
1.1 Background and Motivations	1
1.2 Organization of the Contents	4
1.3 Key Contributions	5
2 THE BASIC FORM OF SPECTRUM SENSING: SIGNAL DETECTION	7
2.1 The Formulation of Signal Detection Problem	7
2.2 Categorization of Signal Detection Algorithms	9
2.3 Energy Detection (EGD)	11
2.4 Matched Filter Detection (MFD)	12
2.4.1 Matched Filtered Energy Detection (MFD-EG)	13
2.4.2 MFD with Featured Sequence (MFD-FS)	14
2.5 Covariance Based Whiteness Detection (CVWD)	14
2.5.1 Equalization of Nonwhite Noise Floor	15
2.5.2 Blind Detection with Maximum-Minimum Eigenvalue (CVWD-MME) and Covariance Absolute Value (CVWD-CAV)	16
2.5.3 Estimator-Correlator Detection with Known Covariance Matrix (CVWD-EC)	17
2.6 Power Spectrum Based Whiteness Detection (PSWD)	17
2.6.1 Equalize Nonwhite Noise Floor and Remove Spurs	19
2.6.2 Blind Detection with the Ratio of Arithmetic-Geometric Means (PSWD-AG)	19
2.6.3 Power Spectrum Whiteness Detection with Known Spectrum Mask (PSWD-SM)	20
2.7 The Equivalence of MFD-EG, CVWD-EC and PSWD-SM	20
2.7.1 Proof of the Equivalence between MFD-EG and CVWD-EC	21
2.7.2 Proof of the Equivalence between CVWD-EC and PSWD-SM	22
2.8 Cyclostationary Detection (CSD)	23
2.9 Autocorrelation Based Detection (ACD)	27
2.9.1 CP Based Detection	27
2.9.2 Feature Sequence Autocorrelation (FSA) Detection	29
2.10 Mitigation of Noise Uncertainty Using Dimension Cancelation (DIC)	33
2.10.1 Influence of the Noise Uncertainty	33
2.10.2 Eliminate Noise Uncertainty with DIC	34
2.11 Cooperative Signal Detection	36
2.11.1 Optimal Soft Combination	36
2.11.2 Hard Combination	38
2.12 Concluding Remarks	38
3 SIMULATIONS OF SIGNAL DETECTION ALGORITHMS	41
3.1 Modeling of Signals	41
3.2 Simulated Results	43
3.2.1 The Noise Uncertainty Problem in MFD-EG and PSWD	43
3.2.2 Comparison of the PSWD and CVWD	44
3.2.3 Equalization of Nonwhite Noise Floor and Removal of Spurs	47
3.2.4 PSWD in Multipath Channel	48

3.2.5	FSA and CP Based Detections with Noise Uncertainty . . .	50
3.2.6	The Influence of CP length on FSA and CP based Detections . . .	51
3.2.7	The Influence of Multipath Channel on FSA and CP based Detections	51
3.2.8	Enhance CP-SW Detection with Pre-alignment	51
3.2.9	CP based Detections of ECMA-392 Signal	54
3.2.10	The Influence of CFO	55
3.2.11	The Influence of SFO	55
3.3	Concluding Remarks	56
4	THE CLASSIFICATION FRAMEWORK BASED ON SIGNAL DETECTION	59
4.1	Introduction	59
4.2	Problem Formulation	60
4.3	Target Signals in TVWS and Their Unique Features	62
4.4	The Classification Framework	64
4.5	Simulation Performances	67
4.6	Concluding Remarks	69
5	EMBEDDED CYCLOSTATIONARY SIGNATURES	71
5.1	Introduction	71
5.2	Generation and Extraction of ECS	75
5.2.1	Scheme 1: Generating ECS with Correlated Constellations on Signature Sub-Carriers (SSC)	75
5.2.2	Scheme 2: Generating ECS with Sinusoids on SSCs	76
5.2.3	SCF Estimator for Extracting ECS	77
5.3	ECS for Signal Classification with Improvement	78
5.4	Extended Information Carried on ECS	81
5.4.1	The Potential Amount of Information	81
5.4.2	Encoding and Decoding of Extended Information on ECS	83
5.4.3	Simulation Performances	86
5.5	Concluding Remarks	88
6	EXPERIMENTS WITH SPECTRUM SENSING TESTBED	89
6.1	Introduction	89
6.2	Methodology	91
6.3	Noise Uncertainty Measurement	93
6.4	Signal Detection	96
6.5	Signal Classification for TVWS	98
6.6	ECS for Signal Classification	103
6.7	ECS for Carrying Extended Information	106
6.8	Concluding Remarks	107
7	CONCLUSIONS AND FUTURE WORKS	109
7.1	Conclusions	109
7.2	Future Works	110
	BIBLIOGRAPHY	112

LIST OF FIGURES

Figure 1	Measured Power Spectrum Density (PSD) from 470 MHz to 862 MHz at both urban and rural locations using Tektronix RSA6114A realtime spectrum analyzer	2
Figure 2	Probability of false alarm (PFA) and mis-detection (PMD) in signal detection problem	9
Figure 3	Categories of signal detection algorithms	10
Figure 4	ACF (normalized SCF) of noise-free QPSK signal, DFT size: 64	25
Figure 5	ACF (normalized SCF) of noise-free BPSK signal, DFT size: 64	26
Figure 6	ACF (normalized SCF) of BPSK signal with noise, DFT size: 64, SNR: -16 dB	26
Figure 7	Illustration of the CP-SW detection for a captured real-world DVB-T signal (530MHz, 8K DFT, 1/4 CP ratio) . .	27
Figure 8	Periodical pilot sub-carrier pattern in DVB-T	30
Figure 9	Illustration of the autocorrelation in FSA detections with an example of the autocorrelation of a captured real-world DVB-T signal(530MHz, 8K DFT, 1/4 CP ratio)	31
Figure 10	Performance of MFD-EG detecting WM signal (loud speaker mode) with NU for different observation time, signal bandwidth: 200 kHz, sampling rate: 500 k/s, passband of the matched filter: 200 kHz, PFA: 0.01, flat fading . . .	44
Figure 11	Performance of PSWD detecting ATSC signal with NU for different observation time, bandwidth: 6 MHz, $N_{DFT} = 64$, $D = 32$, PFA: 0.01, flat fading	45
Figure 12	Comparison of CVWD and PSWD with different shifting steps D for detecting DVB-T signal (any mode), bandwidth: 8 MHz, $D = 16, 32, 64$, $N_{DFT} = 64$, CM size: 32, observation time: 0.125 ms, PFA: 0.01, flat fading	45
Figure 13	Comparison of CVWD and PSWD with different shifting steps for detecting ATSC signal, bandwidth: 6 MHz, $N_{DFT} = 64$, $D = 32, 64$, CM size: 32, observation time: 0.4 ms, PFA: 0.01, flat fading	46
Figure 14	Comparison of PSWD and CVWD for detecting WM signal, bandwidth: 8 MHz, $N_{DFT} = 64$, $D = 32$, CM size: 32, observation time: 1 ms, PFA: 0.01	47
Figure 15	PSD of WM signal with nonwhite noise floor and spurs, sampling rate: 500 k/s, signal carrier: 125kHz, receiver impulse response [1, 0.3], spur frequency: 100kHz & -50kHz, powers of the spurs: 0dB & 4.8dB over noise power	47
Figure 16	PMD of PSWD-AG and CVWD-CAV for detecting WM signal (loud speaker mode) with nonwhite noise floor, bandwidth: 200 kHz, sampling rate: 500 k/s, $N_{DFT} = 64$, $D = 32$, CM size: 32, observation time: 0.2 ms, PFA: 0.01, flat fading	48

Figure 17	PMD of PSWD-AG and CVWD-CAV for detecting WM signal (loud speaker mode) with spurs, bandwidth: 200 kHz, sampling rate: 500 k/s, $N_{\text{DFT}} = 64$, $D = 32$, CM size: 32, observation time: 0.2 ms, PFA: 0.01, flat fading	49
Figure 18	Performance of PSWD detecting ATSC signal in multipath channel (IEEE 802.22 WRAN Type B), bandwidth: 6 MHz, $N_{\text{DFT}} = 64$, $D = 32$, observation time: 0.4ms, PFA: 0.01	49
Figure 19	Performance of PSWD detecting DVB-T signal in multipath channel (COST207BUx12), bandwidth: 8 MHz, $N_{\text{DFT}} = 64$, $D = 32$, CM size: 32, observation time: 1 ms, PFA: 0.01	50
Figure 20	Using DIC to mitigate NU for FSA and CP based detections on DVB-T signal (2K, 1/4 CP mode), observation time: 10 ms, PFA: 0.01	51
Figure 21	The influence of CP length on FSA and CP based detections of DVB-T signal (2K, 1/4 1/32 CP modes), observation time: 10 ms, PFA: 0.01	52
Figure 22	The influence of multipath channel (DVB-T standard defined and IEEE 802.22 WRAN Type B) on FSA and CP based detections of DVB-T signal (2K, 1/32 CP mode), observation time: 10 ms, PFA: 0.01	52
Figure 23	Performance of CP-SW method for detecting TD-LTE downlink (5 MHz, normal CP length, uplink-downlink config: 5) with and without pre-alignment, observation time: 20 ms, pre-alignment length: 0.5 ms (1 slot), PFA: 0.01	53
Figure 24	Performance of CP-SW method for detecting 802.22 downlink (8 MHz, 1/16 CP length) with and without pre-alignment, observation time: 20 ms, pre-alignment length: 10 ms(1 TDD frame), PFA: 0.01	53
Figure 25	Performance of CP based detections on ECMA-392 Signal (8MHz, 1/16 CP mode) with different duty cycles, observation time: 10 ms, PFA: 0.01	54
Figure 26	Performances of FSA-2C, CP-SW and MFD-FS detecting DVB-T signal (2K, 1/16 CP mode) with CFO, observation time: 4.8 ms, PFA: 0.01	55
Figure 27	Performances of FSA-2C and CP-SW methods detecting DVB-T signal (2K, 1/16 CP mode) with SFO, PFA: 0.01	56
Figure 28	Transmission probability matrix from actual hypotheses to classification results in signal classification	60
Figure 29	PSDs of WM signal and DVB-T signal showing large difference in PAR, bandwidth; 8 MHz, SNR: 3 dB	65
Figure 30	Classification framework based on parallel detection algorithms combined with decision rules	65
Figure 31	The overall signal classification performances, target signals listed in Table 6, detection algorithms listed in Table 5, observation time: 20 ms, PFA: 0.01	69
Figure 32	The classification performances of specific signals, target signals: Table 6, detection algorithms: Table 5, observation time: 20 ms, PFA: 0.01	70
Figure 33	Embedded and inherent cyclostationary signatures of OFDM signal revealed in SCF, OFDM DFT size: 64, OFDM CP size: 16	72
Figure 34	Extended information carried on cyclostationary signatures of multi-carrier signal	73

Figure 35	Example of two groups of ECS in OFDM signal revealed by ACF, OFDM DFT length: 64, OFDM CP length: 16, Group 1: 3 SSCs, Group 2: 4 SSCs	76
Figure 36	Digital implementation of SCF and ACF estimator	77
Figure 37	The method of generating ECS with partial correlation of SSCs for signal detection and classification, 3 groups, each with 2 correlated SSCs	79
Figure 38	The method of generating ECS with full correlation of SSCs for signal classification proposed in this thesis, 6 fully correlated SSCs	79
Figure 39	Probability of Correct Classification (PCC) of ECS based signal classification, OFDM DFT size: 64, OFDM CP size: 16, number of sub-carriers: 52, number of SSCs: 6, number of OFDM symbols: 30, 3 groups for partial correlation, number of classes: 4, PFA: 0.01	80
Figure 40	The number of bits can be encoded for different number of SSCs and effective sub-carriers	82
Figure 41	The number of bits can be encoded for different ratios of SSCs among effective sub-carriers	82
Figure 42	Generation of OFDM signal with extended information carried on ECS	83
Figure 43	3D view of the ACF for an OFDM signal with ECS, DFT size: 64, CP length: 16, effective SCs: 52, number of SSCs: 10	84
Figure 44	Top view of the ACF for an OFDM signal with ECS showing PSC of one SSC, DFT size: 64, CP length: 16, effective SCs: 52, number of SSCs: 10	85
Figure 45	Probability of erroneous decoding of the extended information with CFO, DFT size: 256, CP length: 32, number of OFDM symbols: 30, effective SCs(size of A): 200, size of S : 50, number of SSC: 10	87
Figure 46	Probability of erroneous decoding of the extended information with frequency-selective fading channel, DFT size: 256, CP length: 32, number of OFDM symbols: 30, effective SCs(size of A): 200, size of S : 50, number of SSC(size of G): 10	87
Figure 47	The structure of the spectrum sensing testbed	89
Figure 48	Method 1: sensing performance evaluation with simulated signal and noise	91
Figure 49	Method 2: sensing performance evaluation with separately captured signal and noise	92
Figure 50	Method 3: sensing performance evaluation with received signal plus noise	92
Figure 51	PDF of measured noise power from USRP2+WBX and simulated AWGN, sampling rate: 12.5 MS/s, observation time: 1 ms, carrier frequency: 750 MHz, number of measurements: 12000, duration: 12 hours	94
Figure 52	PDF of measured noise power from USRP2+WBX and simulated AWGN, sampling rate: 25 MS/s, observation time: 40 ms, carrier frequency: 750 MHz, number of measurements: 12000, duration: 12 hours	95
Figure 53	PSD of received signal of USRP2+WBX in hypothesis \mathcal{H}_0 , which shows nonwhite noise floor and spurs, carrier frequency: 560 MHz, sampling rate: 12.5 MS/s	96

Figure 54	Performances of detecting DVB-T signals using FSA-2C with DIC, carrier frequency: 560 MHz, receiving sampling rate: 12.5 MS/s, observation time: 20 ms, PFA: 0.01	97
Figure 55	Performance of detecting DVB-T signal (2K, 1/32 CP mode) using FSA-2C with DIC at low SNR, carrier frequency: 560 MHz, receiving sampling rate: 12.5 MS/s, observation time: 20 ms, PFA: 0.01	97
Figure 56	Performance of detecting WM signal by testing PAR of estimated PSD, carrier frequency: 558 MHz, receiving sampling rate: 12.5 MS/s, observation time: 20 ms, PAR threshold: 3.6	98
Figure 57	Signal classification procedures implemented on the spectrum sensing testbed	99
Figure 58	The overall signal classification performance, target signals in Table 6, detection algorithms in Table 5, carrier frequency: 560 MHz, receiving sampling rate: 12.5 MS/s, observation time: 20 ms, PFA: 0.01	100
Figure 59	The PCC for DVB-T signal, target signals in Table 6, detection algorithms in Table 5, carrier frequency: 560 MHz, receiving sampling rate: 12.5 MS/s, observation time: 20 ms, PFA: 0.01	101
Figure 60	The PCC for DVB-T signal, target signals in Table 6, detection algorithms in Table 5, carrier frequency: 560 MHz, receiving sampling rate: 12.5 MS/s, observation time: 20 ms, PFA: 0.01	101
Figure 61	The PCC for DVB-T signal, target signals in Table 6, detection algorithms in Table 5, carrier frequency: 560 MHz, receiving sampling rate: 12.5 MS/s, observation time: 20 ms, PFA: 0.01	102
Figure 62	The PCC for DVB-T signal, target signals in Table 6, detection algorithms in Table 5, carrier frequency: 560 MHz, receiving sampling rate: 12.5 MS/s, observation time: 20 ms, PFA: 0.01	102
Figure 63	The PCC for DVB-T signal, target signals in Table 6, detection algorithms in Table 5, carrier frequency: 560 MHz, receiving sampling rate: 12.5 MS/s, observation time: 20 ms, PFA: 0.01	103
Figure 64	The ACFs of the OFDM signals with four ECS patterns, number of SSC: 6, number of effective SC: 80, DFT length: 128, CP length: 16, number of OFDM symbols: 30, carrier frequency: 750 MHz, receiving sampling rate: 12.5 MS/s	104
Figure 65	The performances of ECS based signal classifications using <i>Scheme 1</i> and <i>Scheme 2</i> , number of classes: 4, number of SSC: 6, number of effective SC: 80, DFT length: 128, CP length: 16, number of OFDM symbols: 30, carrier frequency: 750 MHz, receiving sampling rate: 12.5 MS/s, PFA: 0.01	104
Figure 66	The performances of ECS based signal classifications, number of classes: 4, number of SSC: 2, number of effective SC: 80, DFT length: 128, CP length: 16, number of OFDM symbols: 30, carrier frequency: 750 MHz, receiving sampling rate: 12.5 MS/s, PFA: 0.01	105

Figure 67	The performances of ECS based signal classifications, number of classes: 4, number of SSC: 6, number of effective SC: 80, DFT length: 128, CP length: 16, number of OFDM symbols: 30, carrier frequency: 750 MHz, receiving sampling rate: 12.5 MS/s, PFA: 0.01	105
Figure 68	The performances of ECS based signal classifications, number of classes: 4, number of SSC: 10, number of effective SC: 80, DFT length: 128, CP length: 16, number of OFDM symbols: 30, carrier frequency: 750 MHz, receiving sampling rate: 12.5 MS/s, PFA: 0.01	106
Figure 69	The probability of erroneous decoding (PED) for extended information carried on ECS, DFT length: 256, CP length: 64, effective SCs(size of A): 160, size of S : 78, number of SSC(size of G): 16, carrier frequency: 750 MHz, receiving sampling rate: 12.5 MS/s	107

LIST OF TABLES

Table 1	Dimension Cancellation Factors for Various Detection Methods	36
Table 2	Operating Situations of WM Signal	43
Table 3	Signal Features Utilized by the Detection Algorithms . .	62
Table 4	Useful Parameters of the OFDM Based TVWS Standards for Classification	63
Table 5	Signal Features and Detection Algorithms Used in Classification	67
Table 6	The Target Signals and Modes for Performance Evaluation	67
Table 7	Transition Probabilities for Classification of DVB-T Signal Using FSA-2C, Observation Time: 20 ms, PFA: 0.0064, SNR: -12 dB $\mathcal{H}_{1,2,3,4}$: 8K, 1/4, 1/8, 1/16, 1/32 CP modes, $\hat{\mathcal{H}}_{5,6,7,8}$: 2K, 1/4, 1/8, 1/16, 1/32 CP modes	68
Table 8	Methodologies of Performance Analysis	91
Table 9	Standard Variances of the Measured and Simulated Noise Power	95

ACRONYMS

ACD	Auto-Correlation based Detection
ACF	Auto-Coherence Function
ATSC	Advanced Television Systems Committee
AWGN	Additive White Gaussian Noise
CDF	Cumulative Distribution Function
CEPT	European Conference of Postal and Telecommunications Administrations
CFO	Carrier Frequency Offset
CIC	Cascaded Integrator-Comb
CLT	Central Limit Theorem
CM	Covariance Matrix
CP	Cyclic Prefix
CR	Cognitive Radio
CSD	Cyclostationary Detection
CVWD	Covariance based Whiteness Detections
DFT	Discrete Fourier Transform
DIC	Dimension Cancelation
DS	Degree of Sparsity
DSA	Dynamic Spectrum Access
DVB-T	Digital Video Broadcasting-Terrestrial
ECS	Embedded Cyclostationary Signature
EDF	Equivalent Degree of Freedom
EGD	Energy Detection
FCC	Federal Communications Commission
FS	Feature Sequence
FSA	Feature Sequence Auto-correlation
FS-CCP	Frequency-Smoothed Cyclic Cross Periodogram
LTE	Long Term Evolution
MFD	Matched-Filter Detection
MRC	Maximum Ratio Combining
NU	Noise Uncertainty
OFDM	Orthogonal Frequency-Division Multiplexing
PAR	Peak-to-Average Ratio
PCC	Probability of Correct Classification

PCCD Probability of Correct Classification when Detected
PDF Probability Density Function
PFA Probability of False Alarm
PFC Probability of False Classification
PMD Probability of Mis-Detection
PMSE Programme Making and Special Events
PSD Power Spectrum Density
PSWD Power Spectrum based Whiteness Detection
PU Primary User
QOS Quality of Service
RF Radio Frequency
SCF Spectrum Correlation Function
SDR Software Defined Radio
SFO Sampling Frequency Offset
SNR Signal to Noise Ratio
SSC Signature Sub-Carrier
SU Secondary User
TDD Time-Division Duplex
TS-CCP Time-Smoothed Cyclic Cross Periodogram
TVWS TV band White Space
UHD USRP Hardware Driver
USRP Universal Software Radio Peripheral
WD Whiteness Detection
WM Wireless Microphone

INTRODUCTION

1.1 BACKGROUND AND MOTIVATIONS

The electromagnetic spectrum is a precious natural resource. Nowadays, one of the key problems challenging the innovation in wireless industry and market is the seeming spectrum scarcity caused by the traditional “command-and-control” regulation policy [1], which was shaped dating back to 1920s in the US for solving the chaotic radio broadcasting. In this policy, the electromagnetic spectrum is divided into different bands and assigned to various entities, which is often license-based, exclusive and static in temporal and spatial dimensions. The consequence is that on the one hand, some spectral bands are significantly under-utilized (e.g. some TV bands below 800MHz and radar bands at most of the locations), on the other hand, some spectral bands are heavily used by data-rate-demanding systems or over-crowded with various coexisting systems (e.g. cellular bands and 2.4GHz ISM bands in densely populated areas), which leads to the seeming spectrum scarcity. This phenomenon has been revealed by the Federal Communications Commission (FCC)’s study[2, 3] and the measured results from some other institutions, a survey of them can be found in [4]. We also performed a scanning of the TV band between 470 MHz and 862 MHz at both urban and rural locations (Figure 1), which qualitatively confirmed the significant under-utilization of this band, especially at the rural location.

If the under-utilized spectrum (commonly referred as white space) is allowed to be re-exploited by other wireless applications, it is highly expected that new services and markets will emerge. One example is the big success of the unlicensed WiFi and Bluetooth sharing the 2.4GHz ISM band with other technologies. In fact, since the last decade, the effort of reforming the “command-and-control” policy into a more efficient manner has been greatly strengthened by some regulation bodies, which is mainly driven by the FCC. In 2007 and 2008, FCC performed two actions[5, 6] for evaluating the prototypes of TV band White Space (TVWS) devices submitted by several companies and research institutes, such as Microsoft, Motorola, Philips, Adaptrum and the Institute for Infocomm Research(I²R). The evaluations finally concluded that these prototypes had met the burden of “proof of concept” in their ability to detect and avoid legacy transmissions. On November 4 of 2008, the FCC voted 5-0

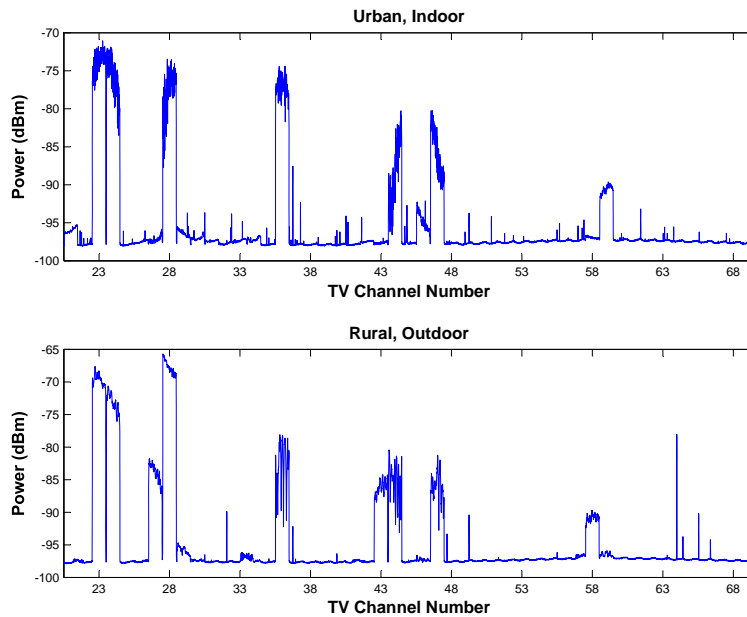


Figure 1: Measured PSD from 470 MHz to 862 MHz at both urban and rural locations using Tektronix RSA6114A realtime spectrum analyzer

to approve the unlicensed use of white space. Some detailed rules are released ten days later in [7] and the final rules are released in [8] on September 23, 2010. The Ofcom, the counterpart of the FCC in UK has also progressed the plan for introducing white space technology[9], which is released on September 1, 2011. The effort in the similar direction is also made by European Conference of Postal and Telecommunications Administrations (CEPT)[10].

The Dynamic Spectrum Access (DSA) is a promising solution for improving the utilization efficiency of the spectrum resource, which receives considerable interests from the wireless industry. It allows secondary radio networks to access the under-utilized spectrum in a dynamic sharing manner. There are three key factors of DSA should be addressed.

1. The legacy licensed user, also called Primary User (PU) should be strictly protected, thus, their Quality of Service (QoS) should not be degraded by the interference generated by the unlicensed Secondary User (SU).
2. Due to the expected innovations in new technologies and new business models, numerous heterogeneous SU networks will share the same spectrum resources. Hence, coordination and coexistence among the heterogeneous networks are desired for satisfying their respective QoS requirements.

3. The wireless systems facilitating the above two requirements should be able to aware the spectrum environment, agilely switch frequency bands, reconfigure the parameters adaptively or even intelligently. These abilities are well driven by the concept of Cognitive Radio (CR) which was firstly introduced by J. Mitola[11] in 1999.

The CR is essentially “*an intelligent wireless communication system that is aware of its environment and uses the methodology of understanding-by-building to learn from the environment and adapt to statistical variations in the input stimuli*”[1]. This definition indicates three key capabilities of CR, they are awareness, learning and adaptation. Among these capabilities, awareness plays the fundamental role since it provides knowledge inputs to CR for further learning and adaptation. According to [12], the awareness capability embodies the awareness of the transmitted waveform, RF spectrum, communication network, geography, locally available services, user needs, language, situation, and security policy. The awareness of the RF spectrum for getting the knowledge of the occupying signal waveforms and vacant channels draws most of the interests in current research and development of CR, because this functionality directly enables the improvement of the spectrum resource’s utilization efficiency.

Spectrum sensing is the most natural form of awareness, since the knowledge of spectrum resource is straightforwardly obtained via passive sensing of the RF spectrum in realtime by applying certain signal processing techniques to the received signal. Spectrum sensing is being widely researched in the reported literatures on CR, especially for detecting the presence of the signal from PU at very low SNR. This is mainly motivated by the regulators’ stringent requirements [7] for protecting the PUs in TV band from the potential interference produced by SUs.

In FCC’s final rules [8] for unlicensed access of TV band, it is pointed out that the available spectrum sensing techniques are not reliable enough to guarantee that the interference from SU is kept at sufficient low level. Then, the requirements on spectrum sensing ability are eliminated in this final rules. Instead, the rules require that the TV band devices can rely only on geo-location and database for getting available spectrum resources. However, the further research on sensing techniques is still encouraged by FCC in the final rules.

According to the original concept of cognitive radio[1, 11], the spectrum sensing is essentially a mean of acquiring knowledge from the RF spectrum for achieving satisfied QoS, which is far beyond the scope of only detecting PU’s signal. Due to the continuing innovations in new technologies and new business models as the result of the rapid increase of people’s demand in various wireless applications,

it is expected that more and more heterogeneous systems will share the same spectrum resources in the future [13, 14]. The challenge arising is not only to protect the legacy PU, but also to optimize the coordination and coexistence among devices and networks, especially heterogeneous ones. In this context, spectrum sensing is still the key to solve the challenges through realtime acquisition of comprehensive knowledge on the RF spectrum shared by many coexisting wireless systems.

Differing from previous studies on spectrum sensing which focus on the detection of PU's signal in DSA[15, 16, 17], this thesis is aimed at exploring the larger potential of spectrum sensing for knowledge acquisition in versatile applications which are listed as follows.

1. The classical PU signal detection is studied with further enhancement of the robustness for receiver with practical imperfections and constraints, such as Noise Uncertainty (NU), clock mismatch, nonwhite noise floor and spurs.
2. Extended from the signal detection techniques, a signal classification framework with the implementation of a classifier for TVWS is proposed in this thesis, which is able to robustly classify the existing and emerging wireless standards.
3. Trying to further enrich the knowledge obtained by spectrum sensing, a novel scheme of delivering extended information on embedded Embedded Cyclostationary Signature (ECS) in Orthogonal Frequency-Division Multiplexing (OFDM) signal is proposed, which enables heterogeneous wireless systems exchanging arbitrary type of knowledge.

In addition to simulation analysis, a testbed is built in this study for performing experimental validation with RF signal. By comparing the experimented results with simulated results, the feasibility and achievable performances of the proposed versatile sensing techniques in real-world implementations are well validated.

1.2 ORGANIZATION OF THE CONTENTS

The contents of this thesis are organized as follows. In Chapter 2, the reported and our proposed signal detection methods are summarized emphasizing on the formulation of detection metrics and thresholds. Chapter 3 further presents the simulated performances of these detection methods with the detailed comparisons of their advantages and disadvantages under the constraints and imperfections in practical receivers. Then, extended from the studied signal detection

methods, the proposed signal classification framework is illustrated in Chapter 4. The novel schemes of applying ECS for signal classification and delivering extended information are presented in Chapter 5. The experimental validation and evaluation of the key spectrum sensing techniques proposed in this thesis are illustrated in Chapter 6. Finally, Chapter 7 draws the conclusion and points out the further research direction.

1.3 KEY CONTRIBUTIONS

This thesis explores the versatile spectrum sensing for optimizing the coordination and coexistence of heterogeneous wireless systems in the future. The major contributions on the versatility and robustness for practical implementation in this thesis are summarized as follows.

1. In Chapter 2, by analyzing the major reported signal detection algorithms, it is found that the problem of ambiguity in Probability of False Alarm (PFA) caused by NU can be completely eliminated by the proposed Dimension Cancellation (DIC) method. The simulated performances presented in Chapter 3 further show that the DIC can lead to some losses in detection performance. However, for the autocorrelation based detection methods, the loss is negligible. It is also shown that the autocorrelation based detection is invulnerable to clock mismatch and multipath channel fading.
2. Two new detection methods using frequency-domain processing are proposed in Chapter 2. They are a blind detection named PSWD-AG and a non-blind detection named PSWD-SM. It is proved that the proposed PSWD-SM is actually equivalent to the reported CVWD-EC and MFD-EG detections using time-domain processing. However, the proposed ones have the advantage that the imperfections of nonwhite noise floor and spurs in practical receivers can be easily mitigated in a straightforward manner.
3. Extended from the signal detection problem, a robust signal classification framework is proposed in Chapter 4, which is essentially the combination of various feature based signal detection algorithms using predefined decision rules. Based on this framework, a signal classifier aiming at major existing and emerging standards in TV band is developed for the first time. The targeted signal classes are the DVB-T, LTE, IEEE 802.22, ECMA-392 and Wireless Microphone (WM) with their different modes.

4. A new scheme of generating ECS is proposed. In this scheme, fully correlated sinusoids on Signature Sub-Carrier (SSC) is applied instead of using correlated constellations on SSC which is common in literatures about ECS [18, 19, 20, 21, 22]. Simulation shows that remarkable performance enhancement can be achieved using the proposed scheme for ECS based signal classification at low SNR. Besides, the knowledge of Cyclic Prefix (CP) length is not required in the proposed scheme, which makes it more favorable to the modulations with multiple options of CP lengths.
5. Extended from the ECS based signal detection and classification, this thesis proposes a novel technique of using the ECS for carrying extended information for the first time, which can greatly enhance the knowledge acquired by spectrum sensing. The extended information includes device or network's identity and parameters, geo-location, spectrum allocation, etc. In Chapter 5, the encoding and decoding methods as well as the simulation considering clock mismatch and multipath fading are presented which shows its feasibility.
6. A testbed is built for validating and evaluating the spectrum sensing techniques studied in this thesis. The testbed consists of the Agilent E4438C vector signal generator for transmitting high quality signals used in sensing test; the USRP2+WBX SDR frontend used as sensing device, which features the imperfections in practical low-cost receiver; a host computer with the spectrum sensing algorithms, standard based waveform generators and controlling software implemented on it. The DVB-T signal transmitted by real TV broadcast is also captured for validating the detection and classification techniques. The experimented results are compared with the simulated results and show good agreement between each other. Besides, the results show that the receiver imperfections of spurs and nonwhite noise floor in the sensing receiver can be mitigated in various sensing algorithms, which leads to only minor harm to the spectrum sensing performances. The experimental validation and evaluation have greatly strengthened the effectiveness and feasibility of applying the signal detection, classification and ECS schemes proposed in this thesis to real-world applications.

THE BASIC FORM OF SPECTRUM SENSING: SIGNAL DETECTION

In cognitive radio, signal detection is the basic form of spectrum sensing, which is aimed at discriminating between the presence and absence of the signal transmitted by Primary User (PU) at very low Signal to Noise Ratio (SNR). It is the most intensively discussed problem in the research on spectrum sensing, which is mainly motivated by the regulators' stringent requirements [7] for protecting the PUs in TV band from the potential interference produced by Secondary User (SU) using Dynamic Spectrum Access (DSA).

The signal detection problem is also the basis of the signal classification schemes presented in Chapter 4 and Chapter 5, because the classification relies on the detection algorithms utilizing the unique features of different signal types. Besides, the signal classifier also needs to identify usable channels in which none of the coexisting signals is presented, which is also the goal of signal detection.

In this Chapter, the major reported signal detection algorithms are summarized with emphasis on the formulation of detection metrics and thresholds. Two signal detection algorithms utilizing frequency domain processing are proposed, which has the advantage of mitigating nonwhite noise and spur more easily comparing with the reported time-domain detection methods. The Dimension Cancellation (DIC) method is proposed for mitigating the Noise Uncertainty (NU) problem which is applicable to nearly all the detection methods. The evaluation of the detection performance via computer simulation will be further given in Chapter 3.

2.1 THE FORMULATION OF SIGNAL DETECTION PROBLEM

In the reported literatures on spectrum sensing summarized in [15, 16, 17], it is commonly defined that the goal of signal detection is to discriminate the following two hypotheses:

$$\begin{aligned} \mathcal{H}_0 : y(t) &= w(t) \\ \mathcal{H}_1 : y(t) &= x(t) + w(t), \end{aligned} \tag{2.1}$$

in which $x(t)$ is the received signal including the effect of fading channel and $w(t)$ is the noise in receiver plus the interference from some other uninterested signals. It is often assumed that $w(t)$ is the

Additive White Gaussian Noise (AWGN) in the reported literatures on spectrum sensing. For achieving the signal detection, certain detection metric

$$\Lambda = \mathcal{F}_{t_0 < t < t_0 + T_d} \{y(t)\} \quad (2.2)$$

is defined, which is the result of a processing on the received signal $y(t)$ within the detection's observation time T_d .

The detection of the interested signal can be achieved straightforwardly by comparing the detection metric Λ with a pre-determined threshold γ and deciding between hypotheses \mathcal{H}_1 and \mathcal{H}_0 :

$$\begin{array}{c} \mathcal{H}_1 \\ \Lambda \underset{\leq}{\overset{\geq}{}} \gamma. \\ \mathcal{H}_0 \end{array} \quad (2.3)$$

The goal of signal detection is to minimize the Probability of Mis-Detection (PMD)

$$P_{MD} = \Pr\{\Lambda < \gamma | \mathcal{H}_1\} = \int_{-\infty}^{\gamma} f_{\Lambda}(\lambda | \mathcal{H}_1) d\lambda \quad (2.4)$$

when the interested signal is presented while maintaining sufficiently small Probability of False Alarm (PFA)

$$P_{FA} = \Pr\{\Lambda \geq \gamma | \mathcal{H}_0\} = \int_{\gamma}^{+\infty} f_{\Lambda}(\lambda | \mathcal{H}_0) d\lambda \quad (2.5)$$

when the interested signal is absent, in which $f_{\Lambda}(\lambda | \mathcal{H}_0)$ and $f_{\Lambda}(\lambda | \mathcal{H}_1)$ are the the Probability Density Function (PDF) of the detection metric Λ for hypotheses \mathcal{H}_0 and \mathcal{H}_1 respectively. The relation between PMD and PFA is also intuitively illustrated in Figure 2.

The following important factors in signal detection problem which should be addressed here:

1. P_{MD} is strongly influenced by SNR

$$SNR = \frac{\int_{t_0}^{t_0 + T_d} |x(t)|^2 dt}{\int_{t_0}^{t_0 + T_d} |w(t)|^2 dt}. \quad (2.6)$$

Generally, for the same P_{FA} , lower P_{MD} can be achieved when SNR is higher, thus, high SNR can give rise to better detection performance.

2. P_{MD} and P_{FA} is affected by the threshold γ . Larger threshold leads to lower P_{FA} and higher P_{MD} . An extreme case is when $\gamma = +\infty$, P_{MD} becomes zero, which means no signal can be

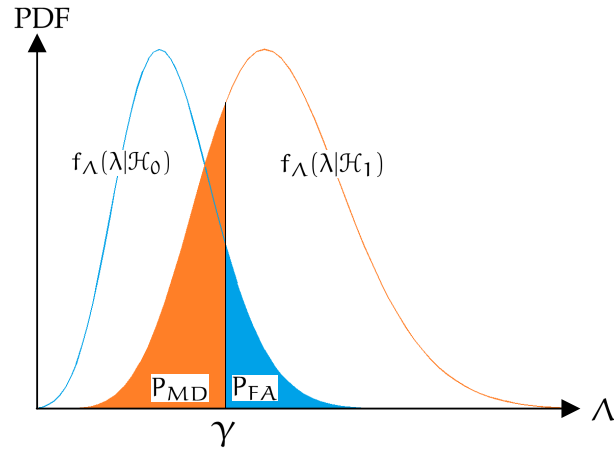


Figure 2: Probability of false alarm (PFA) and mis-detection (PMD) in signal detection problem

detected. On the other hand, when $\gamma = -\infty$, the presence of the interested signal can be always detected no matter how weak the SNR is. However, the resulted P_{FA} of one makes the channel completely unusable since it is always reported as occupied even when it is actually not.

3. The PFA should be known to the sensing receiver for maintaining stable operation. Otherwise, unpredictable overhead of reconfigurations (e.g. switching of frequency channel) may occur due to the unknown false alarm, which can reduce the Quality of Service (QoS) of the CR system significantly. Hence, a predetermined PFA should be given for getting the detection threshold γ . When $f_{\Lambda}(\lambda|\mathcal{H}_0)$ is known, the threshold can be calculated analytically. Otherwise, the threshold can be obtained using large number of empirically tested detection metric in hypothesis \mathcal{H}_0 . The thresholds of various detection methods will be illustrated in the following contents of this chapter.
4. Generally, longer observation time can lead to better detection performance thanks to the reduced ambiguity between hypotheses \mathcal{H}_i and \mathcal{H}_{∞} achieved by averaging with more samples in calculating metric Λ . Specifically, this means that for a fixed SNR and PFA, the increase of observation time can decrease PMD.

2.2 CATEGORIZATION OF SIGNAL DETECTION ALGORITHMS

This chapter summarizes the major signal detection algorithms in the reported literatures, which are essentially the possible formulations of the detection metric $\Lambda = \mathcal{F}_{t_0 < t < t_0 + T_d} \{ \cdot \}$ presented in last section.

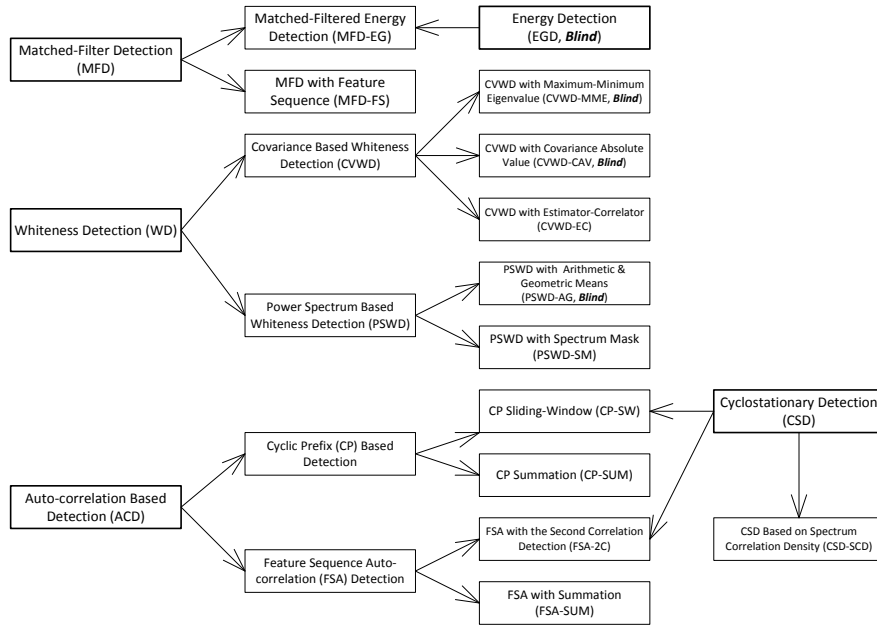


Figure 3: Categories of signal detection algorithms

In reported literatures, spectrum sensing, especially signal detection algorithms are categorized in different ways. For example, in [16], the signal detection algorithms are categorized into energy detection, matched filter detection, cyclostationarity based detection, autocorrelation based detection and covariance matrix based detection. In a more comprehensive survey study [15], the categories are energy detector based, waveform based, cyclostationarity based, radio identification based and matched-filter based sensing.

In order to better characterize the signal detection algorithms, they are categorized in this thesis based on their essential signal processing methods or utilized signal features. Figure 3 shows the categorization with the algorithms' abbreviated names and their relations presented.

In general, there are five main categories of detection algorithms, they are Energy Detection (EGD), Matched-Filter Detection (MFD), Whiteness Detection (WD), Auto-Correlation based Detection (ACD) and Cyclostationary Detection (CSD). An overview of their principles and relations are illustrated as follows.

- The EGD takes the power of received signal as detection metric, which is a blind detector requiring no *a priori* information of the signal.
- The MFD can be based on matching the pulse shape of the signal or matching certain feature sequence in the signal with known structure. The EGD can be combined with MFD by taking the energy of the matched-filtered signal according to the pulse shape as detection metric.

- The WD makes use of the fact that the communication or broadcast signals are normally nonwhite in contrast with the white noise. The whiteness can be tested both in time domain using the covariance matrix and in frequency domain using the estimated Power Spectrum Density (PSD). It is proposed in this thesis that the frequency domain processing has the advantage that the practical imperfections of nonwhite noise floor and spurs can be mitigated more easily. The whiteness can be tested both blindly or non-blindly utilizing known templates of the signal.
- Part of the wireless signals can be characterized by cyclostationary processes which have statistical properties that vary cyclically with time[23]. The cyclostationary property of a signal can be revealed in Spectrum Correlation Function (SCF) which is the extension of PSD with cyclic frequency domain. The SCF for cyclostationary analysis is particularly useful in signal detection and classification with embedded signatures[18, 19, 22]. It is also utilized by the scheme of delivering extended information on Embedded Cyclostationary Signature (ECS) proposed in Chapter 5.
- The known time-frequency structure (e.g. cyclic prefix, preamble, repeated pilot, etc) of wireless signals can be exploited in ACD. When the utilized structure is periodically repeated, the signal exhibits cyclostationarity which can be further used to enhance the detection performance of ACD.

These categorized detection algorithms are illustrated in details in following sections of this chapter. The contents are focused on the formulation of detection metrics and thresholds as well as possible solutions for enhancing the robustness to the constraints and imperfections of practical receivers, such as NU, nonwhite noise floor and spurs.

2.3 ENERGY DETECTION (EGD)

EGD is the most frequently mentioned method in spectrum sensing because it can blindly detect any signal with low computational complexity. Assume the received complex signal with in-phase and quadrature components sampled with period T_s has the following form:

$$\begin{aligned} \mathcal{H}_0 : y[n] &= w[n] \\ \mathcal{H}_1 : y[n] &= x[n] + w[n], \end{aligned} \tag{2.7}$$

in which $w[n]$ is the AWGN with power σ_w^2 and $x[n]$ is the received signal which has already experienced fading channel. The energy of the received signal is straightforwardly taken as detection metric:

$$\Lambda_{\text{EGD}} = \sum_{n=0}^{N-1} |y[n]|^2 = \sum_{n=0}^{N-1} \Re^2(y[n]) + \Im^2(y[n]), \quad (2.8)$$

in which N is the total number of samples used in detection and $\Re(\cdot)$ and $\Im(\cdot)$ are operations of getting real and imaginary part respectively. The observation time in the detection is NT_s . Since the noise is complex AWGN, Λ_{EGD} in hypothesis \mathcal{H}_0 (denoted as $\Lambda_{\text{EGD}}|\mathcal{H}_0$) follows chi-squared distribution with the degree of freedom $2N$ [24]. When N is large, according to Central Limit Theorem (CLT), the probability distributions of $\Lambda_{\text{EGD}}|\mathcal{H}_0$ can be approximated by normal distribution with expectation $N\sigma_w^2$ and variance $N\sigma_w^4$. Then, based on its Cumulative Distribution Function (CDF), the detection threshold for the desired P_{FA} can be derived as:

$$\gamma_{\text{EGD}} = \sigma_w^2 \sqrt{2N} \text{erf}^{-1}(1 - 2P_{\text{FA}}) + N\sigma_w^2, \quad (2.9)$$

in which $\text{erf}^{-1}(\cdot)$ is the inverse Gauss error function.

When the interested signal $x[n]$ is white and independent of the noise, the EGD satisfies the Neyman-Pearson test, which will be further discussed in Section 2.11 which is about cooperative signal detection.

2.4 MATCHED FILTER DETECTION (MFD)

The matched filter is the optimal linear filter for maximizing the SNR in the presence of additive noise. In reported literatures, the MFD is normally taken as a disadvantageous detection [25, 26] because it requires perfect knowledge of the signal's bandwidth, carrier frequency, modulation type, pulse shaping, and frame format [15], although its detection performance is theoretically optimal.

This section presents two partial MFD methods requiring only part of the above knowledge which is easy to obtain in practice. The first one named MFD-EG takes the energy after matched filtering as detection metric, which only needs the carrier frequency, pulse shape or even only the bandwidth of the signal. The other type of MFD is matched with certain known Feature Sequence (FS) of the signal in time domain. The FS is the known preamble or pilot structures in the signal, which is transmitted repeatedly.

2.4.1 Matched Filtered Energy Detection (MFD-EG)

The detection metric of MFD-EG can be simply defined by the energy of the received signal after matched filtering:

$$\begin{aligned} y_f[n] &= \sum_{m=0}^{M-1} f[m]y[n-m] \\ \Lambda_{\text{MFD-EG}} &= \sum_{n=0}^{N-1} |y_f[n]|^2, \end{aligned} \quad (2.10)$$

in which N is the total number of samples used in detection and M is the length of the matched filter. The impulse response $f[n]$ of the matched filter can be taken as a known template of the signal, which has the following relation with the signal's pulse shape $g[n]$:

$$f[n] = g^*[M-n]. \quad (2.11)$$

Similar to the detection metric of EGD (2.8), $\Lambda_{\text{MFD-EG}}$ also follows chi-squared distribution. However, since matched filter introduces coherence between neighboring samples, the chi-squared distribution's Equivalent Degree of Freedom (EDF) is smaller than $2N$ in hypothesis \mathcal{H}_0 . In [27], the energy detection with matched filter is proposed, which addressed that the EDF is two times the time-bandwidth product. The EDF can be also estimated using the known matched filter's impulse response $f[n]$. Define matrix

$$\begin{aligned} \mathbf{G} = \mathbf{f}\mathbf{f}^H &= \begin{bmatrix} f_{0,0} & f_{0,1} & \dots & f_{0,M-1} \\ f_{1,0} & f_{1,1} & \dots & f_{1,M-1} \\ \vdots & \vdots & \ddots & \vdots \\ f_{M-1,0} & f_{M-1,1} & \dots & f_{M-1,M-1} \end{bmatrix} \\ \mathbf{f} &= [f[0] \ f[1] \ f[2] \ \dots \ f[M-1]]^T, \end{aligned} \quad (2.12)$$

in which " $(\cdot)^T$ " and " $(\cdot)^H$ " denote transpose and conjugate transpose of matrix respectively. The EDF of $\Lambda_{\text{MFD-EG}}|\mathcal{H}_0$'s probability distribution can be then calculated by

$$\zeta = \frac{2N \sum_{m=0}^{M-1} f_{m,m}}{\sum_{m=0}^{M-1} \sum_{n=0}^{M-1} f_{m,n}}. \quad (2.13)$$

According to the CLT, when N is large, the probability distributions of $\Lambda_{\text{MFD-EG}}|\mathcal{H}_0$ can be approximated by normal distribution with expectation $\zeta\sigma_w^2/2$ and variance $\zeta\sigma_w^4/2$. Then, based on its CDF, the detection threshold for the desired P_{FA} can be derived as

$$\gamma_{\text{MFD-EG}} = \sigma_w^2 \sqrt{\zeta} \text{erf}^{-1}(1 - 2P_{\text{FA}}) + \frac{\zeta\sigma_w^2}{2}. \quad (2.14)$$

2.4.2 MFD with Featured Sequence (MFD-FS)

Assume the FS in the interested signal is $s[n]$, which is known to the receiver. The matched filter is only matched to the FS and can be denoted by

$$f[n] = s^*[M - n], \quad (2.15)$$

in which M is the length of the FS and “ $(\cdot)^*$ ” denotes conjugate operation. Then the filtered signal is the convolution of the received signal $y[n]$ with the impulse response $f[n]$ of the matched filter.

$$y_f[n] = \sum_{m=0}^{M-1} f[m]y[n - m]. \quad (2.16)$$

The detection is then performed by searching the peak values in $|y_f[n]|^2$ where the local FS is matched with the FS in the signal:

$$\Lambda_{\text{MFD-FS}} = \max_n |y_f[n]|^2. \quad (2.17)$$

If the FS appears periodically in the signal, which exhibits cyclostationarity, the peak values in $y_f[n]$ become also periodical. Hence, the $|y_f[n]|^2$ can be averaged according to the known period for improving the detection performance. Then, the detection metric becomes

$$\Lambda_{\text{MFD-FS,avg.}} = \max_n \sum_{l=0}^{L-1} |y_f[n + lP]|^2 \quad n = 0, \dots, P - 1, \quad (2.18)$$

in which P is the length of period and L is the number of periods within the observation time.

2.5 COVARIANCE BASED WHITENESS DETECTION (CVWD)

When the noise in receiver is AWGN, the nonwhiteness property of wireless signal can be utilized for detecting its presence. The widely discussed Covariance based Whiteness Detections (CVWD) [28, 29, 30, 31, 32] are in essence testing the signal’s whiteness by analyzing the properties of the Covariance Matrix (CM) which is derived from the signal’s autocorrelation in time domain.

There are several types of CVWD, the common key step of them is to estimate the statistical covariance matrix $\hat{\mathbf{R}}_y$ of the received signal $y[n]$:

$$\hat{\mathbf{R}}_y = \frac{1}{N - N_c + 1} \sum_{i=1}^{N - N_c + 1} \mathbf{y}_i \mathbf{y}_i^H, \quad (2.19)$$

in which N is the number of signal samples used in detection and \mathbf{y}_i is a vector consisting of N_c successive samples:

$$\mathbf{y}_i = [\mathbf{y}[i], \mathbf{y}[i + 1], \dots, \mathbf{y}[i + N_c - 1]]^T. \quad (2.20)$$

When the matched filter's impulse response $f[m]$ of the interested signal $x[n]$ is known, its covariance matrix \mathbf{R}_x can be derived as [33]:

$$\mathcal{H} = \begin{bmatrix} f[0] & f[1] & \dots & f[M-1] & 0 & \dots & 0 \\ 0 & f[0] & f[1] & \dots & f[M-1] & \dots & 0 \\ \vdots & \vdots & \ddots & \ddots & \vdots & \ddots & \vdots \\ 0 & \dots & \dots & f[0] & f[1] & \dots & f[M-1] \end{bmatrix}' \quad (2.21)$$

$$\mathbf{R}_x = \mathcal{H}\mathcal{H}^H.$$

Obviously, when the noise $w[n]$ is AWGN,

$$\begin{aligned} \mathcal{H}_0 : \hat{\mathbf{R}}_y &= \sigma_w^2 \mathbf{I} \\ \mathcal{H}_1 : \hat{\mathbf{R}}_y &= \mathbf{R}_x + \sigma_w^2 \mathbf{I}, \end{aligned} \quad (2.22)$$

in which σ_w^2 is the power of noise $w[n]$. The \mathbf{R}_x can be regarded as a known template of the interested signal in the estimator-correlator (EC) detection which will be presented in Section 2.5.3.

2.5.1 Equalization of Nonwhite Noise Floor

The noise in a practical receiver is normally not perfectly white due to the unflat frequency responses of filters in receiver, such as anti-aliasing filter before analog-to-digital converter and Cascaded Integrator-Comb (CIC) filter for sampling rate conversion. The non-white noise leads to non-zero values among the non-diagonal elements of the covariance matrix $\hat{\mathbf{R}}_y$ in hypothesis \mathcal{H}_0 . In Section 3.2.3, it will show that this phenomenon in practical receiver can degrade detection performance notably. In [33], a method is proposed to solve this problem. Assuming the impulse response of receiver is $v[i]$, similar to (2.21), the covariance matrix of the nonwhite noise \mathbf{R}_w can be derived as

$$\mathbf{V} = \begin{bmatrix} v[0] & v[1] & \dots & v[K-1] & 0 & \dots & 0 \\ 0 & v[0] & v[1] & \dots & v[K-1] & \dots & 0 \\ \vdots & \vdots & \ddots & \ddots & \vdots & \ddots & \vdots \\ 0 & \dots & \dots & v[0] & v[1] & \dots & v[K-1] \end{bmatrix}' \quad (2.23)$$

$$\mathbf{R}_w = \mathbf{V}\mathbf{V}^H.$$

The \mathbf{R}_w can also be obtained through applying statistical method in (2.19) to the receiver's noise in hypothesis \mathcal{H}_0 . Then, \mathbf{R}_w is Cholesky

decomposed into $\mathbf{R}_w = \mathbf{Q}^H \mathbf{Q}$. The matrix \mathbf{Q} is used to equalize the estimated covariance matrix $\hat{\mathbf{R}}_y$ as

$$\hat{\mathbf{R}}'_y = (\mathbf{Q}^H)^{-1} \hat{\mathbf{R}}_y \mathbf{Q}^{-1}. \quad (2.24)$$

Then, the equalized covariance matrix $\hat{\mathbf{R}}'_y$ can be used in all the CVWD detection algorithms for correcting the nonwhiteness of the noise in receiver.

2.5.2 Blind Detection with Maximum-Minimum Eigenvalue (CVWD-MME) and Covariance Absolute Value (CVWD-CAV)

When the detector is blind, which means \mathbf{R}_x is completely unknown, the detection can be achieved only by analyzing the statically estimated $\hat{\mathbf{R}}_y$. It is proposed in [34] that a detection method utilizing the Maximum-Minimum Eigenvalues (MME) of $\hat{\mathbf{R}}_y$ has optimal performance, which is presented as follows. First, eigenvalue decomposition is performed on $\hat{\mathbf{R}}_y$:

$$\begin{aligned} \hat{\mathbf{R}}_y &= \Phi_y \Psi_y \Phi_y^{-1} \\ \Phi_y &= [\varphi_{y,1}, \varphi_{y,2}, \dots, \varphi_{y,N_c}] \\ \Psi_y &= \text{diag}\{\psi_{y,1}, \psi_{y,2}, \dots, \psi_{y,N_c}\}, \end{aligned} \quad (2.25)$$

in which $\varphi_{y,n}$ are the eigenvectors and $\psi_{y,n}$ are their corresponding eigenvalues satisfying $\psi_{y,1} \geq \psi_{y,2} \geq \dots \geq \psi_{y,N_c}$. Then the detection metric of CVWD-MME is formulated by

$$\Lambda_{\text{CVWD-MME}} = \frac{\psi_{y,1}}{\psi_{y,N_c}}. \quad (2.26)$$

In [33], an alternative detection method called Covariance Absolute Value (CAV) detection is proposed and implemented. This detection method has the performance which is close to that of CVWD-MME. The simulation performances in Section 3.2.2 will confirm this fact. The detection metric of CVWD-CAV detector is formulated as

$$\Lambda_{\text{CVWD-CAV}} = \frac{\sum_{m=1}^{N_c} \sum_{n=1}^{N_c} |r_{m,n}|}{\sum_{m=1}^{N_c} |r_{m,m}|}, \quad (2.27)$$

in which $r_{m,n}$ is the elements in $\hat{\mathbf{R}}_y$. The advantage of CVWD-CAV detection over CVWD-MME detection is that the computationally costly eigenvalue decomposition on $\hat{\mathbf{R}}_y$ is not required. Obviously, since the detection metrics of CVWD-MME and CVWD-CAV require no information on noise power, they are not affected by the NU problem.

2.5.3 Estimator-Correlator Detection with Known Covariance Matrix (CVWD-EC)

In [28] and [35], an optimal Estimator-Correlator (EC) detector is presented, which takes the noise-free signal's covariance matrix \mathbf{R}_x as known template.

$$\Lambda_{\text{CVWD-EC}} = \frac{1}{N - N_c + 1} \sum_{i=1}^{N-N_c+1} \mathbf{y}_i^H \mathbf{R}_x (\mathbf{R}_x + \sigma_w^2 \mathbf{I})^{-1} \mathbf{y}_i. \quad (2.28)$$

Notice that the diagonal component of \mathbf{R}_x should be equal to the noise-free signal's power σ_x^2 . When the noise-free signal is white, $\mathbf{R}_x = \sigma_x^2 \mathbf{I}$, the EC detector is then reduced to

$$\Lambda_{\text{CVWD-EC,white}} = \frac{1}{N - N_c + 1} \sum_{i=1}^{N-N_c+1} \mathbf{y}_i^H \mathbf{y}_i, \quad (2.29)$$

which is actually equivalent to EGD.

It is impractical to assume that σ_x^2 is known to the receiver due to the unknown SNR of the received signal. However, when the SNR is small, $\mathbf{R}_x + \sigma_w^2 \mathbf{I} \simeq \sigma_w^2 \mathbf{I}$, then the EC detection in (2.28) can be reduced to a more practical form [36]

$$\Lambda_{\text{CVWD-EC,w/o SNR}} = \frac{1}{N - N_c + 1} \sum_{i=1}^{N-N_c+1} \mathbf{y}_i^H \mathbf{R}_x \mathbf{y}_i. \quad (2.30)$$

Obviously, in this detection, the knowledge of SNR is not needed while the signal's covariance matrix \mathbf{R}_x is still required.

2.6 POWER SPECTRUM BASED WHITENESS DETECTION (PSWD)

It is proposed in this thesis that the whiteness of received signal can be also tested in frequency domain using the estimated PSD. In practical receiver, spurs from harmonic components and DC components generated by the receiver itself can cause strong autocorrelation and hence make the covariance matrix no longer equal to $\sigma_w^2 \mathbf{I}$ in hypothesis \mathcal{H}_0 . It will be shown in the simulation results in Section 3.2.3 that this phenomenon can deteriorate CVWD's detection performance significantly. However, since the spurs are very narrowbanded and have fixed frequencies, when the PSD of signal is estimated, the few frequency components with spurs can be simply excluded in the detection algorithm. In this way, the spur's destruction to detection performance can be straightforwardly eliminated in frequency domain. This type of detections are named Power Spectrum based Whiteness Detection (PSWD) in this thesis.

The PSD of the received signal $y[n]$ can be estimated using Welch's method [37]. First, the received signal samples $y[n]$ are split into segments with length N_{DFT} for Discrete Fourier Transform (DFT) operation. Each segment is shifted from previous ones by the step of D samples and there are K segments used in detection. The DFT operations are then performed as

$$Y_i[m] = \sum_{n=0}^{N_{\text{DFT}}-1} y[iD + n]v[n]e^{-2\pi j \frac{nm}{N_{\text{DFT}}}} \quad m = 0, 1, \dots, N_{\text{DFT}} - 1 \quad , \quad (2.31)$$

in which $v[n]$ is a smoothing window of length N_{DFT} . Then the PSD of $y[n]$ can be estimated by

$$\hat{Y}[m] = \frac{\sum_{i=0}^{K-1} |Y_i[m]|^2}{K \sum_{n=0}^{N_{\text{DFT}}-1} v^2[n]} \quad (2.32)$$

From (2.31) it can be inferred that each segment of signal spans N_{DFT} samples and has $N_{\text{DFT}} - D$ samples overlapped with neighboring segments. It can be also inferred that when hypothesis \mathcal{H}_0 is true, $\hat{Y}[m]$ is the average of $2K$ squared gaussian variables, hence it follows chi-squared distribution. In [37], it is pointed out that the overlapping can increase the EDF in estimating $\hat{Y}[n]$ and hence decrease the variance of estimated PSD and improve detection performance, which will be shown in the simulation results in Section 3.2.2. Based on the analysis in [37], the variance of $\hat{Y}[m]$'s components is derived as

$$\text{Var}\{\hat{Y}[m]\} = \frac{\text{Var}\{|Y_i[m]|^2\}}{K} \left\{ 1 + 2 \sum_{k=1}^{K-1} \frac{K-k}{K} \rho[k] \right\}, \quad (2.33)$$

in which

$$\rho[k] = \left\{ \frac{\sum_{n=0}^{N_{\text{DFT}}-1} v[n]v[n+kD]}{\sum_{n=0}^{N_{\text{DFT}}-1} v^2[n]} \right\}^2 \quad (2.34)$$

As $\hat{Y}[m]$ is the average of $|Y_i[m]|^2$, based on (2.32) and (2.33), $\hat{Y}[m]$ follows chi-squared distribution with EDF of

$$\zeta = \frac{2\text{Var}\{|Y_i[m]|^2\}}{\text{Var}\{\hat{Y}[m]\}} = \frac{2K}{1 + 2 \sum_{k=1}^{K-1} \frac{K-k}{K} \rho[k]} \quad (2.35)$$

The multiplication of two in (2.35) is because $Y_i[m]$ are complex values with in-phase and quadrature components. When the observation time thus the total number of samples used in detection N is fixed, the number of segments K becomes a function of the shifting step D :

$$K = \left\lfloor \frac{N - N_{\text{DFT}}}{D} \right\rfloor + 1. \quad (2.36)$$

The K is increased by decreasing D , which leads to the improvement of EDF as is calculated in (2.35).

2.6.1 Equalize Nonwhite Noise Floor and Remove Spurs

There are two issues in practical receiver which need to be addressed. First, in order to eliminate the destruction of spurs, the frequency components with them should be excluded in detection. Then it is assumed that $\mathbf{S} \subseteq \{0, 1, \dots, N_{\text{DFT}} - 1\}$ is the index set of frequency components without spurs. The other issues is that the noise in receiver is not perfectly white due to the unflat frequency response of filters, thus, the noise floor is also not flat. The shape of noise floor can be well estimated using (2.31) and (2.32) with long observation time. Assuming the estimated noise floor is $\hat{W}[m] \quad m = 0, 1, \dots, N_{\text{DFT}} - 1$, it can be then used to equalize the estimated PSD $\hat{Y}[m]$:

$$\hat{Y}_{\text{eq.}}[m] = \frac{\hat{Y}[m]}{\hat{W}[m]}. \quad (2.37)$$

2.6.2 Blind Detection with the Ratio of Arithmetic-Geometric Means (PSWD-AG)

In hypothesis \mathcal{H}_0 , $\hat{Y}_{\text{eq.}}[m]$ converge to a constant when $K \rightarrow \infty$. Since the interested signal $x[n]$ is not white, the $\hat{Y}_{\text{eq.}}[m]$ is not a constant in hypothesis \mathcal{H}_1 , thus, the arithmetic mean of $\hat{Y}_{\text{eq.}}[m] | \mathcal{H}_1$ is always larger than its geometric mean. Therefore, the metric of a blind detection can be formulated using the quotient of the arithmetic mean and geometric mean (AG):

$$\Lambda_{\text{PSWD-AG}} = \frac{\sum_{m \in \mathbf{S}} \hat{Y}_{\text{eq.}}[m]}{L_{\mathbf{S}} \left(\prod_{m \in \mathbf{S}} \hat{Y}_{\text{eq.}}[m] \right)^{\frac{1}{L_{\mathbf{S}}}}}, \quad (2.38)$$

in which $L_{\mathbf{S}}$ is the size of the set \mathbf{S} .

It is difficult to derive the probability distribution of $\Lambda_{\text{PSWD-AG}}$ for calculating the detection threshold in a closed form. Then, large

number of empirically tested detection metric in hypothesis \mathcal{H}_0 can be used to estimate the threshold. The test can be simplified by modeling $\hat{Y}_{\text{eq.}}[m]$ as N independent and identically distributed (i.i.d) random variables following the chi-squared distribution with the EDF calculated by (2.35). When the number of segments K is large, the chi-squared distribution can be approximated by normal distribution.

$$\hat{Y}_{\text{eq.}}[m] \sim \mathcal{N}\left(\sigma_w^2, \frac{\zeta\sigma_w^4}{2K^2}\right). \quad (2.39)$$

It should be noted that the $\Lambda_{\text{PSWD-AG}}$ is a ratio value which is irrelevant to noise power, which is similar to the detection metric of CVWD-MME and CVWD-CAV. Therefore, the PSWD-AG is also not affected by noise uncertainty problem.

2.6.3 Power Spectrum Whiteness Detection with Known Spectrum Mask (PSWD-SM)

The knowledge of the interested signal's PSD can be applied in detection as a template, which can result better detection performance than the blind PSWD-AG (2.38). The known PSD $\check{X}[m]$ is used as a spectrum mask (SM), which is correlated with the estimated PSD of the received signal, resulting the following proposed detection metric

$$\Lambda_{\text{PSWD-SM}} = \sum_{m \in \mathcal{S}} \hat{Y}_{\text{eq.}}[m] \check{X}[m]. \quad (2.40)$$

The idea of using spectrum mask template in PSWD-SM is similar to using the matched filter template in MFD-EG and the covariance matrix template in CVWD-EC. However, thanks to the processing in frequency domain, the destruction of nonwhite noise floor and spurs can be easily eliminated in PSWD-SM. In the next section, it is proved analytically that MFD-EG, CVWD-EC and PSWD-SM are actually equivalent with each other.

2.7 THE EQUIVALENCE OF MFD-EG, CVWD-EC AND PSWD-SM

It can be noticed in Section 2.4, 2.5 and 2.6 that all the three detection methods MFD-EG, CVWD-EC and PSWD-SM require certain templates of the interested signal. They are the impulse response of matched filter $f[m]$, covariance matrix \mathbf{R}_x and the PSD $\check{X}[m]$ of the interested signal respectively. Intuitively, these templates are directly related with each other: the PSD of the signal is decided by the power-frequency response of its matched filter; the PSD is also

the Fourier transform of the signal's autocorrelation function which can be denoted by the covariance matrix. In this section, it is proved analytically that these three signal detection algorithms utilizing different templates are actually equivalent to each other.

2.7.1 Proof of the Equivalence between MFD-EG and CVWD-EC

The convolution operation of matched filtering in (2.10) can be represented in matrix form

$$\mathbf{y}_f = \mathbf{F}^H \mathbf{y}, \quad (2.41)$$

in which $\mathbf{y} = [y[0], y[1], \dots, y[N-1]]^T$ is the vector of received signal's samples and \mathbf{F} is the composed of the matched filter's impulse response $f[n]$:

$$\mathbf{F} = \begin{bmatrix} f[0] & f[1] & \dots & f[M-1] & 0 & \dots & 0 \\ 0 & f[0] & f[1] & \dots & f[M-1] & \dots & 0 \\ \vdots & \vdots & \ddots & \ddots & \vdots & \ddots & \vdots \\ 0 & \dots & \dots & f[0] & f[1] & \dots & f[M-1] \end{bmatrix}, \quad (2.42)$$

The detection metric of MFD-EG can be then rewritten in matrix form as

$$\begin{aligned} \Lambda_{\text{MFD-EG}} &= \frac{1}{N} \sum_{n=0}^{N-1} |y_f[n]|^2 \\ &= E(\mathbf{y}_f^H \mathbf{y}_f) \\ &= E(\mathbf{y}^H \mathbf{F} \mathbf{F}^H \mathbf{y}), \end{aligned} \quad (2.43)$$

In which $E(\cdot)$ denotes the expectation of a random process. The impulse response of the interested signal's pulse shaping filter can be written as $\mathbf{g} = [f[M-1], f[M-2], \dots, f[0]]^H$. Then, the transmitted signal \mathbf{x} can be modeled as an i.i.d. process \mathbf{z} filtered by the pulse shaping filter, if the non-random structures, such as preambles, pilot tones and cyclic prefix are ignored. The pulse shaping filtering can be denoted by

$$\mathbf{x} = \mathbf{F} \mathbf{z}^*. \quad (2.44)$$

Assume the variance of \mathbf{z} is normalized to 1, based on (2.19), the covariance matrix of \mathbf{z} becomes an identity matrix:

$$E(\mathbf{z} \mathbf{z}^H) = E(\mathbf{z}^* \mathbf{z}^T) = \mathbf{I}. \quad (2.45)$$

Then, referring (2.19), the covariance matrix of the interested signal \mathbf{x} can be obtained by

$$\begin{aligned}
\mathbf{R}_x &= \mathbb{E}(\mathbf{x}\mathbf{x}^H) \\
&= \mathbb{E}(\mathbf{F}\mathbf{z}^*\mathbf{z}^T\mathbf{F}^H) \\
&= \mathbf{F}\mathbb{E}(\mathbf{z}^*\mathbf{z}^T)\mathbf{F}^H \\
&= \mathbf{F}\mathbf{F}^H.
\end{aligned} \tag{2.46}$$

Recalling the detection metric of MFD-EG in (2.43),

$$\begin{aligned}
\Lambda_{\text{MFD-EG}} &= \mathbb{E}(\mathbf{y}^H\mathbf{F}\mathbf{F}^H\mathbf{y}) \\
&= \mathbb{E}(\mathbf{y}^H\mathbf{R}_x\mathbf{y}) \\
&= \Lambda_{\text{CVWD-EC, w/o SNR}}.
\end{aligned} \tag{2.47}$$

This complete the proof of the equivalence of MFD-EG and CVWD-EC(without SNR).

2.7.2 Proof of the Equivalence between CVWD-EC and PSWD-SM

The DFT operation for estimating the PSD of the interested signal using Welch's method can be written in the following matrix form

$$\mathbf{x}_F = \mathbf{W}\mathbf{x}, \tag{2.48}$$

in which \mathbf{W} is the DFT matrix defined by

$$\mathbf{W} = \begin{bmatrix} 1 & 1 & 1 & \dots & 1 \\ 1 & w & w^2 & \dots & w^{N_{\text{DFT}}-1} \\ 1 & w^2 & w^4 & \dots & w^{2(N_{\text{DFT}}-1)} \\ \vdots & \vdots & \vdots & & \vdots \\ 1 & w^{N_{\text{DFT}}-1} & w^{2(N_{\text{DFT}}-1)} & \dots & w^{(N_{\text{DFT}}-1)(N_{\text{DFT}}-1)} \end{bmatrix}, \tag{2.49}$$

in which $w = e^{-j2\pi/N_{\text{DFT}}}$. The matrix \mathbf{W} satisfies $\mathbf{W}\mathbf{W}^H = \mathbf{I}$. Define another matrix

$$\begin{aligned}
\mathbf{S}_x &= \mathbf{W}\mathbf{R}_x\mathbf{W}^H \\
&= \mathbf{W}\mathbb{E}(\mathbf{x}\mathbf{x}^H)\mathbf{W}^H \\
&= \mathbb{E}(\mathbf{W}\mathbf{x}\mathbf{x}^H\mathbf{W}^H) \\
&= \mathbb{E}(\mathbf{x}_F\mathbf{x}_F^H) \\
&= \text{diag}\{\check{X}[0], \check{X}[1], \dots, \check{X}[N_{\text{DFT}} - 1]\},
\end{aligned} \tag{2.50}$$

in which $\check{\chi}[m]$ is the estimated PSD of the interested signal \mathbf{x} . The detection metric of PSWD-SM can be then formulated by

$$\begin{aligned}
\Lambda_{\text{PSWD-SM}} &= \mathbb{E}(\mathbf{y}_F^H \mathbf{S}_x \mathbf{y}_F) \\
&= \mathbb{E}((\mathbf{W}\mathbf{y})^H \mathbf{S}_x (\mathbf{W}\mathbf{y})) \\
&= \mathbb{E}(\mathbf{y}^H \mathbf{W}^H \mathbf{W} \mathbf{R}_x \mathbf{W}^H \mathbf{W} \mathbf{y}) \\
&= \mathbb{E}(\mathbf{y}^H \mathbf{R}_x \mathbf{y}) \\
&= \Lambda_{\text{CVWD-EC}, w/o \text{ SNR}}.
\end{aligned} \tag{2.51}$$

Then the equivalence of PSWD-SM and CVWD-EC(without SNR) is proved.

2.8 CYCLOSTATIONARY DETECTION (CSD)

The communication and broadcasting signals normally exhibit non-stationarity due to their time-varying statistical properties. However, the statical properties of some signals are cyclical due to the periodically repeated structures in the signal, such as preamble, pilot, Cyclic Prefix (CP), sinusoid carrier and spreading code, etc. This kind of signals are characterized by cyclostationary process which can be examined for detecting and classifying the signal at low SNR regime. The cyclostationary signal are often analyzed using SCF, which is formulated as follows.

A signal $x(t)$ is defined as wide-sense cyclostationary if its mean and autocorrelation are periodical with period T_0 :

$$\begin{aligned}
M_x(t) &= \mathbb{E}\{x(t)\} = M_x(t + T_0), \\
R_x(t, \tau) &= \mathbb{E}\{x(t - \tau/2)x^*(t + \tau/2)\} \\
&= R_x(t + T_0, \tau).
\end{aligned} \tag{2.52}$$

The period T_0 in time t can lead to the expression of $R_x(t, \tau)$ using Fourier series [38]:

$$R_x(t, \tau) = \sum_{\alpha} R_x^{\alpha}(\tau) e^{j2\pi\alpha t}, \tag{2.53}$$

in which $\alpha = m/T_0$ is the cyclic frequency and m is an integer. The Fourier coefficient can be calculated by

$$R_x^{\alpha}(\tau) = \lim_{T \rightarrow \infty} \frac{1}{T} \int_{-T/2}^{T/2} R_x(t, \tau) e^{-j2\pi\alpha t} dt. \tag{2.54}$$

The cyclic Wiener relation [39] states that the SCF can be obtained from the Fourier transform of the cyclic autocorrelation in (2.54):

$$S_x^{\alpha}(f) = \int_{-\infty}^{\infty} R_x^{\alpha}(\tau) e^{-j2\pi f \tau} d\tau. \tag{2.55}$$

In discussing the measurement of spectral correlation[38, 39], Gardner showed that the SCF can be estimated in both time-smoothing approach and frequency-smoothing approach. The Time-Smoothed Cyclic Cross Periodogram (TS-CCP) is utilized in time-smoothing approach, which is formulated by

$$S_x^\alpha(f) = \lim_{\Delta f \rightarrow 0} \lim_{T \rightarrow \infty} \frac{1}{\Delta f} \int_{-T/2}^{T/2} \Delta f X_{1/\Delta f}(t, f + \alpha/2) X_{1/\Delta f}^*(t, f - \alpha/2) dt. \quad (2.56)$$

in which $X_{1/\Delta f}(t, f)$ is the Fourier transform within time interval $1/\Delta f$:

$$X_{1/\Delta f}(t, f) = \int_{t - \frac{1}{2\Delta f}}^{t + \frac{1}{2\Delta f}} x(u) e^{-j2\pi f u} du. \quad (2.57)$$

Gardner showed that the time-smoothing approach in (2.56) is completely equivalent to the frequency-smoothing approach using the Frequency-Smoothed Cyclic Cross Periodogram (FS-CCP):

$$S_x^\alpha(f) = \lim_{\Delta f \rightarrow 0} \lim_{T \rightarrow \infty} \frac{1}{\Delta f} \int_{f - \Delta f/2}^{f + \Delta f/2} \frac{1}{T} X_T(t, v + \alpha/2) X_T^*(t, v - \alpha/2) dv, \quad (2.58)$$

in which $X_T(t, f)$ is the Fourier transform within time interval T :

$$X_T(t, f) = \int_{t - \frac{T}{2}}^{t + \frac{T}{2}} x(u) e^{-j2\pi f u} du. \quad (2.59)$$

The T and Δf are the temporal resolution and spectral resolution respectively. The time-smoothing approach requires

$$T \gg \frac{1}{\Delta f}, \quad (2.60)$$

while the frequency-smoothing approach requires

$$\Delta f \gg \frac{1}{T}. \quad (2.61)$$

Hence, for both approaches the product of temporal and spectral resolutions should greatly exceed one:

$$\Delta f T \gg 1. \quad (2.62)$$

It is often useful to examine the spectral coherence without considering the absolute power of the signal. This can be achieved using the

Auto-Coherence Function (ACF) which is essentially the normalized SCF:

$$C_x^\alpha(f) = \frac{|S_x^\alpha(f)|}{[S_x^0(f + \alpha/2)S_x^0(f - \alpha/2)]^{1/2}}. \quad (2.63)$$

Obviously, its value is within $[0, 1]$. Since the result of ACF is the dimensionless coherence value without considering the absolute power, the signal detection and classification based on ACF have the big advantage of invulnerable to noise uncertainty problem comparing with the spectrum sensing based on SCF.

In Figure 4 and Figure 5, the ACFs of BPSK and QPSK are presented, which shows some signatures on the plain of cyclic-spectral frequencies. It can be noticed that there is a strong and unique signature only in the ACF of BPSK, which is due to the conjugate symmetric property of BPSK's spectrum density. It is shown in Figure 6 that this strong signature of BPSK can still be clearly revealed even at the SNR as low as -16 dB. The classification of BPSK and QPSK using cyclostationary signature is analyzed in [40].

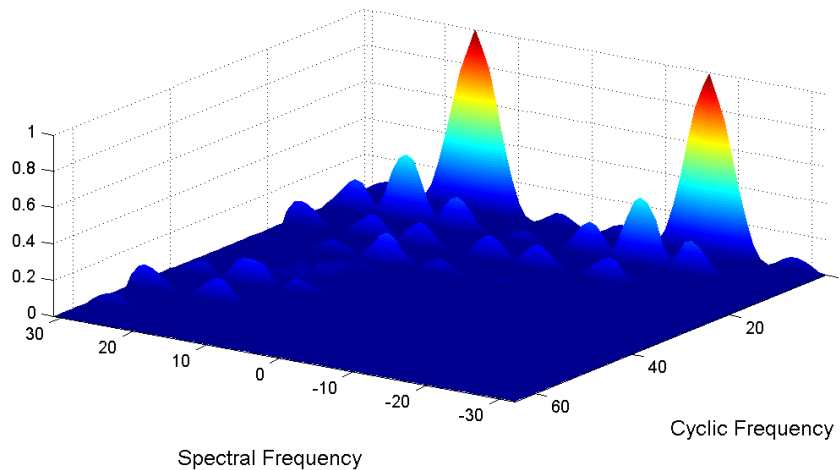


Figure 4: ACF (normalized SCF) of noise-free QPSK signal, DFT size: 64

The SCF analysis is particularly helpful in extracting the cyclostationary signatures embedded intentionally in multi-carrier signal for assisting signal detection and classification [19, 20, 21, 41, 42]. In this thesis, the application of embedded cyclostationary signatures (ECS) is further extended to the scheme of delivering arbitrary extended information, which is illustrated in details in Chapter 5. Other than the SCF analysis, the cyclostationarity of wireless signals can be exploited in other forms for signal detection, such as the CP-SW and the FSA-2C detections presented in Section 2.9.1.1 and Section 2.9.2.2 respectively.

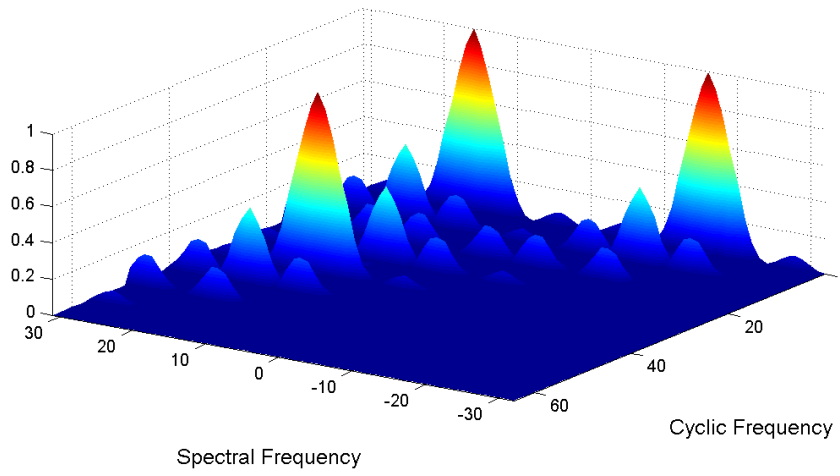


Figure 5: ACF (normalized SCF) of noise-free BPSK signal, DFT size: 64

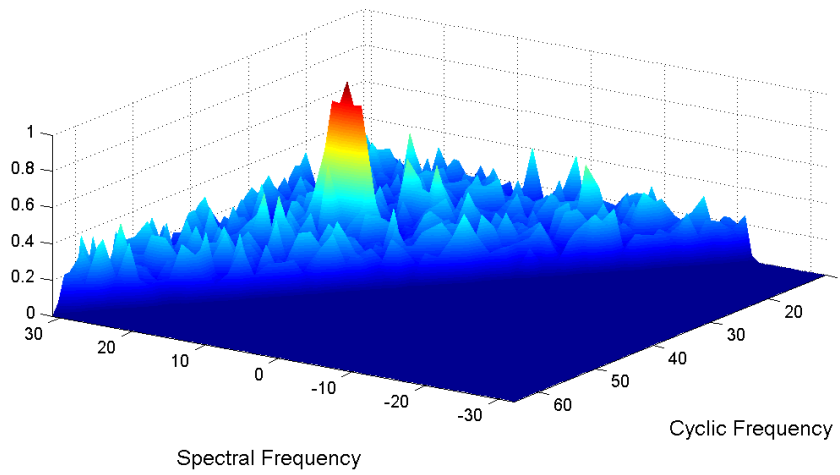


Figure 6: ACF (normalized SCF) of BPSK signal with noise, DFT size: 64,
SNR: -16 dB

2.9 AUTOCORRELATION BASED DETECTION (ACD)

The MFD introduced in Section 2.4 is essentially based on cross-correlating the received signal with a known sequence which is either the pulse shaping filter or a FS in the preamble or pilot structures. When some repeated structure such as CP and repeated FS are in the interested signal, the autocorrelation of the signal with its delayed version can be also used to compose the detection metrics, which doesn't require the knowledge of the sequence.

2.9.1 CP Based Detection

The reported sensing techniques show big interest in the CP of OFDM signal [43, 44, 45], which is the copy of the tail part of a OFDM symbol and placed at the beginning of a symbol. Strong autocorrelation can be then generated at time lag of DFT size N_{DFT} :

$$r[n] = y[n]y^*[n + N_{DFT}]. \tag{2.64}$$

2.9.1.1 CP Sliding Window Detection (CP-SW)

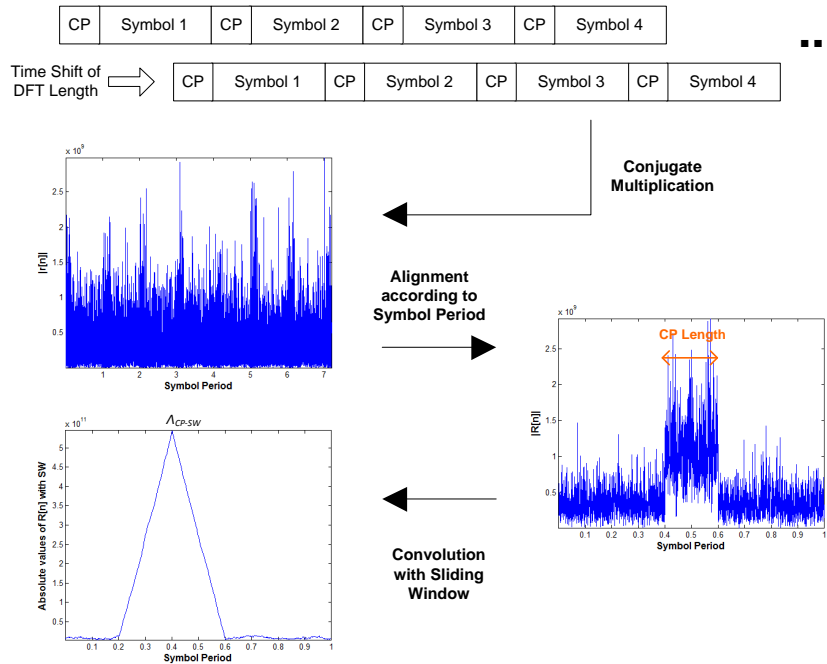


Figure 7: Illustration of the CP-SW detection for a captured real-world DVB-T signal (530MHz, 8K DFT, 1/4 CP ratio)

When $r[n]$ is the correlation between samples in CP and its corresponding tail part of the symbol, its expectation becomes nonzero, thus $r[n]$ is nonstationary. When the OFDM symbols are continuously

and periodically transmitted, as the statistical property is repeated every symbol period, $r[n]$ becomes a cyclostationary process, which can be further split into segments with symbol length $N_{\text{DFT}} + N_{\text{CP}}$ and averaged:

$$\begin{aligned} R[n] &= \frac{1}{\lfloor \frac{N - N_{\text{DFT}} + 1}{N_{\text{DFT}} + N_{\text{CP}}} \rfloor} \sum_{l=0}^{\lfloor \frac{N - N_{\text{DFT}} + 1}{N_{\text{DFT}} + N_{\text{CP}}} \rfloor - 1} r[n + l(N_{\text{DFT}} + N_{\text{CP}})] \\ n &= 0, \dots, N_{\text{DFT}} + N_{\text{CP}} - 1. \end{aligned} \quad (2.65)$$

In this way, the time locations with correlated CPs are aligned, which strengthens the correlation of CPs. It lead to the CP Sliding-Window (SW) detector [43] with test statistic

$$\Lambda_{\text{CP-SW}} = \max_i \left| \sum_{n=i}^{i+N_{\text{CP}}-1} \tilde{R}[n] \right| \quad i = 0, 1, \dots, N_{\text{DFT}} + N_{\text{CP}} - 1, \quad (2.66)$$

in which $\tilde{R}[n]$ is the cyclic extension of $R[n]$ with one CP length. The procedure of generating the detection metric of CP-SW is also presented in Figure 7 showing the intermediate values of processing a captured real-world Digital Video Broadcasting-Terrestrial (DVB-T) signal.

In hypothesis \mathcal{H}_0 , the $|\sum_{n=i}^{i+N_{\text{CP}}-1} \tilde{R}[n]|$ with different i are statistically correlated. Their real and imaginary parts can be approximated by two identical and independent normal distributions with CLT. Therefore, $|\sum_{n=i}^{i+N_{\text{CP}}-1} \tilde{R}[n]|$ follows joint Rayleigh distribution which is, still an open research problem for more than 4 variables and with arbitrary covariance matrix[46, 47]. Hence the exact probability distribution of $\Lambda_{\text{CP-SW}}$ is hard to known and the detection threshold cannot be directly calculated in a closed form. However, the threshold can still be estimated through empirical method with large amount of detection tests in hypothesis \mathcal{H}_0 .

In some standards, such as the 3GPP Long Term Evolution (LTE) and the IEEE 802.22, although the signal has the periodical frame structure, the OFDM symbols in a frame are however not completely periodically and continuously transmitted. For example, the Time-Division Duplex (TDD) frame of IEEE 802.22 standard has the period of 10 ms, in each frame, the periodicity is broken by the TTG (Transmit/Receive Transition Gap) and RTG (Receive/Transmit Transition Gap) which are used for accommodating the transmission delay of wireless channel. For LTE with normal CP length, the CP of the first OFDM symbol in a time slot is longer than the CP of the other symbols in the same time slot. These two properties of IEEE 802.22 and LTE disables the alignment and correlation strengthen

performed in (2.65) for the autocorrelation $r[n]$ and makes the CP-SW detection in (2.66) unsuitable for detecting them.

In order to enable the CP-SW detection with aligned CP's correlation, a method is proposed in this thesis that the $r[n]$ in (2.64) is pre-aligned according to the signal's frame period:

$$r'[n] = \sum_k r[n + kL_{\text{frm}}], \quad (2.67)$$

in which L_{frm} is the period of a frame. For example, the period for the LTE signal is the slot length of 0.5 ms; the period for the 802.22 signal is the TDD frame length of 10 ms. Since most of the OFDM symbols in a period are continuously and periodically transmitted, the further alignment with symbol length in (2.65) and the CP-SW detection in (2.66) are still effective to the pre-aligned $r'[n]$. The performances with and without the pre-alignment for detecting LTE and 802.22 signals will be presented in Section 3.2.8.

2.9.1.2 CP Summation Detection (CP-SUM)

For noncontinuous OFDM transmissions, such as IEEE 802.11a/g and ECMA-392 with CSMA/CA (Carrier Sense Multiple Access with Collision Avoidance) MAC (Media Access Control) layer, the number of OFDM symbols in a burst as well as the intervals between bursts are both random. In this case $r[i]$ is not cyclostationary anymore and the alignment in (2.65) may have no advantage since the OFDM symbols are not periodically transmitted. However, the signal can still be detected ignoring the nonstationary property of $r[n]$ using simple summation of $r[n]$ [48], which is named CP-SUM detector in this thesis. The detection metric of it is formulated by

$$\Lambda_{\text{CP-SUM}} = \frac{1}{\sqrt{N - N_{\text{DFT}} + 1}} \left| \sum_{n=0}^{N - N_{\text{DFT}} - 1} r[n] \right|, \quad (2.68)$$

in which N is the total number of samples used in detection.

Based on CLT, in hypothesis \mathcal{H}_0 , the real and imaginary parts of $\sum_{n=0}^{N - N_{\text{DFT}} - 1} r[n]$ follow zero-mean normal distribution with variance of $\frac{\sigma_w^4}{2}$. Then $\Lambda_{\text{CP-SUM}}$ follows Rayleigh distribution which can be used to calculate the detection threshold

$$\gamma_{\text{CP-SUM}} = \sigma_w^2 \sqrt{-\ln P_{\text{FA}}}. \quad (2.69)$$

2.9.2 Feature Sequence Autocorrelation (FSA) Detection

If the FS in the preamble or pilot structures are repeated, autocorrelation can be used to formulate detection metrics, which is named

feature sequence autocorrelation (FSA) in this thesis. An typical example which has this property is DVB-T. According to [49], every transmitted OFDM symbol of DVB-T signal contains two kinds of pilot sub-carriers, they are continued pilots and scattered pilots. The frequency locations of continued pilots are the same for all transmitted OFDM symbols. while the scattered pilots are inserted every twelve sub-carriers and their frequency locations are shifted by three sub-carriers in the next OFDM symbol. Hence the positions of scattered pilots are repeated every four OFDM symbols, which is depicted in Figure 8. The number of scattered pilots is also much larger than the continued pilots, which makes the scattered pilots' period a major issue considered in FSA detections.

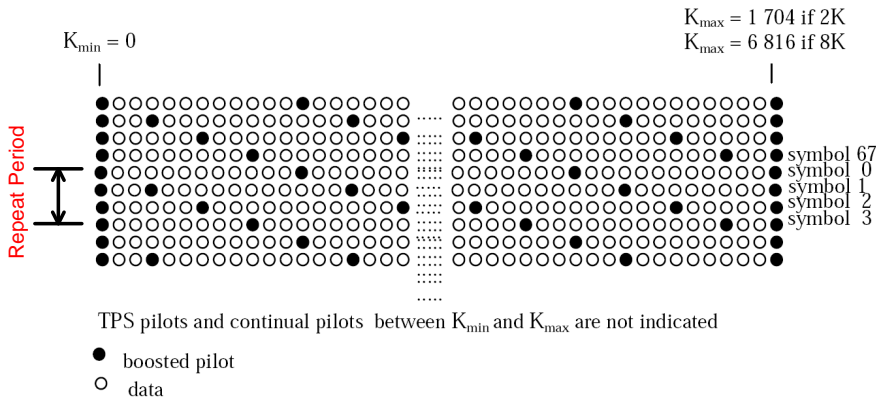


Figure 8: Periodical pilot sub-carrier pattern in DVB-T

In the studies in [50, 46], two TDSC (Time-Domain Symbol Cross-correlation) based detection methods named TDSC-NP and TDSC-MRC for DVB-T are proposed. The TDSC-NP is based on the derivation using Neyman-Pearson test while the TDSC-MRC utilizes Maximum Ratio Combining (MRC). In [51], We further investigated these two methods with more concise reformulation of the detection metrics and considering practical issues. Since the pilots in time domain are taken as FS for autocorrelation, the TDSC methods are actually the FSA detections presented in this sections.

Assume $y[n]$ is the received signal with noise, the period of the repeated FS in the signal is L and there are totally N_p periods thus $N_p L$ samples are used in detection. Define

$$R_k^L = \frac{1}{\sqrt{L}} \sum_{n=0}^{(N_p-k)L-1} y[n]y^*[n+kL] \quad k = 1, 2, \dots, N_p - 1 \quad (2.70)$$

as the autocorrelations of received signal $y[n]$ with time lags which are multiple of L .

The generation of the autocorrelations R_k^L in FSA detections is also exhibited illustratively in Figure 9. Besides, an example of the autocorrelation of a captured real-world DVB-T signal is also presented in this figure. It clearly reveals the strong peaks in the autocorrelation generated by the periodical FS when time shift equals to kL , which are utilized in detecting the signal. Figure 9 also shows some smaller peaks in the autocorrelation with period of $L/4$, which is generated by the continued pilot sub-carriers.

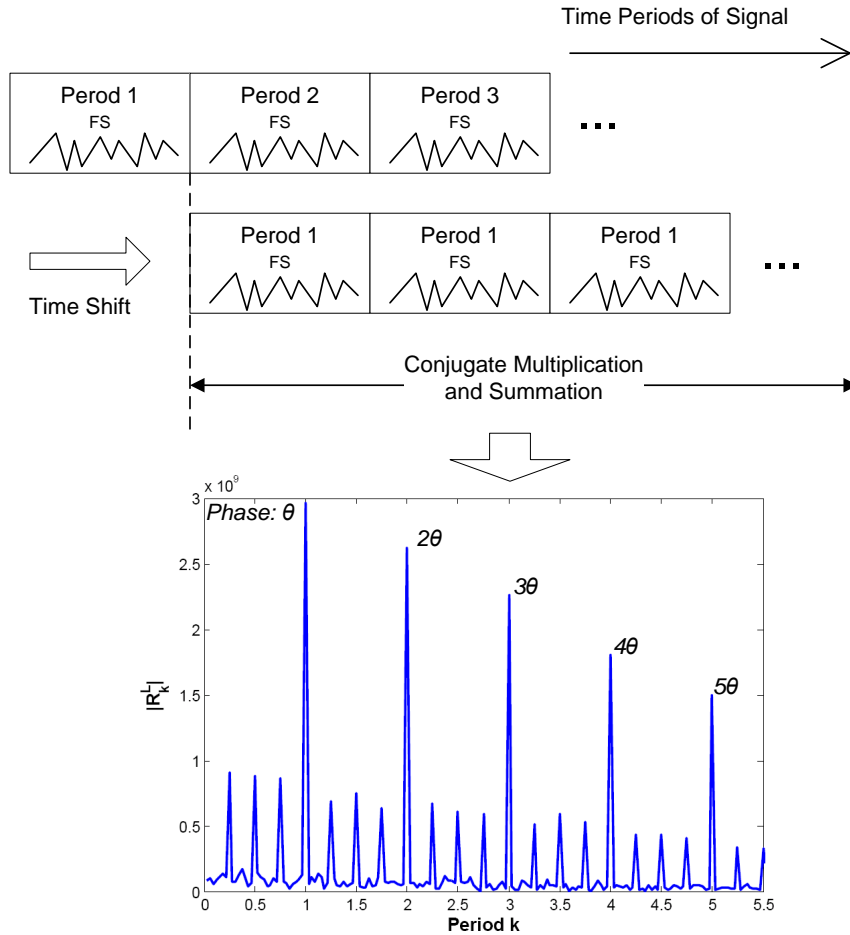


Figure 9: Illustration of the autocorrelation in FSA detections with an example of the autocorrelation of a captured real-world DVB-T signal(530MHz, 8K DFT, 1/4 CP ratio)

2.9.2.1 FSA with Summation Detection (FSA-SUM)

The absolute value of the summed autocorrelation with time shift of length L can be taken as detection metric. In [50] and [46], it is illustrated that this detection metric satisfies the condition of NP test and was named TDSC-NP in the two papers. Since it is based on the

summed autocorrelation according to FS, we renamed it FSA-SUM in this thesis. The detection metric is formulated as

$$\Lambda_{\text{FSA-SUM}} = |\mathbf{R}_1^L| = \sqrt{\Re^2(\mathbf{R}_1^L) + \Im^2(\mathbf{R}_1^L)}. \quad (2.71)$$

For hypothesis \mathcal{H}_0 , $\mathbf{y}[n]$ contains the noise $w[n]$ only, which results

$$\mathbf{R}_1^L | \mathcal{H}_0 = \frac{1}{\sqrt{L}} \sum_{n=0}^{(N_p-1)L-1} w[n]w[n+L]. \quad (2.72)$$

According to CLT, the $\Re(\mathbf{R}_k^L | \mathcal{H}_0)$ and $\Im(\mathbf{R}_k^L | \mathcal{H}_0)$ can be approximated by uncorrelated zero mean normal distributions, the variance of which becomes

$$\text{Var}\{\Re(\mathbf{R}_k^L | \mathcal{H}_0)\} = \text{Var}\{\Im(\mathbf{R}_k^L | \mathcal{H}_0)\} = \frac{(N_p - k)\sigma_w^4}{2}. \quad (2.73)$$

Then, the detection metric $\Lambda_{\text{FSA-SUM}}$ follows Rayleigh distribution. Based on its CDF, the detection threshold can be calculated by

$$\gamma_{\text{FSA-SUM}} = \sigma_w^2 \sqrt{-(N_p - 1) \ln P_{\text{FA}}}. \quad (2.74)$$

It should be noted that the FSA-SUM detection is similar to the CP-SUM detection in (2.68). The only difference is that the FS length of L is taken in FSA-SUM as autocorrelation's time lag instead of the DFT size N_{DFT} used in CP-SUM.

2.9.2.2 FSA with Twice Correlations (FSA-2C)

When the FS in the interested signal is repeated periodically, cyclostationarity is exhibited and can be utilized to compose detection metric which is more sophisticated than FSA-SUM. An optimal method using MRC of the secondary correlation values is proposed in [50, 46], which is named FSA-2C (twice correlation) in this thesis and can be concisely denoted as

$$\Lambda_{\text{FSA-2C}} = \left| \sum_{k=1}^J \mathbf{R}_k^L \mathbf{R}_{k+1}^{L*} \right| \quad J = 1, 2, \dots, N_p - 2, \quad (2.75)$$

in which J is the number of autocorrelation values used in FSA-2C detection. Generally, larger J can lead to better detection performance at the cost of higher computational complexity.

Using (2.73), the variance of the real and imaginary part of $\mathbf{R}_k^L \mathbf{R}_{k+1}^{L*}$ is calculated by

$$\begin{aligned} \text{Var}\{\Re(\mathbf{R}_k^L \mathbf{R}_{k+1}^{L*}) | \mathcal{H}_0\} &= \text{Var}\{\Im(\mathbf{R}_k^L \mathbf{R}_{k+1}^{L*}) | \mathcal{H}_0\} \\ &= \frac{(N_p - k)(N_p - k - 1)\sigma_w^8}{2}. \end{aligned} \quad (2.76)$$

When J is large, based on CLT, $\Lambda_{\text{FSA-2C}}$ can be approximated with Rayleigh distribution. Then the detection threshold can be derived as

$$\gamma_{\text{FSA-2C}} = \sigma_w^4 \sqrt{-\sum_{k=1}^J (N_p - k)(N_p - k - 1) \ln P_{\text{FA}}}. \quad (2.77)$$

2.10 MITIGATION OF NOISE UNCERTAINTY USING DIMENSION CANCELATION (DIC)

2.10.1 Influence of the Noise Uncertainty

In practical receivers, the power of noise cannot be exactly known even when the receiver is calibrated due to the following reasons [52]:

- uncertainty in thermal noise caused by changing temperature;
- uncertainty in amplifier gain caused by changing temperature;
- error in calibration;
- interference during calibration.

The lack of exact knowledge on noise power is called Noise Uncertainty (NU). In some detection methods, it can lead to inaccuracy in detection threshold resulting higher PFA and PMD than expected values. Besides, for EGD [52] and other moment based detectors [53], NU can cause the ‘‘SNR wall’’ phenomenon which makes the detection completely failed when the SNR is below certain limit, no matter how long the observation time is.

2.10.1.1 Unlimited Detectability and the Case of EGD

In order to describe the NU’s impact to PMD, we define the *unlimited detectability*, which means the successful detection at arbitrary low SNR can be achieved as long as the observation time is long enough. It is described mathematically by

$$\lim_{N \rightarrow +\infty} P_{\text{MD}} = \lim_{N \rightarrow +\infty} \Pr\{\Lambda < \gamma | \mathcal{H}_1\} = 0, \quad (2.78)$$

in which N is the number of signal samples used in detection.

As was illustrated in Section 2.3, the probability distribution of the detection metric of EGD can be approximated by normal distributions using CLT:

$$\begin{aligned} \Lambda_{\text{EGD}} | \mathcal{H}_0 &\sim \mathcal{N}(N\sigma_w^2, N\sigma_w^4) \\ \Lambda_{\text{EGD}} | \mathcal{H}_1 &\sim \mathcal{N}(N(\sigma_w^2 + \sigma_x^2), N(\sigma_w^2 + \sigma_x^2)^2) \end{aligned} \quad (2.79)$$

Based on (2.9), the threshold of EGD with known noise power σ_w^2 is formulated by

$$\gamma_{\text{EGD}}(\sigma_w^2) = \sigma_w^2 \sqrt{2N} \text{erf}^{-1}(1 - 2P_{\text{FA}}) + N\sigma_w^2, \quad (2.80)$$

When the noise power σ_w^2 is perfectly known, the PMD when $N \rightarrow +\infty$ is

$$\begin{aligned} \lim_{N \rightarrow +\infty} P_{\text{MD}} &= \lim_{N \rightarrow +\infty} \Pr\{\Lambda_{\text{EGD}} < \gamma_{\text{EGD}}(\sigma_w^2) | \mathcal{H}_1\} \\ &= \lim_{N \rightarrow +\infty} \frac{1}{2} \left[1 + \text{erf} \left(\frac{\sigma_w^2 \sqrt{(2N)} \text{erf}^{-1}(1 - 2P_{\text{FA}}) + N\sigma_w^2 - N(\sigma_w^2 + \sigma_x^2)}{\sqrt{2N}(\sigma_w^2 + \sigma_x^2)} \right) \right] \\ &= \lim_{N \rightarrow +\infty} \frac{1}{2} \left[1 + \text{erf} \left(\frac{\sigma_w^2 \text{erf}^{-1}(1 - 2P_{\text{FA}}) - \sqrt{N/2} \sigma_x^2}{(\sigma_w^2 + \sigma_x^2)} \right) \right] \\ &= 0, \end{aligned} \quad (2.81)$$

which means that the unlimited detectability can be achieved. However, when the detector's expected noise power σ_e^2 differs from the actual value σ_w^2 , particularly, when $\sigma_e^2 > \sigma_w^2$, the PMD when $N \rightarrow +\infty$ becomes

$$\begin{aligned} \lim_{N \rightarrow +\infty} P_{\text{MD}} &= \lim_{N \rightarrow +\infty} \Pr\{\Lambda_{\text{EGD}} < \gamma_{\text{EGD}}(\sigma_e^2) | \mathcal{H}_1\} \\ &= \lim_{N \rightarrow +\infty} \frac{1}{2} \left[1 + \text{erf} \left(\frac{\sigma_w^2 \sqrt{(2N)} \text{erf}^{-1}(1 - 2P_{\text{FA}}) + N\sigma_e^2 - N(\sigma_w^2 + \sigma_x^2)}{\sqrt{2N}(\sigma_w^2 + \sigma_x^2)} \right) \right] \\ &= \lim_{N \rightarrow +\infty} \frac{1}{2} \left[1 + \text{erf} \left(\frac{\sigma_w^2 \text{erf}^{-1}(1 - 2P_{\text{FA}}) + \sqrt{N/2}(\sigma_e^2 - \sigma_w^2 - \sigma_x^2)}{(\sigma_w^2 + \sigma_x^2)} \right) \right] \\ &= 1 \quad \left(\frac{\sigma_x^2}{\sigma_w^2} < \frac{\sigma_e^2}{\sigma_w^2} - 1 \right), \end{aligned} \quad (2.82)$$

in which $\frac{\sigma_x^2}{\sigma_w^2}$ is the actual SNR of the received signal. Thus, when the SNR is smaller than the limit $\frac{\sigma_e^2}{\sigma_w^2} - 1$, the detection can be completely failed no matter how the N corresponding to observation time is increased.

2.10.2 Eliminate Noise Uncertainty with DIC

In (2.9), (2.14), (2.69), (2.74) and (2.77), it can be noticed that all the thresholds of EGD, MFD-EG, CP-SUM, FSA-SUM and FSA-2C detections include the multiplication term σ_w^2 or σ_w^4 . This means that the knowledge of noise power σ_w^2 is required in these detection methods. Practically, since the noise power σ_w^2 cannot be perfectly known due to the NU problem, the threshold calculation therefore becomes inaccurate, which leads to unpredicted PFA and PMD.

In this section, a novel method of eliminating the destruction from NU is proposed, which is essentially based on removing the requirement on noise power knowledge through canceling the dimension of

the detection metrics. In this way, no matter how noise power varies, the threshold as well as its corresponding PFA remain unchanged.

The power of the received signal $y[n]$ is estimated by

$$\hat{\sigma}_y^2 = E(|y[n]|^2) = \frac{1}{N} \sum_{n=0}^{N-1} |y[n]|^2. \quad (2.83)$$

In hypothesis \mathcal{H}_0 , $E(\hat{\sigma}_y^2|\mathcal{H}_0)$ equals to the noise power σ_w^2 . The knowledge of noise power in threshold can be removed through dividing the detection metrics by the cancellation factor $E^2(|y[n]|^2)$ or $E(|y[n]|^2)$ depending on whether the noise power term in the threshold is squared or not.

From another point of view, it can be noticed that the dimension of the cancellation factor should be the same as the dimension of the detection metric and its corresponding threshold. For example, assume the dimension of received samples is in volt (V), the detection metric of MFD-EG in (2.10) is V^2 , then the cancellation factor $E(|y[n]|^2)$ with dimension V^2 should be applied; the detection metric of FSA-2C in (2.75) needs twice correlation operations resulting the dimension of V^4 , hence the cancellation factor of $E^2(|y[n]|^2)$ with the same dimension is used.

Based on this idea, the DIC can be applied to nearly all the detection metrics introduced in Chapter 2 which require the knowledge of noise power thus have dimensions. One exception is the EGD which has the detection metric $\Lambda_{EGD} = N\hat{\sigma}_y^2 = NE(|y[n]|^2)$, if it is divided by the according cancellation factor $E(|y[n]|^2)$, the detection metric becomes a constant N for both \mathcal{H}_0 and \mathcal{H}_1 , which makes the signal detection impossible.

The detection metrics of CVWD-MME, CVWD-CAV and PSWD-AG have no dimensions inherently: $\Lambda_{CVWD-MME}$ is the ratio between maximum and minimum eigenvalues of the estimated covariance matrix; $\Lambda_{CVWD-CAV}$ is the ratio between the sum of all elements in the covariance matrix and the sum of diagonal elements; $\Lambda_{PSWD-AG}$ is the ratio between arithmetic mean and geometric mean of the components in estimated PSD. Their detection metrics in \mathcal{H}_0 and resulted PFA are irrelevant to noise power. Therefore, the DIC is not needed by them.

By analyzing the dimensions of the detection metrics illustrated in this chapter, their according DIC factors Ψ_{method} are summarized in Table 1. The detection metrics after DIC can be then defined by

$$\Lambda'_{\text{method}} = \frac{\Lambda_{\text{method}}}{\Psi_{\text{method}}}. \quad (2.84)$$

Table 1: Dimension Cancellation Factors for Various Detection Methods

Detection Methods	DIC Factor Ψ_{method}
EGD	not available
MFD-EG/FS	$E(y[n] ^2)$
CVWD-MME/CAV	not needed
CVWD-EC	$E(y[n] ^2)$
PSWD-AG	not needed
PSWD-SM	$E(y[n] ^2)$
CSD using ACF	$E(y[n] ^2)$
CP-SW/SUM	$E(y[n] ^2)$
FSA-SUM	$E(y[n] ^2)$
FSA-2C	$E^2(y[n] ^2)$

In Chapter 3 and Chapter 4, the effectiveness of applying DIC for eliminating NU problem completely in signal detection and classification is validated in various spectrum sensing scenarios.

2.11 COOPERATIVE SIGNAL DETECTION

The previous parts of this chapter discuss only the local signal detection methods which are applied only on single sensing node. The reported literatures have shown that the combination of the sensing measurements from multiple sensing nodes can effectively improve the overall detection performance at low SNR, reduce the sensitivity requirement on single sensing node, mitigation channel fading, shadowing and noise uncertainty [54, 55, 56, 17]. In this section, we briefly review the major algorithms used in cooperative signal detection.

2.11.1 Optimal Soft Combination

Consider the spectrum sensing scenario with K cooperating sensing nodes, each of them senses the same channel simultaneously using the following observed signal in the two hypotheses:

$$\begin{aligned}
 \mathcal{H}_0 : \mathbf{y}_k &= \mathbf{w}_k \\
 \mathcal{H}_1 : \mathbf{y}_k &= \mathbf{x}_k + \mathbf{w}_k
 \end{aligned} \tag{2.85}$$

$k = 1, 2, \dots, K.$

It is assumed that both the elements in the target signal vector \mathbf{x}_k and the noise vector \mathbf{w}_k are all independent and normally distributed

with zero means, thus $\mathbf{x}_k \sim \mathcal{N}(\mathbf{0}, \eta_k^2 \mathbf{I})$ and $\mathbf{w}_k \sim \mathcal{N}(\mathbf{0}, \sigma_k^2 \mathbf{I})$. Then the likelihood ratio between the joint observations in both hypotheses can be composed by

$$\begin{aligned}
 L(\mathbf{y}_1, \dots, \mathbf{y}_K) &= \frac{\prod_{k=1}^K f_k(\mathbf{y}_k | \mathcal{H}_1)}{\prod_{k=1}^K f_k(\mathbf{y}_k | \mathcal{H}_0)} \\
 &= \prod_{k=1}^K \frac{\frac{1}{(\sigma_k^2 + \eta_k^2)^N} \exp\left(-\frac{\|\mathbf{y}_k\|^2}{\sigma_k^2 + \eta_k^2}\right)}{\frac{1}{\sigma_k^{2N}} \exp\left(-\frac{\|\mathbf{y}_k\|^2}{\sigma_k^2}\right)} \\
 &= \prod_{k=1}^K \frac{\sigma_k^{2N}}{(\sigma_k^2 + \eta_k^2)^N} \exp\left(\frac{\eta_k^2 \|\mathbf{y}_k\|^2}{\sigma_k^2 (\sigma_k^2 + \eta_k^2)}\right) \\
 &= \prod_{k=1}^K \frac{\sigma_k^{2N}}{(\sigma_k^2 + \eta_k^2)^N} \cdot \exp\left(\sum_{k=1}^K \frac{\eta_k^2 \|\mathbf{y}_k\|^2}{\sigma_k^2 (\sigma_k^2 + \eta_k^2)}\right),
 \end{aligned} \tag{2.86}$$

in which N is the number of signal samples used in EGD on each node and η_k^2 and σ_k^2 are the signal power and noise power on the node k respectively. It should be noted that $\|\mathbf{y}_k\|^2$ is the detection metric of EGD on sensing node k :

$$\|\mathbf{y}_k\|^2 = \sum_{n=1}^N |y_k[n]|^2. \tag{2.87}$$

According to the Neyman-Pearson lemma[57], the likelihood ratio test which rejects \mathcal{H}_0 in favor of \mathcal{H}_1

$$L(\mathbf{y}_1, \dots, \mathbf{y}_K) \geq \xi_\alpha \tag{2.88}$$

when

$$\Pr\left\{L(\mathbf{y}_1, \dots, \mathbf{y}_K) \geq \xi_\alpha | \mathcal{H}_0\right\} = \alpha \tag{2.89}$$

is the most powerful test with a given size α and its corresponding threshold ξ_α . The α is the probability of detecting the actual hypothesis \mathcal{H}_0 mistakenly as \mathcal{H}_1 , thus the PFA. Removing all the constants in (2.86), the optimal Neyman-Pearson based detection can be expressed as

$$\Lambda_{\text{opt.}} = \sum_{k=1}^K \frac{\eta_k^2 \|\mathbf{y}_k\|^2}{\sigma_k^2 (\sigma_k^2 + \eta_k^2)} \underset{\mathcal{H}_0}{\overset{\mathcal{H}_1}{\geq}} \gamma_{\text{opt.}} \tag{2.90}$$

It should be noted that when $K = 1$, it is reduced to the signal-node EGD, which is also Neyman-Pearson test based on the analysis in (2.88).

2.11.2 Hard Combination

The optimal cooperative detection requires the *a priori* knowledge of the signal powers received on each sensing nodes, which is difficult to be obtain in practical applications. A paradox arising in the optimal detection is that if the cognitive radio network hasn't identify whether the interested signal is existing or not, how can it know the SNRs of the signal on each sensing nodes? Besides, it is very difficult to accurately estimate the SNR when the SNR itself is low[58]. Another limitation on the optimal cooperative detection is that the complete detection metrics from different sensing nodes need to be send to a fusion center for combination as (2.90), which may result in a large amount of data traffic.

A much simpler form of cooperative detection for practical application is that each sensing node makes their own decision and send only the one-bit result to the fusion center in which the hard combination is performed for making the final decision. The typical hard combination are based on the *AND*, *OR* and *voting* rules.

Assume $\bar{\Lambda}_k$ is the local decision made by sensing node k , which is either 1 or 0 for the result detected or not detected. The *AND* rule decides the interested signal is detected, thus \mathcal{H}_1 , when

$$\sum_{k=1}^K \bar{\Lambda}_k = K. \quad (2.91)$$

The *OR* rule decides \mathcal{H}_1 when

$$\sum_{k=1}^K \bar{\Lambda}_k \geq 1. \quad (2.92)$$

Both *AND* and *OR* rules are actually the special cases of the *voting* rule, which decides \mathcal{H}_1 only when at least M out of the K sensing nodes report that the interested signal is detected:

$$\sum_{k=1}^K \bar{\Lambda}_k \geq M. \quad (2.93)$$

2.12 CONCLUDING REMARKS

Signal detection is the basic form of spectrum sensing. It is also the foundation of the signal classification and cyclostationary signature extraction and decoding presented in later contents of this thesis.

In this chapter, the key algorithms of the major signal detection methods are summarized with concise formulation of their detection metrics and thresholds. Besides, two new detection methods

using frequency-domain processing are proposed. They are a blind detection named PSWD-AG and another non-blind detection named PSWD-SM which takes the PSD of the interested signal as a known template. It is proved that the proposed PSWD-SM is actually equivalent to CVWD-EC and MFD-EG detections which use time-domain processing. However, the proposed ones have the advantage that the imperfections of nonwhite noise floor and spurs in practical receivers can be easily mitigated in a more straightforward manner.

Further more, the DIC scheme is proposed in this chapter for eliminating the NU problem which is very harmful to spectrum sensing. The DIC can be applied to nearly all the detection methods introduced in this chapter, which require the knowledge of noise power, thus have dimensions in their detection metrics.

In the next chapter, the simulation performances of these methods for detecting different signals are evaluated and compared under practical conditions such as noise uncertainty, nonwhite noise floor, spurs, clock mismatch and multipath fading channel.

SIMULATIONS OF SIGNAL DETECTION ALGORITHMS

In this chapter, the signal detection algorithms illustrated in Chapter 2 are further evaluated through Monte Carlo simulations. The simulation platform are build on Matlab software with the full implementation of the detection algorithms with the formulation of detection threshold, SNR scaling and statistical testing cycles taken into account. The major interested signal types in the spectrum sensing issue are modeled according to their respective standard specifications emphasizing on the features utilized by different detection algorithms. The algorithms are compared under simulated practical conditions such as Noise Uncertainty (NU), clock mismatch, nonwhite noise floor, spurs, and multipath fading channel.

3.1 MODELING OF SIGNALS

Proper modeling of the target signals is very important to the correct evaluation of spectrum sensing techniques. Hence, before the presentation of simulation performances of various signal detection algorithms, in this section, the modeling methods of the different types of signals are first introduced. Apart from the evaluation of signal detection algorithms using simulation in this chapter, the modeled signals are also applied for validating the signal classifier for TVWS which is presented in Chapter 4. Besides, the modeled signals are also adopted in the experimental tests using real-world signal transmissions, which will be introduced in Chapter 6.

Seven types of signals are modeled for spectrum sensing, they are DVB-T, 3GPP LTE, IEEE 802.22, ECMA-392, Wireless Microphone (WM) and Advanced Television Systems Committee (ATSC) digital TV. The modeling of theses signals conforms their respective standard specifications with all the properties and parameters utilized by spectrum sensing techniques covered, such as CP and DFT lengths in OFDM, structure of pilots, signal bandwidth and sampling rate etc. Reasonable simplification are conducted on other properties and parameters which are irrelevant to the spectrum sensing techniques.

1. *DVB-T*

Based on the DVB-T standard defined in [49], the signal is simulated mainly considering the CP and DFT lengths, the

signal bandwidth and the time-frequency pilot structure with the period of four OFDM symbols which is shown in Figure 8. There are two options of the DFT lengths (2048, 8192) and four options of the CP length ratio ($1/4$, $1/8$, $1/16$, $1/32$) which result totally eight modes of the DVB-T signal. They are all taken into account especially in the proposed signal classifier presented in Chapter 4. The DVB-T signal from real-world TV broadcast is also captured and stored for spectrum sensing tests. It will be shown in Section 6.4 that the signal detection performances for both simulated and captured DVB-T signal are well matched.

2. *3GPP LTE*

The modeling of the LTE signal is based on the 3GPP TS 36.211 standard document [59]. The signal classifier presented in Chapter 4 mainly utilizes the LTE's properties of CP/DFT lengths and the slot period of 0.5 ms. Therefore, the modeling mainly focuses on its frame/slot structure, normal/extended CP lengths, TDD and FDD modes, different bandwidth configurations and their corresponding sampling rates.

3. *IEEE 802.22*

Referencing the IEEE 802.22-2012 standard specification [60], the signal modeling mainly focuses on the CP/DFT lengths in OFDM, the frame structure, different bandwidth configurations and their corresponding sampling rate, which is similar to the modeling of LTE signal.

4. *ECMA-392*

The modeling of ECMA-392 signal focuses on the CP/DFT lengths, bandwidth configurations and the sampling rate defined in [61]. Considering the random bursty behavior due to the CSMA/CA MAC layer, a duty cycle factor is defined for characterizing the signal's occupancy of the channel. As was illustrated in Section 2.9.1.2, the CP-SUM method is suitable for detecting the ECMA-392 signal with random bursty behavior.

5. *WM*

There is no standard definition of WM signal. However, most of the WM devices use analog frequency modulation (FM) and their signal bandwidths are normally less than 200 kHz [62]. Considering the TV channel of 6 or 8 MHz, the signal power of WM is highly concentrated in frequency domain. There are two reported methods for modeling the WM signal. The first one takes sinusoid tone as audio signal source for the frequency

modulation, which is proposed by IEEE 802.22 WRAN working group in [62]. There are three operating situations with different input audio signal characteristics defined in this method, the sinusoid frequencies and the FM deviation of these situations are listed in Table 2. In the second method, the audio signal source is modeled more accurately using the colored noise generated by passing white noise through a circuit described in [63]. In this thesis, the second method is adopted. The FM deviation of 32.6 kHz in the loud speaker situation shown in Table 2 is mainly considered, since it characterizes the highest bandwidth of the FM signal which leads to a worst case evaluation of the sensing performance. This fact was previously revealed in [64, 65].

6. *ATSC* The modeling of ATSC [66] signal focuses on its PSD shape which is utilized in CVWD and PSWD investigated in this thesis. The pilot tones at 309440.6 Hz and 328843.6 Hz from the edge of 6 MHz TV channel and modeled which become a unique feature of its PSD.

Table 2: Operating Situations of WM Signal

Situation	Sinusoid Frequency	FM Deviation
Silent	32 kHz	5 kHz
Soft Speaker	3.9 kHz	15 kHz
Loud Speaker	13.4 kHz	32.6 kHz

3.2 SIMULATED RESULTS

3.2.1 *The Noise Uncertainty Problem in MFD-EG and PSWD*

As is illustrated in Section 2.10.1, due to the practical reasons, the noise power in receiver cannot be exactly known resulting the NU problem which is harmful to spectrum sensing. It is analyzed in Section 2.10.1.1 that the EGD is lack of the unlimited delectability when the NU is presented, which causes the “SNR wall” phenomenon making the detection in lower SNR regime impossible no matter how the observation time is increased.

In this section, the detections of the the WM and ATSC signals with NU are evaluated. The MFD-EG detection’s performances for WM signal is presented in Figure 10, which is essentially the energy detection after matched filtering. The NU is modeled with the “robust

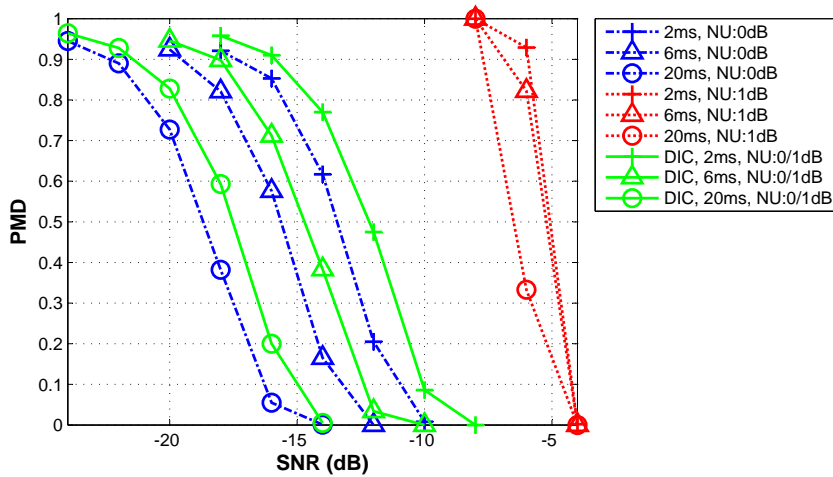


Figure 10: Performance of MFD-EG detecting WM signal (loud speaker mode) with NU for different observation time, signal bandwidth: 200 kHz, sampling rate: 500 k/s, passband of the matched filter: 200 kHz, PFA: 0.01, flat fading

statistic” methods presented in [52], in which the upper limit of noise power is used to calculate the PFA while the lower limit is used to calculate the PMD. Hence, the worst-case evaluation of the impact of NU can be modeled. The WM is modeled in the loud speaker mode introduced in Section 3.1. Figure 10 clearly shows the “SNR wall” at about -6 dB which prevents the improvement of detection performance even when observation time is increased to tenfold. This result confirmed the reported result presented in [52]. However, when the Dimension Cancellation (DIC) is enabled, the SNR wall phenomenon is eliminated although the detection performances become a little worse than the detection without DIC and NU. It should be noticed that using DIC, the detection performances with or without NU are actually the same, which indicates the complete mitigation of NU problem.

For detecting ATSC signal using the proposed PSWD methods, the similar results as for detecting WM can be obtained, which is shown in Figure 11. The PSD of ATSC signal is taken as template in PSWD-SM. When DIC is enabled, the PSWD-SM becomes insensitive to NU. It shows that the blind PSWD-AG is inherently insensitive to NU and requires no *a priori* information, however the performance is worse than the non-blind PSWD-SM.

3.2.2 Comparison of the PSWD and CVWD

The CVWD-CAV, CVWD-MME and PSWD-AG are all blind detections based on testing the whiteness of received signal but in different

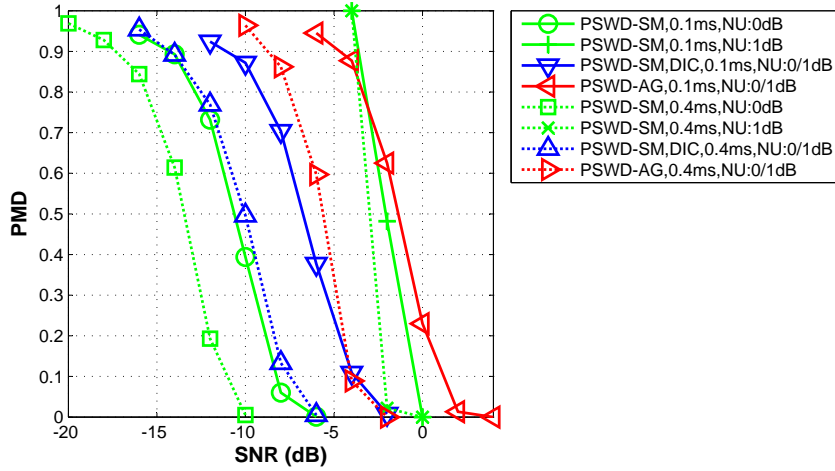


Figure 11: Performance of PSDW detecting ATSC signal with NU for different observation time, bandwidth: 6 MHz, $N_{DFT} = 64$, $D = 32$, PFA: 0.01, flat fading

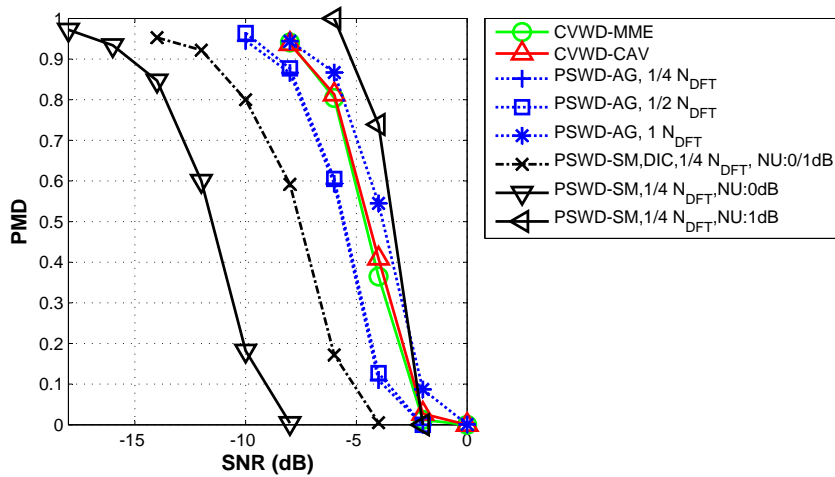


Figure 12: Comparison of CVWD and PSDW with different shifting steps D for detecting DVB-T signal (any mode), bandwidth: 8 MHz, $D = 16, 32, 64$, $N_{DFT} = 64$, CM size: 32, observation time: 0.125 ms, PFA: 0.01, flat fading

approaches. In Figure 12, the detection performances on DVB-T signal using CVWDs and PSWDs are compared in several different aspects. First, similar performances are achieved by the blind CVWD-CAV, CVWD-MME and PSWD-AG methods. Second, when the shifting step D is reduced to a half or a quarter of the DFT size, an obvious performance improvement can be achieved thanks to the increase of Equivalent Degree of Freedom (EDF) in PSD estimation illustrated in (2.35). Third, the PSWD-SM using the PSD of the DVB-T signal as template has better performance than the blind detections, however, it is susceptible to NU which is shown in Figure 12 and also in Figure 11. Figure 12 shows that when DIC is enabled, the PSWD-SM becomes unsusceptible to NU.

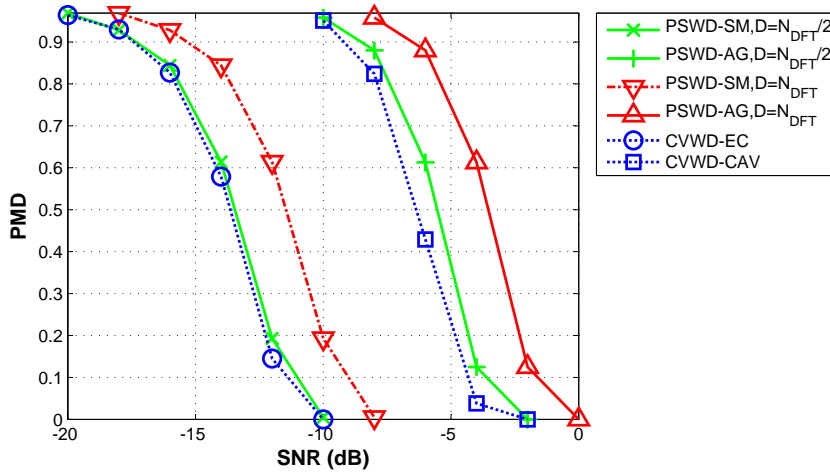


Figure 13: Comparison of CVWD and PSWD with different shifting steps for detecting ATSC signal, bandwidth: 6 MHz, $N_{DFT} = 64$, $D = 32, 64$, CM size: 32, observation time: 0.4 ms, PFA: 0.01, flat fading

It is proved analytically in Section 2.7 that the CVWD-EC (without SNR knowledge), PSWD-SM and MFD-EG are actually equivalent to each other. Figure 13 confirmed this fact by showing very similar performance of CVWD-EC and PSWD-SM for detection ATSC signal. The PSWD-SM and MFD-EG for detecting WM signal in both “silent” and “loud speaker” situations have also the similar performances, which is shown in Figure 14.

It is illustrated in (2.35) and (2.36) that the estimation variance of PSD can be reduced and the detection performance can be improved through increasing the EDF of estimate by reducing shifting step D . Figure 12 and Figure 13 show that when the shifting step D in PSD estimation becomes a half of the DFT size, notable performance gain can be obtained over the case when $D = N_{DFT}$. However, the gain by further decreasing the shifting step to $D = N_{DFT}/4$ becomes marginal. The notable performance improvement when $D = N_{DFT}/2$ can be

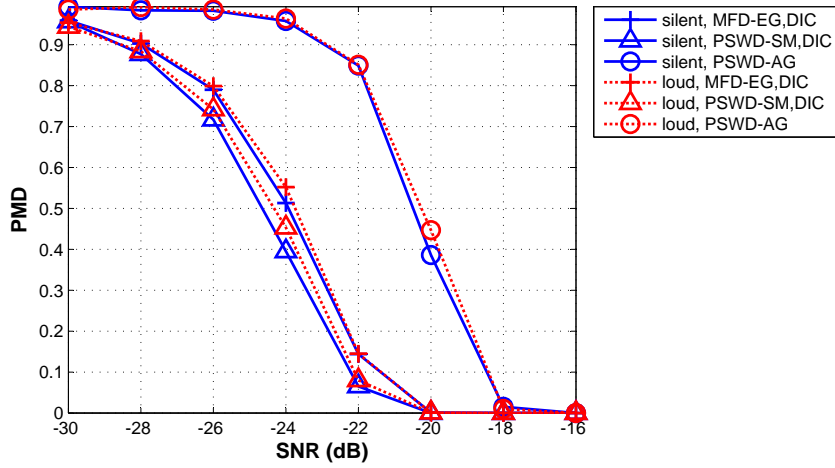


Figure 14: Comparison of PSWD and CVWD for detecting WM signal, bandwidth: 8 MHz, $N_{DFT} = 64$, $D = 32$, CM size: 32, observation time: 1 ms, PFA: 0.01

explained by the increase of the EDF in PSD estimation by about 34% calculated using (2.35). However, the gain by further decreasing D becomes very limited, for example, the increase of EDF by reducing D from $N_{DFT}/2$ to $N_{DFT}/4$ is only 8.5%.

3.2.3 Equalization of Nonwhite Noise Floor and Removal of Spurs

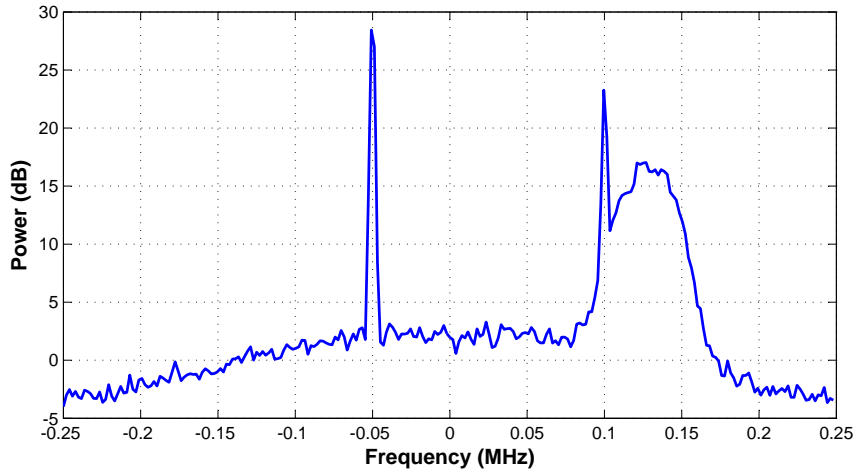


Figure 15: PSD of WM signal with nonwhite noise floor and spurs, sampling rate: 500 k/s, signal carrier: 125kHz, receiver impulse response [1, 0.3], spur frequency: 100kHz & -50kHz, powers of the spurs: 0dB & 4.8dB over noise power

As was illustrated in Section 2.6, the proposed PSWD methods has the advantage of mitigating the nonwhite noise floor and spurs in practical receivers straightforwardly. Simulation results of detecting WM signal with a nonwhite noise floor and two spurs are presented in this sections, the PSD of which is shown in Figure 15.

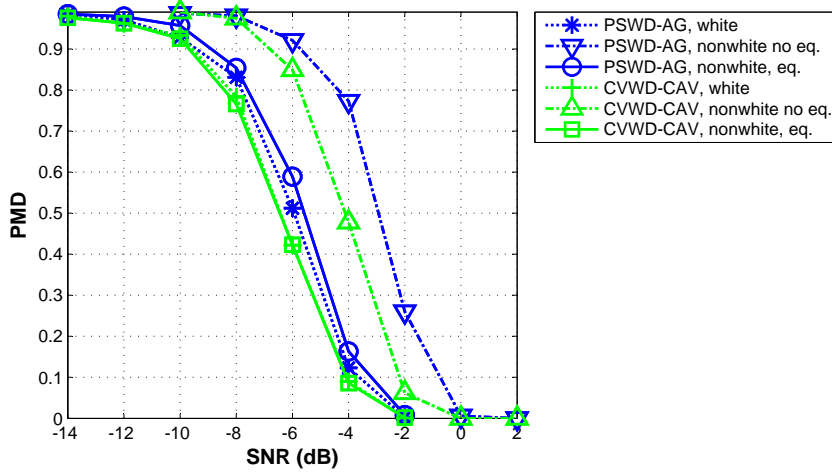


Figure 16: PMD of PSWD-AG and CVWD-CAV for detecting WM signal (loud speaker mode) with nonwhite noise floor, bandwidth: 200 kHz, sampling rate: 500 k/s, $N_{\text{DFT}} = 64$, $D = 32$, CM size: 32, observation time: 0.2 ms, PFA: 0.01, flat fading

It is illustrated in (2.37) and (2.24) that the nonwhite noise floor can be equalized in both PSWD and CVWD methods. Figure 16 shows that in the blind PSWD-AG and CVWD-CAV detection, the nonwhite noise floor can degrade the performance notably. However, when equalization in time or frequency domains is applied, the performance can be recovered to about the same level as the ideal case when noise floor is white.

In PSWD methods, the destruction from spurs to detection performance can be straightforwardly removed as illustrated in Section 2.6.1. Figure 17 shows that when the spurs are presented, the CVWD-CAV detection becomes completely failed. With the removal of spurs in frequency domain, the PSWD-AG's detection performance is only slightly worse than the ideal case when there is no spur.

3.2.4 PSWD in Multipath Channel

The detection performances of PSWD methods for detecting ATSC and DVB-T signals in multipath channels are presented in Figure 18 and Figure 19 respectively. The channel models used here are the IEEE 802.22 WRAN Type B channel defined in [67] and the COST 207 bad urban channel with 12 taps (COST207BUx12) defined in [68].

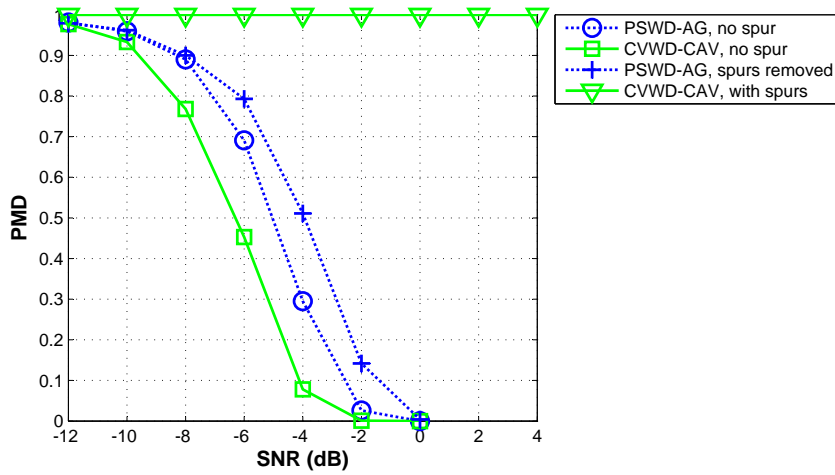


Figure 17: PMD of PSWD-AG and CVWD-CAV for detecting WM signal (loud speaker mode) with spurs, bandwidth: 200 kHz, sampling rate: 500 k/s, $N_{DFT} = 64$, $D = 32$, CM size: 32, observation time: 0.2 ms, PFA: 0.01, flat fading

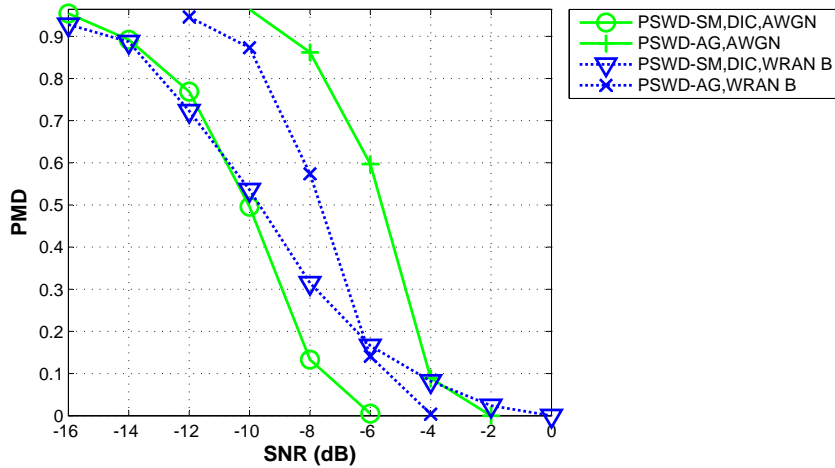


Figure 18: Performance of PSWD detecting ATSC signal in multipath channel (IEEE 802.22 WRAN Type B), bandwidth: 6 MHz, $N_{DFT} = 64$, $D = 32$, observation time: 0.4ms, PFA: 0.01

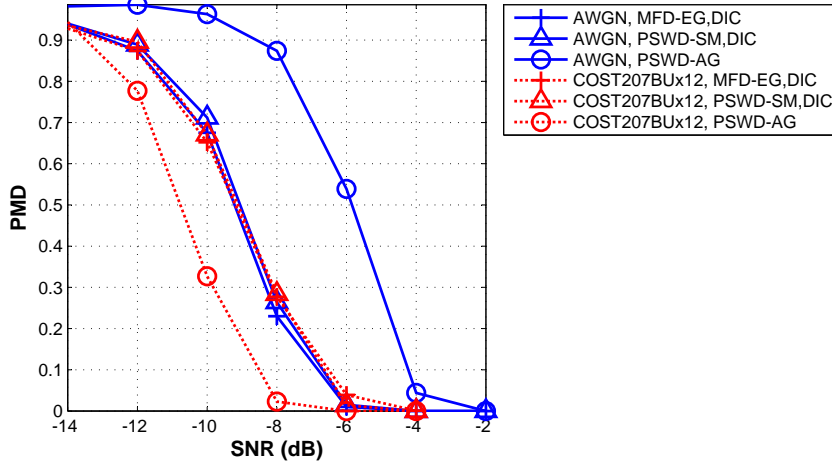


Figure 19: Performance of PSWD detecting DVB-T signal in multipath channel (COST207BU_{x12}), bandwidth: 8 MHz, $N_{\text{DFT}} = 64$, $D = 32$, CM size: 32, observation time: 1 ms, PFA: 0.01

It is shown that the blind PSWD-AG detection can even perform better in multipath channel than in AWGN channel. This is because that the nonwhiteness of the target signal is actually strengthened by the frequency selective fading caused by multipath channel. It is also shown in Figure 19 that the PSWD-SM and MFD-EG methods have the same detection performances, which confirms their equivalence proved analytically in Section 2.7.

3.2.5 FSA and CP Based Detections with Noise Uncertainty

In previous sections of this chapter, the effectiveness of using DIC to mitigate the NU problem for the three similar template based detections (MFD-EG, CVWD-EC and PSWD-SM) is already shown. The simulation results of them are presented in Figure 10, Figure 11 and Figure 12.

The proposed DIC scheme is also effective to the autocorrelation based FSA and CP detection algorithms. Their performances for detecting DVB-T signals with DIC are simulated and presented in this section. The NU is modeled with the “robust statistic” methods presented in [52] for giving worst-case evaluations. It is shown in Figure 20 that without DIC, the detection performances can be notably decreased by 1 dB NU for all the four detection methods. The advantage of using DIC is clearly revealed in Figure 20 that the performances of all the autocorrelation based detections become insensitive to NU. Meanwhile, it is worth to mention that DIC causes

nearly no degradation to detection performances comparing with the ideal case when there is no NU.

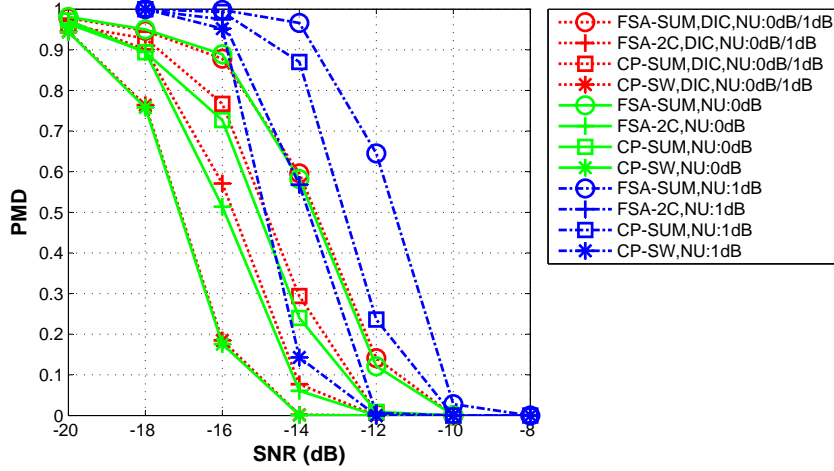


Figure 20: Using DIC to mitigate NU for FSA and CP based detections on DVB-T signal (2K, 1/4 CP mode), observation time: 10 ms, PFA: 0.01

3.2.6 The Influence of CP length on FSA and CP based Detections

In Figure 21 it is shown that the performances of CP based detections are very dependent on the length of CP. Thus, the larger the CP length, the better detection performance can be achieved. On the contrary, the FSA detections are not insensitive to CP ratio, which is a favorable property that the detection performances for different CP length are nearly identical.

3.2.7 The Influence of Multipath Channel on FSA and CP based Detections

The performances of FSA and CP detections in multipath channels are shown in Figure 22. The channel models used here are the IEEE 802.22 WRAN Type B channel profile defined in [67] and the rayleigh channel profile defined in DVB-T standard [49]. It shows that the detection performances of these two types of autocorrelation based methods are not sensitive to multipath fading.

3.2.8 Enhance CP-SW Detection with Pre-alignment

In some standards, such as the LTE and the IEEE 802.22, although the signal has the periodical frame structure, the OFDM symbols in

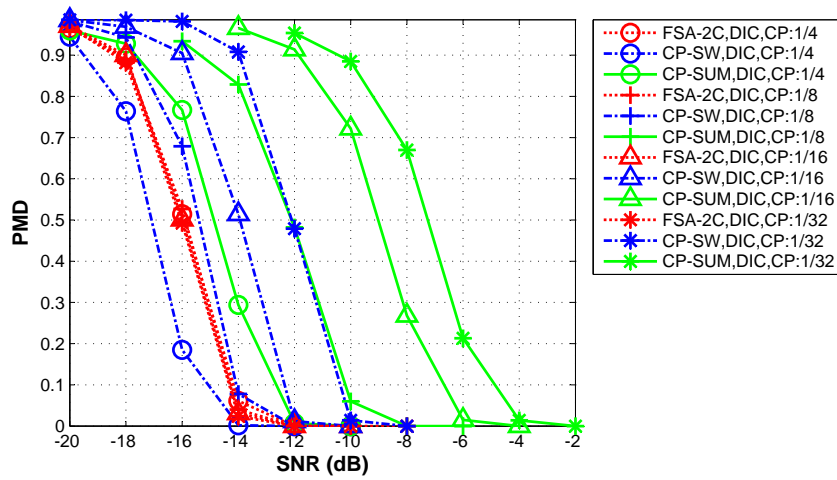


Figure 21: The influence of CP length on FSA and CP based detections of DVB-T signal (2K, 1/4 1/32 CP modes), observation time: 10 ms, PFA: 0.01

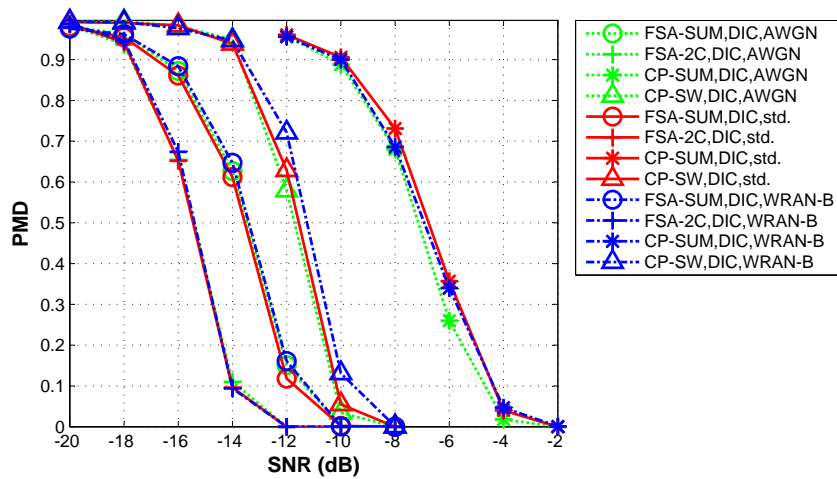


Figure 22: The influence of multipath channel (DVB-T standard defined and IEEE 802.22 WRAN Type B) on FSA and CP based detections of DVB-T signal (2K, 1/32 CP mode), observation time: 10 ms, PFA: 0.01

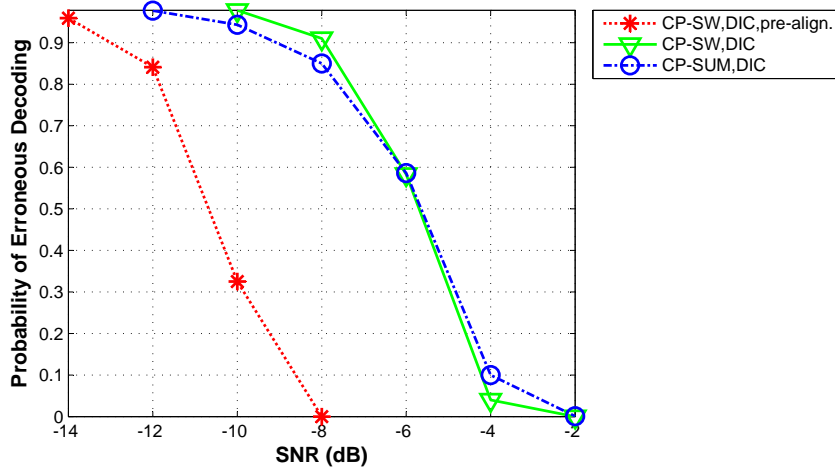


Figure 23: Performance of CP-SW method for detecting TD-LTE downlink (5 MHz, normal CP length, uplink-downlink config: 5) with and without pre-alignment, observation time: 20 ms, pre-alignment length: 0.5 ms (1 slot), PFA: 0.01

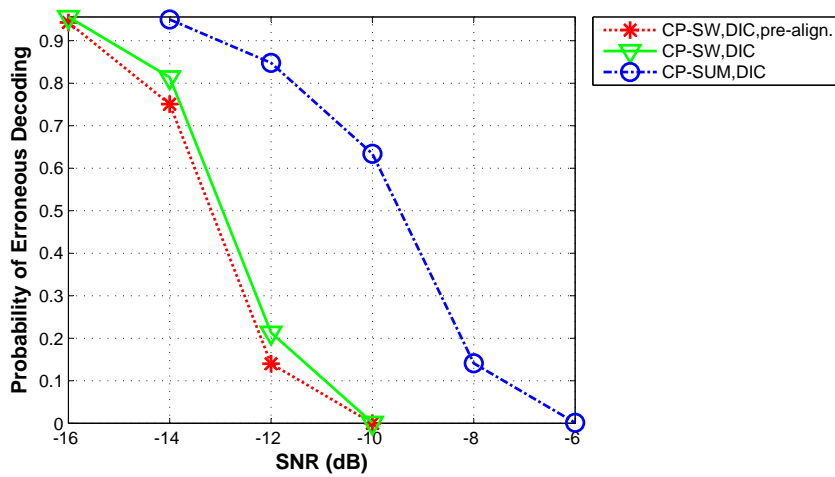


Figure 24: Performance of CP-SW method for detecting 802.22 downlink (8 MHz, 1/16 CP length) with and without pre-alignment, observation time: 20 ms, pre-alignment length: 10 ms (1 TDD frame), PFA: 0.01

one frame are however not completely periodically and continuously transmitted, which makes the CP-SW detection not applicable to these standards. In Section 2.9.1.1, a method is proposed which can enable the CP-SW detection by pre-aligning the autocorrelation with frame period (2.67). The performances of detecting TD-LTE and IEEE 802.22 signals with CP based detections are simulated and presented in Figure 23 and Figure 24 respectively. The gain of applying the pre-alignment is clearly shown in the result, especially for detecting the TD-LTE signal. Figure 24 shows that for the CP-SW detection of the 802.22 signal, the gain of applying pre-alignment is limited. This is because there are only two 10 ms TDD frames in the observation time of 20 ms so the alignment of CP in (2.65) can still be maintained to some extent even without the pre-alignment according to TDD frames.

3.2.9 CP based Detections of ECMA-392 Signal

Differs from the OFDM symbols' periodical structures in DVB-T, LTE and IEEE 802.22, the ECMA-392 has the random bursty signal structure due to its CSMA/CA MAC layer. Since there is no strong periodicity in ECMA-392 signal, the CP-SW detection which relies on the periodicity of OFDM symbols may perform worse than the CP-SUM detection. In this simulation, the ECMA-392 signal is characterized by the randomly presence of bursts with certain duty cycle. The detection performances with different duty cycles are presented in Figure 25. It shows that when the duty cycle is low, the performance of CP-SUM can be even better than the CP-SW detection.

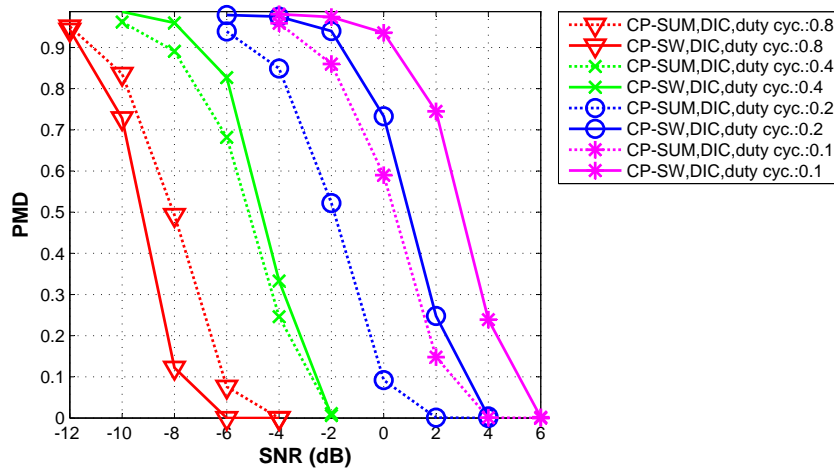


Figure 25: Performance of CP based detections on ECMA-392 Signal (8MHz, 1/16 CP mode) with different duty cycles, observation time: 10 ms, PFA: 0.01

3.2.10 The Influence of CFO

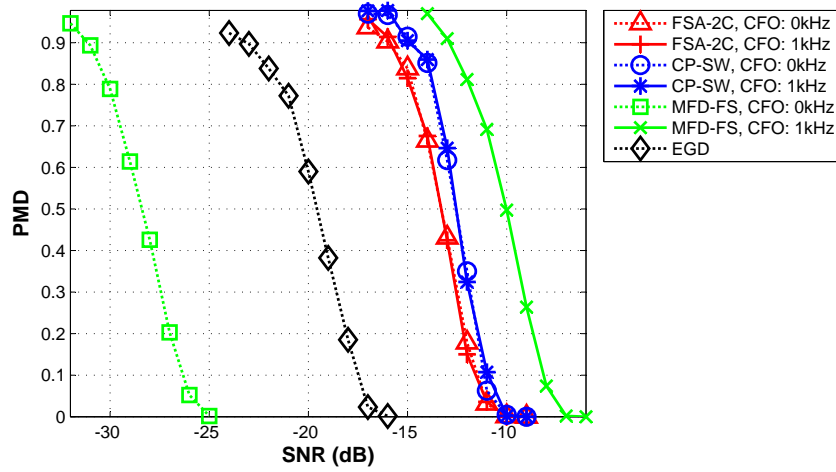


Figure 26: Performances of FSA-2C, CP-SW and MFD-FS detecting DVB-T signal (2K, 1/16 CP mode) with CFO, observation time: 4.8 ms, PFA: 0.01

Figure 26 presents the detection performances of FSA-2C, CP-SW and MFD-FS for DVB-T signal with Carrier Frequency Offset (CFO). The feature sequence used in MFD-FS is the time domain response of the pilots in DVB-T signal. It shows that the cross-correlation based MFD-FS is very vulnerable to CFO. It can be explained by that the phase rotation along the time caused by CFO can destruct the cross-correlation in time domain. In frequency domain, this phenomenon can be translated into the mismatch of the local filter which is intended to match the frequency response of the feature sequence, as the result of CFO. Figure 26 also shows that the autocorrelation based FSA-2C and CP-SW are insensitive to CFO at all. This can be explained by that the phase rotation along time caused by CFO is converted into a constant phase shift after autocorrelation. Since only the amplitude of the autocorrelation values are taken as detection metrics, which is irrelevant to the phase shift, the detection performance is not affected by CFO.

3.2.11 The Influence of SFO

Figure 27 shows that the detection performance of FSA-2C can be degraded notably by Sampling Frequency Offset (SFO), especially when observation time becomes longer. The CP-SW detection is not sensitive to SFO. This can be explained by that the FSA-2C utilizes the autocorrelation R_k^L with large time lag factor k in (2.70). Since

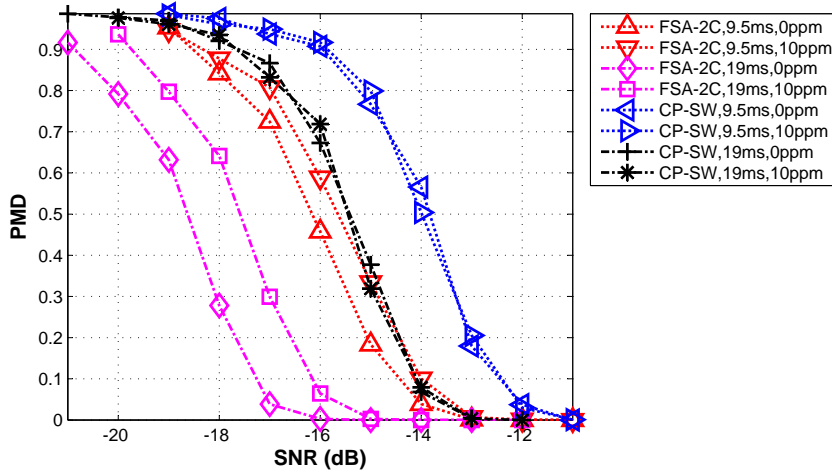


Figure 27: Performances of FSA-2C and CP-SW methods detecting DVB-T signal (2K, 1/16 CP mode) with SFO, PFA: 0.01

the effect of SFO is the accumulated sampling location error along with the increase of time, when the time lag becomes large, the autocorrelation property can be destructed obviously by this error. The CP-SW detection utilizes the autocorrelation with time lag of the DFT length of OFDM modulation, which is much smaller than that of the FSA-2C detection. Therefore, the performance of it is not sensitive to SFO.

3.3 CONCLUDING REMARKS

In this chapter, the signal detection algorithms illustrated in Chapter 2 are evaluated using computer simulations. The signals involved in simulation tests are DVB-T, WM, 3GPP LTE, IEEE 802.22 and ECMA-392, which covers the major PU and SU signals in TV band. The conclusions regarding the performances of the evaluated detection algorithms are drawn as follows:

- The proposed DIC method can effectively mitigate the NU problem and can be applied to all the detection algorithms which have dimensions in their detection metrics. Notably, for autocorrelation based detection, such as CP-SUM, CP-SW, FSA-SUM and FSA-2C, the DIC causes nearly no degradation to detection performances.
- The proposed PSWD methods using frequency domain processing have very similar performance to CVWD using time domain processing. However, the PSWD methods can mitigate the nonwhite noise floor and spurs in practical receivers more easily comparing with CVWD.

- If the time-frequency structure of the signal is known to the detector. The FSA and CP based detections utilizing autocorrelation are more favorable in terms of robustness against multipath fading, insensitivity to clock mismatch and there is nearly no degradation to detection performance when DIC is applied.

The simulation analysis of the detection algorithms provides important insights for the design of the signal classification framework in Chapter 4 and facilitates the implementation of the spectrum sensing testbed presented in Chapter 6.

THE CLASSIFICATION FRAMEWORK BASED ON SIGNAL DETECTION

4.1 INTRODUCTION

In Chapter 2 and Chapter 3, we investigated the major signal detection methods and presented our proposed PSD algorithms as well as the Dimension Cancellation (DIC) method for mitigating the Noise Uncertainty (NU) problem which is applicable to nearly all the detection methods. The reported studies on spectrum sensing pay most of the attentions to signal detection problem which is mainly motivated by the regulators' stringed requirements on protecting the legacy TV broadcast users as the necessary condition of opening TV band for secondary Dynamic Spectrum Access (DSA).

Due to the continuing innovations in new technologies and new business models, it is expected that numerous heterogeneous systems will share the same spectrum resources in the future [13, 14]. For example, apart from the primary TV broadcast, some of the other technologies or standards, such as IEEE 802.22[60], IEEE 802.11af[69], ECMA-392[61], LTE[59] and cognitive Programme Making and Special Events (PMSE)[70] are targeted at exploiting the TV band White Space (TVWS) for providing new services. As a result, the challenge arising is not only to protect the legacy PU, but also to optimize the coordination and coexistence among different devices and networks, especially heterogeneous ones. In this context, in addition to the detection of PU's signal, it is also desired to use spectrum sensing for acquiring knowledge on other coexisting networks or devices. For this purpose, based on the study on signal detection in Chapter 2 and Chapter 3, we propose a signal classification framework with the robust implementation aiming at the major primary and secondary standards coexisting in TV band.

We first review the representative signal classification schemes for spectrum sensing reported in literatures. In [71, 72, 73], the authors mainly focus on the classification based on signal's PSD shape. The Guard Interval (GI) with CP is taken into account for classifying OFDM signals with similar PSD shapes. Most of the targeted signals are actually not coexisting in the same frequency band, such as UMTS, DVB-S, HiperLAN and IS-95. In [40, 74, 75, 76], classification schemes for OFDM signals are proposed which are based on the analysis of their cyclostationarity. Only the general signal models are

discussed in these studies and the classification of standard-specific signals is not considered. In [77], a classifier for LTE and WiMax is proposed based on detailed analysis of the cyclostationary features from both CP and pilot sub-carriers.

The reported studies on signal classification for CR have shown great interest in OFDM since it is becoming the dominant modulation scheme in today's communication and broadcast standards. Most of the standards in TV band are based on OFDM, such as DVB-T, IEEE 802.22, IEEE 802.11af, ECMA-392 and LTE. Comparing with the reported studies, the classification scheme proposed in this thesis covers the major standard in TV band for the first time. Besides, the robustness in real-world implementation is emphasized in the design of the classifier and further validated in real-world experiment which will be presented in Chapter 6.

4.2 PROBLEM FORMULATION

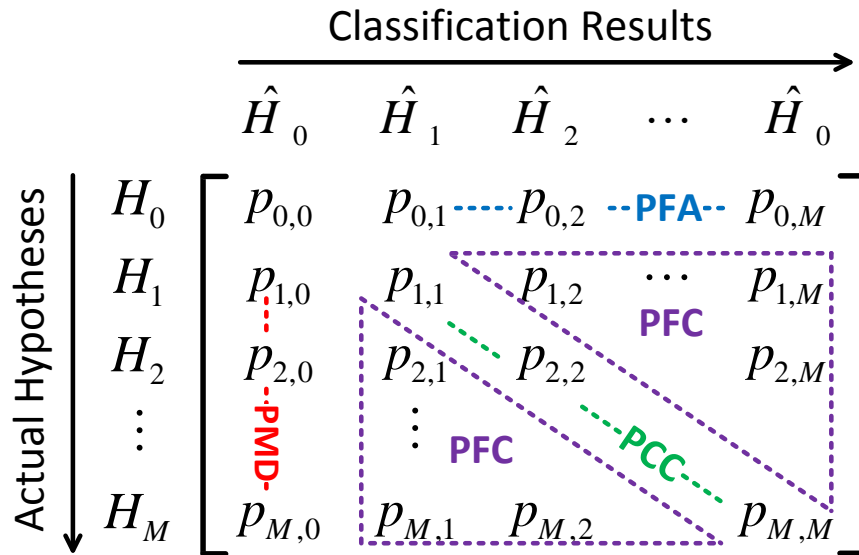


Figure 28: Transmission probability matrix from actual hypotheses to classification results in signal classification

The signal classification is essentially based on and extended from the signal detection algorithms which are presented in Chapter 2 and Chapter 3. Assume there are M classes of interested signal types which need to be classified and only one type of signal is presented in the measured channel. The goal of the classification is to decide correctly which type of signal is actually presented in the channel. We define the hypothesis \mathcal{H}_0 being the case when no signal is presented, which is the same as in the signal detection problem. The hypotheses

\mathcal{H}_m ($m = 1, 2, \dots, M$) are defined for the cases when the signal type m is presented. The transition probabilities from the actual hypotheses to the classification results can be denoted in matrix form as shown in Figure 28. The row numbers of the matrix denote the actual presented signal's types while the column numbers of the matrix denote the resulted signal types by classification. Obviously, the matrix of transition probability for ideal signal classification should be an identity matrix \mathbf{I} .

The following probabilities and the specific requirements on them in signal classification problem are defined based on the matrix of transmission probability:

- Probability of False Alarm (PFA):

$$P_{\text{FA}} = \sum_{m=1}^M p_{0,m}. \quad (4.1)$$

The P_{FA} is predefined according to the user's requirement. It should be insensitive to NU, which can be achieved using the DIC method proposed in Section 2.10 for signal detection.

- Probability of Correct Classification (PCC) of signal type n :

$$P_{\text{CC}}^n = p_{n,n} \quad n > 0. \quad (4.2)$$

The P_{CC}^n should be as large as possible for achieving accurate classification. Particularly, the Primary User (PU) signals such as DVB-T normally needs to be more stringently protected. Thus, they need to be detected and correctly classified at lower SNR comparing with other secondary unlicensed signals. Therefore, more robust detection methods should be taken into account for them.

- Probability of False Classification (PFC) of signal type n :

$$P_{\text{FC}}^n = \sum_{m>0, m \neq n} p_{n,m} \quad n > 0. \quad (4.3)$$

The P_{FC}^n characterizes the ambiguity of falsely classifying signal type n as other types, which should be minimized. It is worth to mention that although the classification of the signal is false, it still means that the presence of the signal is detected.

- Probability of Mis-Detection (PMD) of signal type n :

$$P_{\text{MD}}^n = p_{n,0} = 1 - P_{\text{CC}}^n - P_{\text{FC}}^n \quad n > 0. \quad (4.4)$$

When the presented signal is neither correctly nor falsely classified, the mis-detection occurs, which should also be minimized, especially for PU's signal at low SNR.

- Probability of Correct Classification when Detected (PCCD) of signal n :

$$P_{\text{CCD}}^n = \frac{p_{n,n}}{\sum_{m>0} p_{n,m}} = \frac{P_{\text{CC}}^n}{P_{\text{CC}}^n + P_{\text{FC}}^n} = \frac{P_{\text{CC}}^n}{1 - P_{\text{MD}}}, n > 0. \quad (4.5)$$

The PCCD is the probability of correct classification of the signal on condition that the signal is already detected. Comparing with PCC, PCCD only characterizes the accuracy of differentiating among the interested signals without considering the hypothesis \mathcal{H}_0 .

4.3 TARGET SIGNALS IN TVWS AND THEIR UNIQUE FEATURES

The unique and signal-specific features are utilized by different detection algorithms which makes unmatched signal appears to be like noise. In this way, the classification is achieved by matching the detection algorithms to received signal with properly designed decision rules.

Since the goal of the signal classification is to identify the types or standards of target signals, the signal-specific features are essential to the success of classification. Therefore, the blind detections such as EGD, CVWD-MME/CAV and PSWD-AG, which don't require the known features of the target signals are not applicable to the signal classification. Instead, the detection algorithms utilizing certain unique features of the target signals should be employed. The features of different signals utilized by the detection algorithms illustrated in Section 2 and Section 3 are summarized in Table 3.

Table 3: Signal Features Utilized by the Detection Algorithms

Detection Methods	Utilized Features
PSWD-SM	the shape of PSD
CVWD-EC	the Covariance Matrix (CM)
MFD	the pulse shaping filter or feature sequence
CP-SUM/SW	the CP and DFT length of OFDM signal
FSA-SUM/ $2C$	the repeating period of feature sequence
CSD	the features in spectral-cyclic frequency domain

The major systems operating or will potentially operate in TVWS are considered in the proposed classification scheme. They are:

- DVB-T: digital TV broadcast, licensed PU;
- IEEE 802.22 Wireless Regional Area Network (WRAN): bring low-cost broadband access to hard-to-reach, low population density areas instead of wireline accesses (e.g. DSL, optical fiber);
- ECMA-392: for communications of personal/portable devices, e.g. delivering high-definition (HD) video, campus-wide wireless coverage and interactive TV broadcasting services;
- 3GPP LTE: the 4G cellular and mobile communication standard, may potentially operate in TV white space[78, 79];
- Wireless Microphone (WM): normally analog FM with bandwidth which is less than 200 kHz.

It can be noticed that all the target signals listed above are OFDM-based except the WM signal. These OFDM based standards have similar bandwidths which lead to the similar flat-top PSD shapes. It is shown in Table 4 that DVB-T, IEEE 802.22 and ECMA-392 in 8 MHz mode have almost the same bandwidth of more than 7 MHz, while the LTE has several bandwidth configurations ranging from 1.25 MHz to 20 MHz and the 5 MHz mode suits one TV channel well. The narrowband WM signal has the bandwidth of less than 200 kHz. Therefore, the PSD shape is not a feature which is sufficiently unique for classifying these signal types. Hence, the standard classification scheme proposed in [71, 72] based on PSD shape is not applicable here. The similar conclusion is also drawn in [73] and a more robust classifier utilizing the difference in the guard interval (GI) with CP is proposed in that paper. It is proved in Section 2.7 that the covariance matrix utilized by the CVWD-EC and the pulse shaping filter response utilized by MFD-EG are features similar to PSD, which are therefore also not sufficiently unique for differentiating the OFDM standards.

Table 4: Useful Parameters of the OFDM Based TVWS Standards for Classification

Standards	Bandwidth	Sampling Rate	DFT Size	CP ratio
DVB-T	7.612 MHz	64/7 MS/s	8192, 2048	1/4, 1/8, 1/16, 1/32
802.22 (8MHz mode)	7.178 MHz	9.136 MS/s	2048	1/4, 1/8, 1/16, 1/32
ECMA-392 (8MHz mode)	7.357 MHz	64/7 MS/s	128	1/8, 1/16, 1/32
LTE (5MHz mode)	4.5 MHz	7.68 MS/s	512	long: 1/4; normal: 9/128×6 10/128×1
WM	< 200 kHz	N/A	N/A	N/A

Inspired by the studies in [73, 75, 76, 77], we further explore some other unique features for signal classification in addition to CP. The cross-correlation based MFD-FS detection is very sensitive to CFO as is shown in Figure 26, which is impractical for robust implementation with low-cost hardware. According to the CSD based on SCF analysis, if the OFDM symbols are continuously and periodically transmitted exhibiting cyclostationarity, the CP can generate signatures in SCF at cyclic frequencies n/T_s [18, 19]. The T_s is the length of the OFDM symbol. Apart from this, the listed signals in Table 4 don't have features which can be revealed easily in the estimated SCF. Besides, the CP feature can be more straightforwardly exploited using the time-domain autocorrelation based methods, such as CP-SUM and CP-SW illustrated in Section 2.9.1. The DVB-T signal also has the unique periodical pilot tone structure which is utilized in the FSA detections introduced in Section 2.9.2. It is concluded in Chapter 3 that the autocorrelation based detection has the advantages of insensitivity to clock mismatch and multipath channel. Based on the above analysis, the proposed signal classification scheme mainly adopts the detections based on autocorrelation as the foundation. Some basic parameters of these OFDM standards are listed in Table 4 showing their unique sampling rates, DFT length, CP length, etc., which decides the features at different time lags in autocorrelation.

The other special type of signal is the narrowband WM signal. There is no standard-defined parameters of WM signal. Normally, the signal is Frequency Modulated (FM) with bandwidth which is less than 200 kHz and the carrier frequencies are allocated from channel edge in the step of 25 kHz [80]. Since the narrowband WM signals are normally sparsely distributed in the TV channels, if the signal in the whole channel is received by a wideband receiver, the Peak-to-Average Ratio (PAR) of the estimated PSD is generally larger than the PAR of other OFDM signals' flat-top PSD. For example, considering a 8 MHz TV channel, Figure 29 shows that the PAR of WM's PSD is much larger than the PAR of DVB-T's PSD, when the SNRs of both signal are the same. This property of WM signal can be taken as an unique feature in signal classification.

4.4 THE CLASSIFICATION FRAMEWORK

The proposed classification framework is based the combination of the detection algorithms presented in Section 2. For OFDM based standards, it is concluded in Section 4.3 that the autocorrelation-based CP and FSA detections together with DIC are more robustness against receiver's practical imperfections such as NU, clock mismatching and multipath channel. Besides, Reported studies in [73, 75, 76, 77]

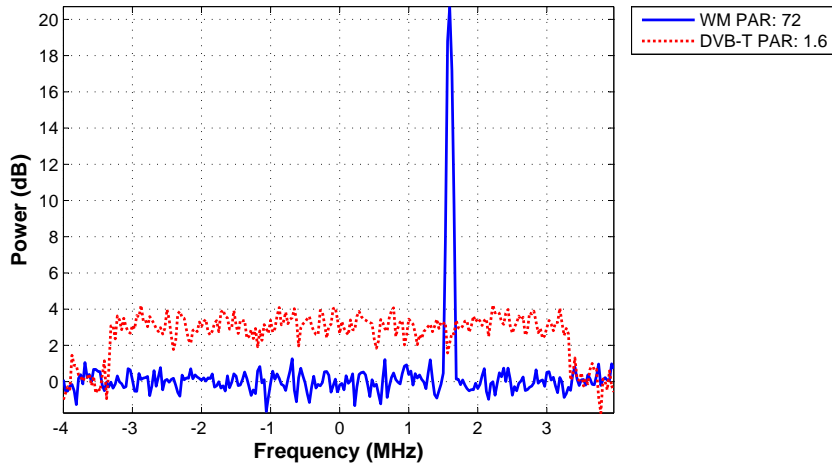
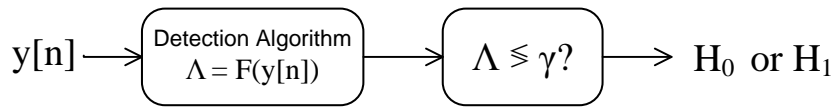


Figure 29: PSDs of WM signal and DVB-T signal showing large difference in PAR, bandwidth; 8 MHz, SNR: 3 dB

shows good uniqueness of CP and Feature Sequence (FS) for signal classification. For the sparsely distributed narrowband WM signal, there is no deterministic features in autocorrelation, however, the PAR of its PSD is generally larger than the flat-top PSDs of the wideband OFDM signals, which can be utilized to classify it.

Signal Detection



Signal Classification

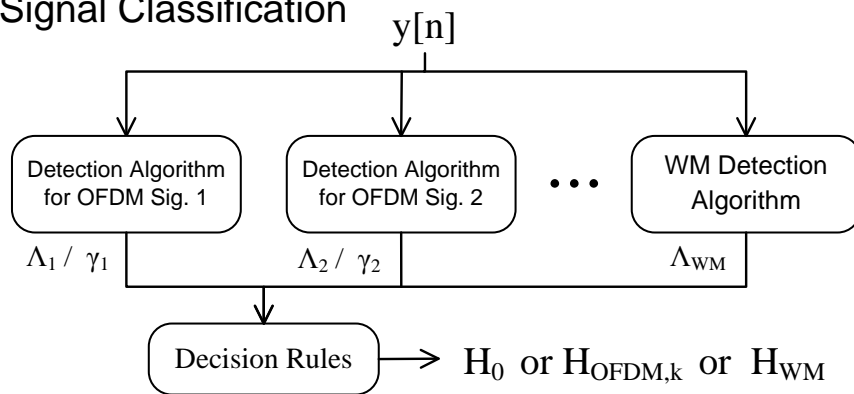


Figure 30: Classification framework based on parallel detection algorithms combined with decision rules

In the proposed classification framework, various feature-based signal detection algorithms are selected based on previous characterization of the signal detection algorithms in terms of robustness, uniqueness and feasibility. These detection algorithms are performed

in parallel on the received signal with deterministic observation time. The resulted detection metrics from different algorithms are analyzed and compared using certain logic rules to decide which standard or type of signal is actually received in the measured channel. The classification framework is depicted intuitively in Figure 30.

Assume Λ_i is the metric of the detection algorithm which matches OFDM signal class i :

$$\Lambda_i = \mathcal{F}_i(y[n]) \quad i = 1, 2, \dots, K. \quad (4.6)$$

The effective classification of the OFDM signals that identifies signal type i from other signal types accurately should satisfy the following condition:

$$\begin{aligned} \Pr\{\Lambda_i | \mathcal{H}_i > \Lambda_i | \mathcal{H}_j\} &= 1 \quad (j \neq i \quad i, j = 1, 2, \dots, K) \\ \text{and} & \\ \Lambda_i | \mathcal{H}_i &> 1. \end{aligned} \quad (4.7)$$

If the featured time lags in OFDM signals' autocorrelation are unique for different signals, the above condition is expected to be well satisfied.

Specially, for classifying WM signal, we utilize its narrowband (< 200 KHz) feature which exhibits sparse distribution and high PAR in estimated power spectrum density (PSD) of the signal in one TV channel. The PAR of the estimated PSD $\hat{Y}[m]$ from (2.32) is calculated as

$$\Phi = \max(\hat{Y}[m]) / \bar{\hat{Y}}, \quad (4.8)$$

in which $\bar{\hat{Y}}$ denotes the mean value of the estimated PSD $\hat{Y}[m]$. This method for detection and classification of narrowband transmissions is also applied in our previous development of the Cognitive Agile Spectrum Testbed (COAST)[81].

Since the targeted OFDM signals may also exhibit high PAR in their PSD if they experience frequency-selective fading, another property called the Degree of Sparsity (DS) is also used together with PAR to classify the WM signal:

$$\Psi = \sum_{\hat{Y}[m] \geq (1+\rho)\bar{\hat{Y}}} m / M \quad (4.9)$$

The detection metric for WM signal is the logic result of if Φ and Ψ are both larger than their respective thresholds:

$$\Lambda_{WM} = (\Phi \geq \phi \quad \text{AND} \quad \Psi \leq \psi), \quad (4.10)$$

which is either 0 or 1.

After the received signal are processed by the detection algorithms resulting detection metrics Λ_i for OFDM class i and Λ_{WM} for WM, the rules in (4.11) are used for deciding which signal occupies the channel (hypotheses $\hat{\mathcal{H}}_{\text{OFDM},k}$, $\hat{\mathcal{H}}_{\text{WM}}$) or the channel is vacant (hypothesis $\hat{\mathcal{H}}_0$). It should be noted that the WM signal is classified as long as the PAR and DS satisfies the condition. Since the different OFDM detection algorithms has different threshold γ_i , we take Λ_i/γ_i as unified metrics with common threshold of 1 for finding the matched algorithm. Because each algorithms is specific to certain standards and mode, one signal can be classified as long as its corresponding algorithm is matched.

$$\begin{aligned} \hat{\mathcal{H}}_{\text{OFDM},k} : k &= \arg \max_i (\Lambda_i/\gamma_i), \quad \Lambda_{\text{WM}} = 0 \text{ and } \max_i (\Lambda_i/\gamma_i) \geq 1 \\ \hat{\mathcal{H}}_{\text{WM}} : \Lambda_{\text{WM}} &= 1 \\ \hat{\mathcal{H}}_0 : \max_i (\Lambda_i/\gamma_i) &< 1 \text{ and } \Lambda_{\text{WM}} = 0 \end{aligned} \quad (4.11)$$

4.5 SIMULATION PERFORMANCES

Table 5: Signal Features and Detection Algorithms Used in Classification

Standards/Types	Algorithms	Utilized Feature
DVB-T	FSA-2C	periodical pilot tone structure in time domain
LTE (5 MHz mode)	CP-SW (pre-align.)	CP and DFT length, slot length
802.22 (8 MHz mode)	CP-SUM	DFT length, indifferent to CP length
ECMA-392 (8 MHz mode)	CP-SUM	DFT length, indifferent to CP length
WM	PAR and DS of PSD	high PAR & low DS in PSD due to narrowband

Table 6: The Target Signals and Modes for Performance Evaluation

Standards/Types	Modes
DVB-T	8 modes: all the CP and DFT lengths
LTE DL (5 MHz mode)	2 modes: TD-LTE (UL/DL conf. 2), long CP and normal CP
802.22 DL (8 MHz mode)	1 mode: 8 MHz, 1/16 CP
ECMA-392 (8 MHz mode)	1 mode: 8 MHz, 1/16 CP, duty cycle: 0.5
WM	1 mode: FM, loud speaker

The selected target signals and their different modes involved in performance evaluation are listed in Table 6, which are fully covered by the selected detection algorithms show in Table 5. For the eight modes of DVB-T signal, the configurations of FSA-2C are different due to the various lengths of CP and DFT. Therefore, eight mode-specific FSA-2C detectors are applied in the implemented classifier.

Similarly, the CP-SW detection also relies on the two different CP length of the LTE signal. Hence, two mode-specific CP-SW detectors are applied. The CP-SUM detection for IEEE 802.22 and ECMA-392 signal rely only on the DFT length and are indifferent to their different CP lengths. Hence, the CP-SUM with one configuration can be applied to all the modes with the same DFT length. It should be noted that the longer the CP length, the better the detection performance can be achieved by CP-SUM and CP-SW as was presented in Section 3.2.6.

Table 7: Transition Probabilities for Classification of DVB-T Signal Using FSA-2C, Observation Time: 20 ms, PFA: 0.0064, SNR: -12 dB
 $\mathcal{H}_{1,2,3,4}$: 8K, 1/4, 1/8, 1/16, 1/32 CP modes,
 $\mathcal{H}_{5,6,7,8}$: 2K, 1/4, 1/8, 1/16, 1/32 CP modes

	$\hat{\mathcal{H}}_1$	$\hat{\mathcal{H}}_2$	$\hat{\mathcal{H}}_3$	$\hat{\mathcal{H}}_4$	$\hat{\mathcal{H}}_5$	$\hat{\mathcal{H}}_6$	$\hat{\mathcal{H}}_7$	$\hat{\mathcal{H}}_8$
\mathcal{H}_1	0.980	0	0	0	0.02	0	0	0
\mathcal{H}_2	0	0.966	0	0	0	0.034	0	0
\mathcal{H}_3	0	0	0.984	0	0	0	0.016	0
\mathcal{H}_4	0	0	0	0.976	0	0	0	0.024
\mathcal{H}_5	0	0	0	0	1	0	0	0
\mathcal{H}_6	0	0	0	0	0	1	0	0
\mathcal{H}_7	0	0	0	0	0	0	1	0
\mathcal{H}_8	0	0	0	0	0	0	0	1

The transition probability matrix in Table 7 shows that for classifying different modes of DVB-T, there are some small ambiguities among the modes with different DFT lengths but the same CP length ratio. This can be explained by that when the CP length ratios are the same, the FS length of the signal in 8K mode is just four times of the signal in 2K mode. Thus the FSA-2C configured for the 8K mode can also detect the signal in 2K mode. However, this ambiguity doesn't affect the classification of DVB-T from other standards. Since the main goal of classification is to recognize the standards of the signal, the different modes of DVB-T are combined into one class in the simulation. Similarly, the TD-LTE signal in both normal CP mode and long CP mode are also combined into one class. Therefore, there are totally five targeted classes of signals as listed in Table 6.

The simulation performances of signal classification are presented in Figure 31 and Figure 32. For each SNR, the actually appeared signal is randomly chosen from the standards and modes listed in Table 6 with equal probabilities. Then the classification is performed following the rules in (4.11) which concludes which class of signal is

received or none is received, thus \mathcal{H}_0 . Figure 31 presents the overall classification performances of all the signal types, which shows that the PCCD is always higher than PCC and for most of the simulated SNRs, the PCCD are one. This means that as long as the existence of the signal is successfully detected, it can be nearly always correctly classified. This is a favorable result showing very small ambiguity among different standards in classification. Figure 32 presents the PCC of each type of signals. It shows that when the SNR is large enough, each class of signal can be perfectly detected and classified. It should be noted that higher robustness at low SNR for classifying the primary signal DVB-T is also achieved.

The signal classification scheme will be further validated using the experiments carried on our spectrum sensing testbed. Good match between the simulated results and experimented results is achieved which will be presented in Section 6.5.

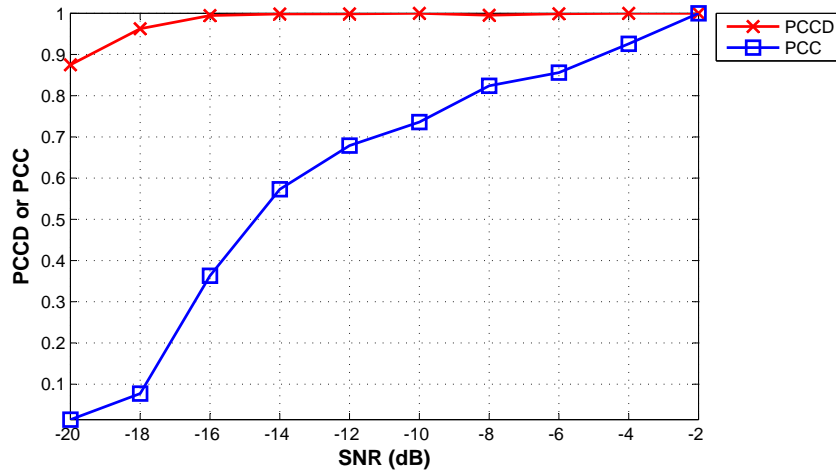


Figure 31: The overall signal classification performances, target signals listed in Table 6, detection algorithms listed in Table 5, observation time: 20 ms, PFA: 0.01

4.6 CONCLUDING REMARKS

Based on the signal detection algorithms and their performance evaluation using simulation presented in Chapter 2 and Chapter 3, a classifier for the signals in TV band is proposed in this chapter.

Section 4.1 illustrates the motivation and application of designing the signal classifier. Due to the continuous emerging of new standards in TV band, the coexistence among heterogeneous networks becomes more and more complex. Then the goal of spectrum sensing is not limited to the detection of the primary TV signal at low

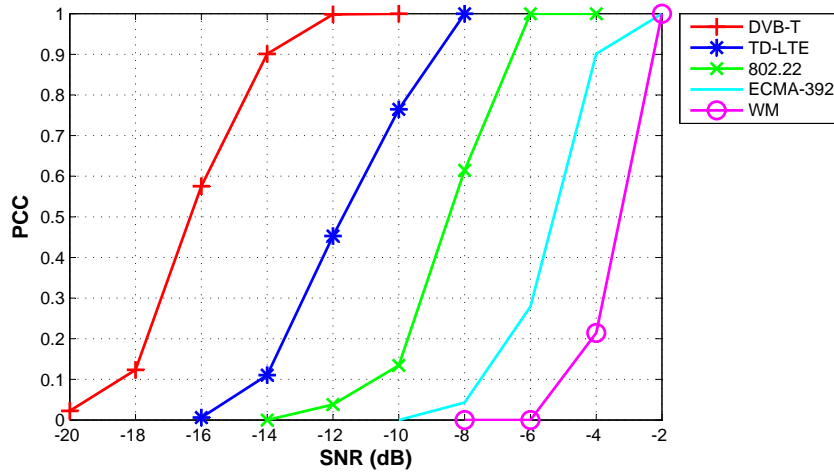


Figure 32: The classification performances of specific signals, target signals: Table 6, detection algorithms: Table 5, observation time: 20 ms, PFA: 0.01

SNR. Meanwhile, the knowledge on other coexisting networks and devices should be also obtained for optimizing the coordination and coexistence among heterogeneous wireless systems. This leads to the demand of developing a versatile signal classifier which is more capable than the single-purposed signal detector.

In Section 4.2, the signal classification problem is clearly formulated based on the transition probability matrix from actual hypotheses to classification results. Extended from the PMD and PFA in the signal detection problem, several other performance indicators are defined. They are the PFC, PCC and PCCD.

Section 4.3 specifies the target signals of DVB-T, TD-LTE, IEEE 802.22, ECMA-392 and WM and summarizes their features which can be utilized in classification. It is concluded that CP and FSA based detections utilizing the unique time lags in autocorrelation are most suitable for classifying the different OFDM-based standards, which are caused by the unique FFT and CP lengths as well as the pilot structure. The WM signal can be classified using the property of higher PAR in the estimated PSD.

The proposed classification framework is illustrated in Section 4.4, which is essentially the combination of various feature based detection algorithms together with a properly designed decision rules. Using this framework, in Section 4.5, simulation tests are performed for classifying the five classes of signals with different modes. The results shows that the proposed scheme can achieve robust classification with small ambiguity among different standards.

In Chapter 6, the further evaluation of the signal classifier with real-world implementation on our sensing testbed will be presented.

ENHANCED SPECTRUM SENSING WITH EMBEDDED CYCLOSTATIONARY SIGNATURES

5.1 INTRODUCTION

Part of the communication and broadcast signals exhibit inherent cyclostationarity due to their periodical structures, such as preamble, pilot, CP, sinusoid carrier and spreading code, etc. In Section 2.8, the Spectrum Correlation Function (SCF) and its normalized version Auto-Coherence Function (ACF) are introduced which are taken as the tools for analyzing signal's cyclostationarity. The examples of the inherent cyclostationary signatures of BPSK and QPSK modulated signals revealed by ACF are shown in Figure 4, Figure 5 and Figure 6 respectively. In Gardner's work [82, 83], the different signatures of BPSK and QPSK are also presented.

If the OFDM symbols are continuously and periodically transmitted, cyclostationary signatures generated from CP can be revealed in SCF and ACF at cyclic frequencies n/T_s [19, 18], in which T_s is the length of the OFDM symbol including the CP segment. Illustrated in Section 2.9.1 and Section 4.3, the feature of CP can be also explored using CP-SUM and CP-MAX detections based on time-domain auto-correlation for detecting or classifying the OFDM based standards. Apart from the inherent signatures from CP, it was proposed in [18, 19, 20, 21] that Embedded Cyclostationary Signature (ECS) can be artificially generated by manipulating the correlation among part of the sub-carriers (SC). As an example, Figure 33 shows the SCF of an OFDM signal exhibiting both of its inherent signatures from CP and an ECS generated by two correlated Signature Sub-Carrier (SSC).

The artificially generated ECS provides much higher flexibility than the signal's inherent signature. As a result, it can open wide possibilities for enhancing the information which can be obtained via spectrum sensing. Extending further from the signal detection and classification with inherent standard-specific features discussed in previous contents, in this chapter, the novel spectrum sensing schemes utilizing the flexible ECS for signal classification and delivering arbitrary extended information are proposed.

According to the multi-carrier signals such as CP-OFDM and OFDM-OQAM, the information bits are coded and modulated on sub-carriers which are orthogonally and compactly allocated in frequency domain. It was proposed in [18, 19, 20, 21] by Sutton and his

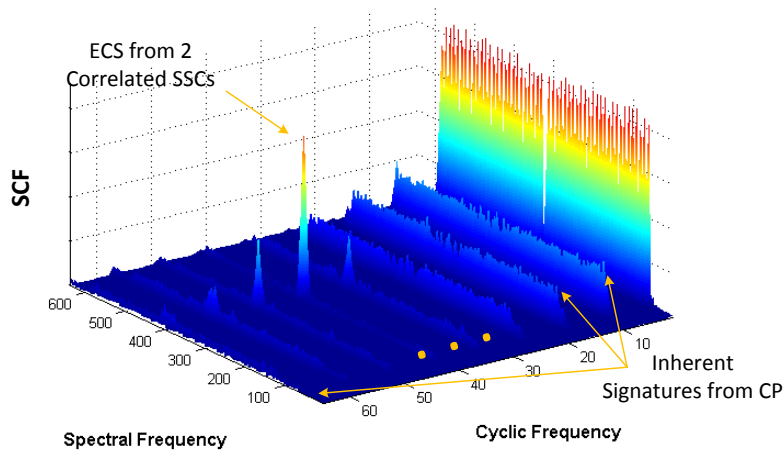


Figure 33: Embedded and inherent cyclostationary signatures of OFDM signal revealed in SCF, OFDM DFT size: 64, OFDM CP size: 16

colleagues that the flexible ECS can be created by manipulating the correlation among SSCs in OFDM waveform, which doesn't interfere with the normal data transmission on other sub-carriers. In this way, signal detection, device/network identification, frequency acquisition and spectrum rendezvous can be achieved by extracting the ECS at receiver side. This approach is essentially a mean of enriching the knowledge which can be obtained via spectrum sensing. Based on their pioneering work, it is proposed by us in [42] and [41] that a stand-alone beacon signal utilizing the cyclostationary signature can be further applied for indicating spectrum allocations for enhancing Dynamic Spectrum Access (DSA).

In the traditional DSA scenarios, it is challenging for devices or networks, especially heterogeneous ones to obtain comprehensive knowledge on each other for optimizing their coordination and coexistence:

1. In classical signal detection problem of spectrum sensing, SU can only sense the presence or absence of certain type or standard of signal in the interested bands.
2. Moving one step forward, using signal classification and identification, SU can further recognize the types or standards and may extract minor parameters of unknown signals.
3. In the geo-location database approach, abundant information of other devices or networks can possibly be obtained. The access to a remote database is required which is not always available in all the applications. Besides, in a very dynamic spectrum

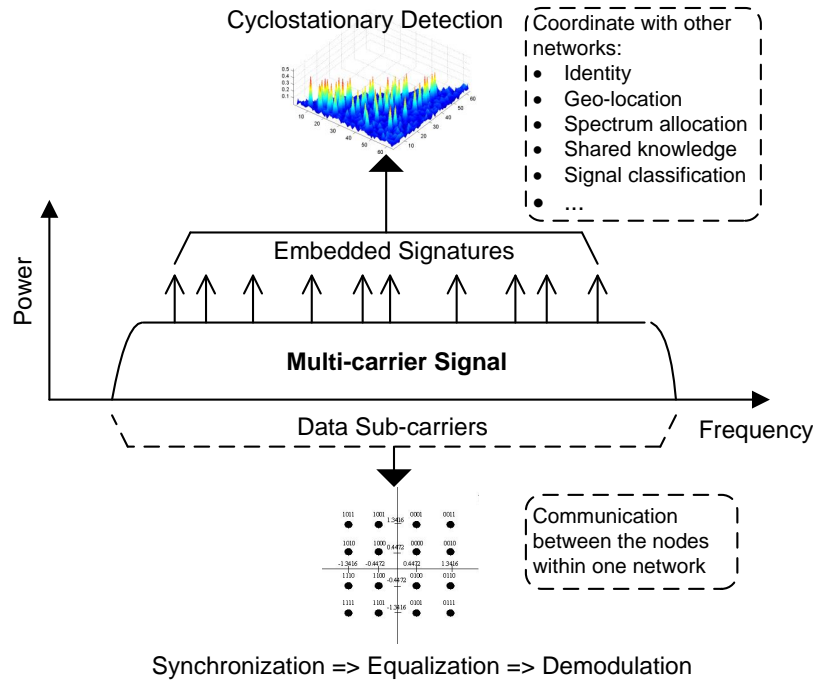


Figure 34: Extended information carried on cyclostationary signatures of multi-carrier signal

sharing scenario, frequent update of database is needed which may become difficult. The current development of the geo-location database is aimed at protecting Primary User (PU)s [84], such as TV broadcasting and PMSE users, other coexisting Secondary User (SU)s are mostly ignored. Hence, this approach is not adequate for improving the coordination and coexistence among dynamic SUs.

Trying to solve these challenges, a scheme of delivering extended information using ECS for multi-carrier signal is proposed in this thesis, which enables the heterogeneous systems to get much more knowledge on each other via spectrum sensing than the traditional signal detection and classification approaches. Some examples of the potential applications of the extended information and their benefits are listed as follows.

1. *Device/Network's Identity and Parameters*
 The identity and parameter information can assist users to quickly discover available services, recognize and synchronize to peer devices in spectrum rendezvous [19, 18].
2. *Geo-location*
 With this information, networks can estimate and optimize their

mutual interference levels through calculation of their relative locations. When positioning via GPS, cellular network or WiFi network is not possible, users can make use of nearby networks' geo-location information.

3. *Spectrum Allocation*

Networks can declare their spectrum allocations to each other, which facilitates their coordination of spectrum usages. The knowledge of each other's geo-location can be also involved in the optimization of their coordination.

4. *Shared Knowledge*

The knowledge obtained by spectrum sensing or access of database can be shared among heterogeneous networks or devices to reduce the overhead of redundant sensing and database inquiries. Besides, it can help to mitigate the hidden-node problem for devices which are blind to some other networks due to deep shadow fading.

It should be noted that the decoding of the extended information carried on ECS requires only the proposed cyclostationary detection techniques which will be illustrated later. The much more complicated procedures in normal digital receivers including synchronization, channel estimation/equalization and demodulation/decoding are avoided. Thus, the decoding of the extended information is unified in one framework which is much more cost-efficient than the integration of multiple standard-specific receivers. In the proposed scheme, only a small part of sub-carriers are taken as SSC for generating ECS resulting small increase of overhead.

In the following contents of this chapter, we first introduce the generation and extraction of ECS with an improved scheme presented. Then, the ECS based signal classification is introduced showing the advantage of the improved ECS generation scheme. The novel scheme of using ECS for delivering extended information is further presented in Section 5.4 with detailed illustration on the amount of information, encoding and decoding as well as some simulation results in practical conditions. The proposed spectrum sensing based on ECS in this chapter is further validated using real-world experiments with RF signal which is further presented in Chapter 6.

5.2 GENERATION AND EXTRACTION OF ECS

5.2.1 *Scheme 1: Generating ECS with Correlated Constellations on Signature Sub-Carriers (SSC)*

The OFDM signal is essentially a set of statistically independent streams of modulated constellations which are transmitted on parallel sub-carriers. Assuming the set includes all the effective sub-carriers is \mathbf{A} , the OFDM signal can be then represented by

$$x[p] = \sum_k \sum_{n \in \mathbf{A}} x_{k,n} e^{2\pi j \frac{np}{M}} q[p - kN_s], \quad (5.1)$$

in which $x_{k,n}$ is the modulated QAM or PSK constellation on the n th sub-carrier of the k th OFDM symbol, $q[p]$ is the pulse shaping window and N_s is the period of OFDM symbol. The generation of OFDM symbols is essentially an Inverse Discrete Fourier Transform (IDFT) operation and is usually implemented with the more efficient Inverse Fast Fourier Transform (IFFT). Normally, an OFDM symbol period include a segment of CP for relaxing channel equalization, which leads to a symbol length which larger than the actually DFT size:

$$N_s = N_{CP} + N_{DFT}. \quad (5.2)$$

Since in multi-carrier signal, the modulated constellations are carried independently on many narrowband sub-carriers, which give rise to the possibility of manipulating the spectral correlation in frequency domain with small granularity. Part of the sub-carriers are taken for embedding special signal with intended correlation pattern, which are name signature sub-carrier (SSC) in this thesis. The SSCs are grouped into several mutually exclusive sets $\mathbf{G}_1, \mathbf{G}_2, \dots, \mathbf{G}_R$ and the constellations on the SSCs in the same group are correlated with each other:

$$x_{k,n_1} = x_{k,n_2} \quad n_1, n_2 \in \mathbf{G}_i, n_1 \neq n_2, \quad (5.3)$$

and the constellations on SSCs belonging to different groups are statistically independent:

$$\lim_{K \rightarrow \infty} \sum_{k=1}^K x_{k,n_1} x_{k,n_3}^* = 0 \quad n_1 \in \mathbf{G}_u, n_3 \in \mathbf{G}_v, \mathbf{G}_u \neq \mathbf{G}_v. \quad (5.4)$$

Thanks to the orthogonality among different sub-carriers, the SSCs don't interfere the normal data transmissions on other sub-carriers. The signatures in estimated SCF are generated by the correlation of each of the two SSCs within one group. Thus, for the group \mathbf{G}_i

having g_i number of SSCs, the total number of signatures from the group in SCF is

$$\binom{g_i}{2} = \frac{g_i!}{2(g_i - 2)!} \quad g_i \geq 2. \quad (5.5)$$

This scheme is adopted in all the literatures about applying ECS in multi-carrier signal and is named *Scheme 1* in this thesis. An example of assigning signatures into two groups for an OFDM signal is given in Figure 35. In Group 1, there are 3 SSCs assigned resulting $\binom{3}{2} = 3$ ECSs in SCF. And in Group 2, there are 4 SSCs resulting $\binom{4}{2} = 6$ ECSs.

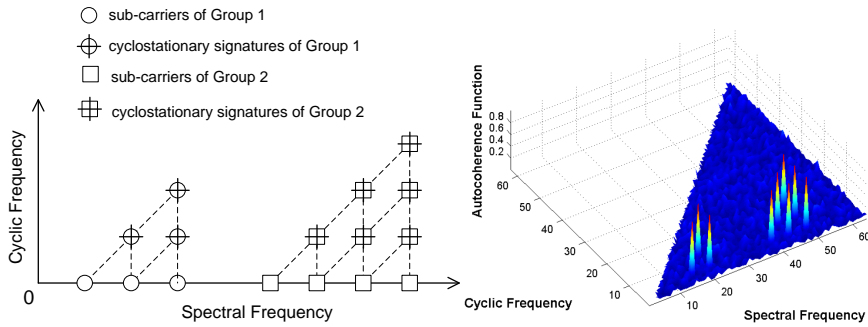


Figure 35: Example of two groups of ECS in OFDM signal revealed by ACF, OFDM DFT length: 64, OFDM CP length: 16, Group 1: 3 SSCs, Group 2: 4 SSCs

5.2.2 Scheme 2: Generating ECS with Sinusoids on SSCs

Another scheme is proposed in this thesis that the SSCs with correlated constellations can be replaced by sinusoid tones when there is only one group of SSCs for embedding signature in the signal. As a result, there is no need to consider the statistical independence among the SSCs in different groups, which enables the use of the fully correlated sinusoids. In this scheme, the normal data transmitted on other sub-carriers are modulated by

$$x_{\text{data}}[p] = \sum_k \sum_{n \in \mathbf{A}-\mathbf{G}} x_{k,n} e^{2\pi j \frac{np}{M}} q[p - kN_s], \quad (5.6)$$

which can be implemented using DFT. The \mathbf{G} is the set of SSCs with sinusoids for generating signature signal

$$x_{\text{SSC}}[p] = \sum_{n \in \mathbf{G}} e^{2\pi j \frac{np}{M}}. \quad (5.7)$$

Then the OFDM signal with ECS becomes the summation of the data signals and the signature signals.

$$x[p] = x_{\text{data}}[p] + x_{\text{SSC}}[p]. \quad (5.8)$$

This proposed scheme is called *Scheme 2* in this thesis and rooted from our previous work in [41].

5.2.3 SCF Estimator for Extracting ECS

In Section 2.8, the analysis of cyclostationarity using SCF estimated by both Time-Smoothed Cyclic Cross Periodogram (TS-CCP) and Frequency-Smoothed Cyclic Cross Periodogram (FS-CCP) is presented. The TS-CCP has lower complexity since the constraint (2.60) can be satisfied with shorter DFT length [19, 18]. Therefore, the TS-CCP is adopted in our implementation of SCF estimator using digital processing.

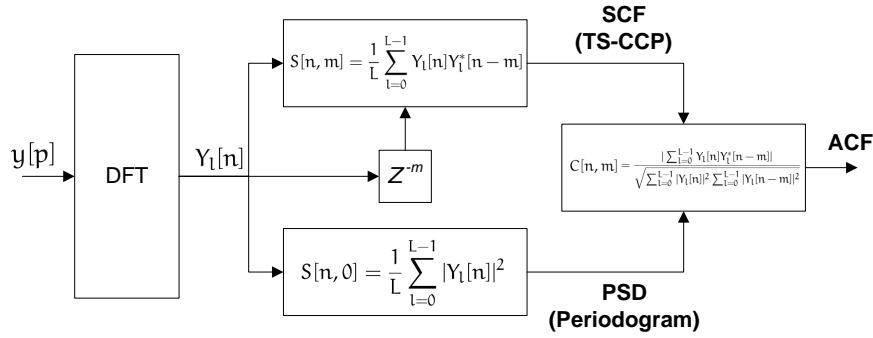


Figure 36: Digital implementation of SCF and ACF estimator

The digital TS-CCP estimator is formulated as:

$$S[n, m] = \frac{1}{L} \sum_{l=0}^{L-1} Y_l[n] Y_l^*[n-m] \quad m, n = 0, 1, \dots, N_{\text{DFT}} - 1, \quad (5.9)$$

in which

$$Y_l[n] = \sum_{i=0}^{N_{\text{DFT}}-1} y[lD + i] v[i] e^{-2\pi j \frac{ni}{N_{\text{DFT}}}} \quad n = 0, 1, \dots, N_{\text{DFT}} - 1 \quad (5.10)$$

is the N_{DFT} -point DFT of the received signal $y[p]$. Since the smallest granularity of the cyclostationary signatures in frequency domain is the sub-carrier's spacing, the inherent OFDM signal's DFT length is also used here for ACF estimation, which provides sufficient frequency resolution. The $v[i]$ is the smoothing window of length N_{DFT} . We use rectangular window featuring high frequency resolution

which can differentiate adjacent signatures well. The spectral frequencies and the cyclic frequencies are indexed by n and m respectively. The ACF can be further estimated by normalizing the SCF:

$$\begin{aligned} C[n, m] &= \frac{|S[n, m]|}{\sqrt{(S[n, 0]S[n - m, 0])}} \\ &= \frac{|\sum_{l=0}^{L-1} Y_l[n]Y_l^*[n - m]|}{\sqrt{\sum_{l=0}^{L-1} |Y_l[n]|^2 \sum_{l=0}^{L-1} |Y_l[n - m]|^2}}. \end{aligned} \quad (5.11)$$

It should be noted that the shifting step D in (5.10) for calculating the TS-CCP is different in *Scheme 1* and *Scheme 2*. In *Scheme 1*, $D = N_s$, because the cyclic period of the SSCs with correlated constellations is the same as the OFDM symbol period N_s . In *Scheme 2*, $D = N_{\text{DFT}}$ which is shorter than the OFDM symbol period, because the cyclic period of the SSCs carrying sinusoids with continuous phase is the same as the DFT length. For the same observation time, since the cyclic period of *Scheme 2* is shorter, more number of averaging is performed in estimating SCF, which can lead to some performance improvement in detecting the signatures. The other advantage of *Scheme 2* is that only the knowledge of DFT length is needed while the CP length is not needed by the detector, which is particularly favorable for detecting the OFDM signal which has multiple options of CP lengths.

5.3 ECS FOR SIGNAL CLASSIFICATION WITH IMPROVEMENT

The signature generations reported in [18, 19, 22] are essentially the manipulation of M SSC groups, each group has only two correlated SSCs which has the same frequency separation. There is no SSC shared by different groups. In this way, all the signatures have the same cyclic frequency which is equal to the frequency separation of the two SSCs in a group. This method is actually a specific configuration of the *Scheme 1* presented in Section 5.2.1 and the correlation among SSCs are only partially explored. The amount of signatures N_{sig} in estimated SCF or ACF is equal to the amount of groups M . The generation of the signature using this method as well as the estimated ACF is presented in Figure 37.

It is expected that the classification performance can be improved by further exploiting the spectral correlations of all the SSCs. An example showing the method placing all six SSCs in one group and its resulted ACF are presented in Figure 38. When sinusoids are placed on the SSCs, this assignment of signatures becomes actually the *Scheme 2* introduced in Section 5.2.2. For fair comparison with the reported signature assignment for signal classification in [18, 19], the total number of sub-carriers $2M$ and

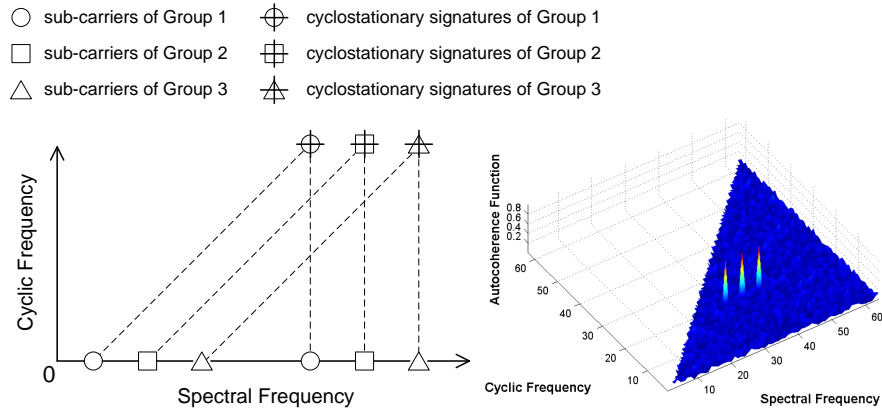


Figure 37: The method of generating ECS with partial correlation of SSCs for signal detection and classification, 3 groups, each with 2 correlated SSCs

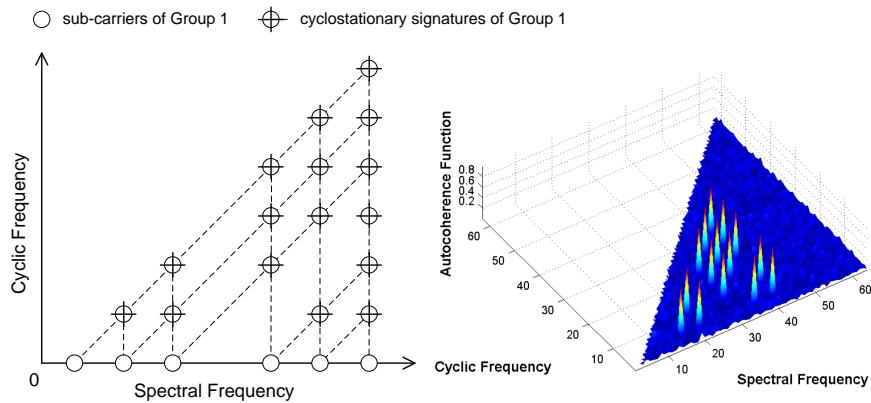


Figure 38: The method of generating ECS with full correlation of SSCs for signal classification proposed in this thesis, 6 fully correlated SSCs

their assignment patterns are kept the same. Then, the number of signatures revealed in the proposed method becomes $N_{sig.} = \binom{2M}{2} = M(2M - 1)$.

In the ECS based signal classification, a group of templates are correlated with the estimated ACF and the one with maximum correlation value is taken as the classification result. A template $\{(n_{k,i}, m_{k,i})\}$ is essentially the spectral and cyclic frequencies pair of the signature for class k . The correlations of the estimated ACF with the templates are taken as the detection metrics:

$$\Lambda_k = \frac{\sum_{i=1}^{N_{sig.,k}} C[n_{k,i}, m_{k,i}]}{N_{sig.,k}}. \quad (5.12)$$

The hypothesis \mathcal{H}_0 when there is actually no signal received should also be detected using a threshold γ according to a desired PFA. However, this issue is not taken into account in the classifier reported in [19, 18]. Define hypothesis $\mathcal{H}_k, k > 0$ being the situation when signal of class k is transmitted, which is under the same signal classification framework illustrated in Section 4.4. The classification is performed as

$$\begin{aligned} \hat{\mathcal{H}}_k : \hat{k} &= \arg \max_k (\Lambda_k), \max_k (\Lambda_k) \geq \gamma \\ \hat{\mathcal{H}}_0 : \max_k (\Lambda_k) &< \gamma \end{aligned} \quad (5.13)$$

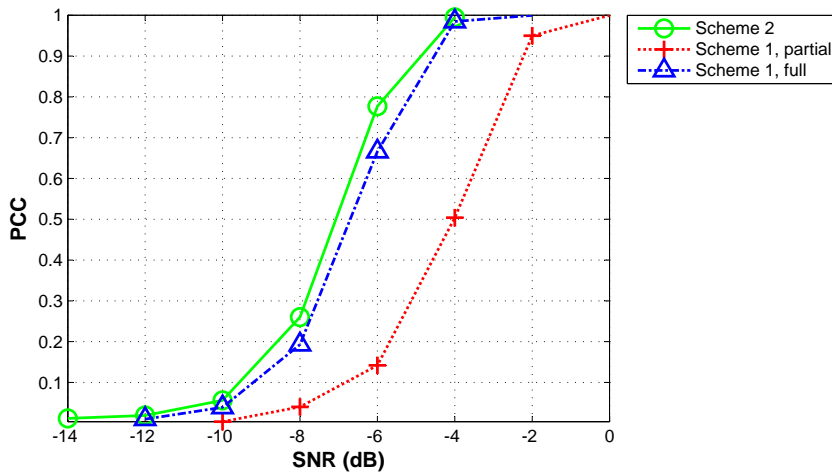


Figure 39: PCC of ECS based signal classification, OFDM DFT size: 64, OFDM CP size: 16, number of sub-carriers: 52, number of SSCs: 6, number of OFDM symbols: 30, 3 groups for partial correlation, number of classes: 4, PFA: 0.01

The performance of signal classification using ECS with different schemes are simulated and presented in Figure 39. The “partial” case is the way in [18, 19] that the six SSCs are divided into three groups, each of them has two correlated SSCs, which can generate three ECSs as presented in Figure 37. The “full” case is that all the six SSCs are in one group, thus they are fully correlated resulting 15 ECSs as shown in Figure 38. These two cases

are actually specific configurations of *Scheme 1* illustrated in Section 5.2.1. In *Scheme 2*, the six SSCs are fully correlated sinusoids which generates the same ECS pattern as the “full” case in *Scheme 1* (Figure 38). Figure 39 shows that the *Scheme 2* and the “full” case of *Scheme 1* have remarkable gain over the “partial” case of *Scheme 1*, which is caused by the increased number of ECS due to full correlation among SSCs. The performance of *Scheme 2* is slightly better than the “full” case of *Scheme 1*, which is due to the increased times of averaging L in (5.9) as the result of using smaller shifting step $D = N_{\text{DFT}}$ instead of using $D = N_s$.

5.4 EXTENDED INFORMATION CARRIED ON ECS

The proposed scheme of carrying extended information on multi-carrier signal is based on the abundant ECS patterns generated by different combinations of SSCs’ frequency locations. The *Scheme 2* using fully correlated sinusoids as SSCs are adopted thanks to its favorable properties such as indifferent to CP lengths and more times of averaging in estimating ACF, which are already presented in previous sections of this chapter.

5.4.1 The Potential Amount of Information

It can be noticed in Figure 37 and Figure 38 that on the spectral-cyclic frequency plain of ACF, the spectral frequency of an ECS is equal to the larger one of its two corresponding SSCs’ frequencies while the cyclic frequency of an ECS is equal to the difference of its two corresponding SSCs. Based on this relation, the frequency locations of the SSCs can be detected by the coordinates of ECSs on the spectral-cyclic frequency plain of ACF.

Assume an OFDM system has N_C effective sub-carriers which belong to the set \mathbf{A} , among which there are totally N_{SSC} sub-carriers are taken as SSCs for generating ECSs in ACF. The information is encoded in the combinations of the SSCs. There are totally

$$K_1 = \binom{N_C}{N_{\text{SSC}}} \quad (5.14)$$

combinations can be achieved for the given number of effective sub-carriers and SSCs. All these combinations are indexed using unique numbers, which result the total number of encoded information bits:

$$N_{\text{bit}} = \lfloor \log_2 K_1 \rfloor = \left\lfloor \log_2 \frac{N_C!}{N_{\text{SSC}}!(N_C - N_{\text{SSC}})!} \right\rfloor. \quad (5.15)$$

For example, according to a multi-carrier system with 200 effective sub-carriers, if 10% thus 20 sub-carriers are taken as SSCs, the number of information can be encoded is $\lfloor \binom{200}{20} \rfloor = 90$ bits. The amount of bits can be carried on ECS with different overhead ratios is further presented in Figure 41. It shows that when the overhead ratio of SSC is fixed, the potential number of encoded bits increases linearly along with the increase of the effective sub-carriers.

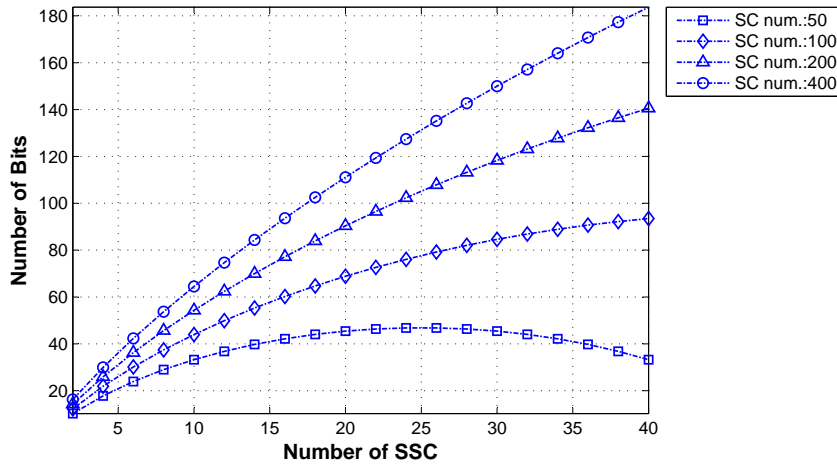


Figure 40: The number of bits can be encoded for different number of SSCs and effective sub-carriers

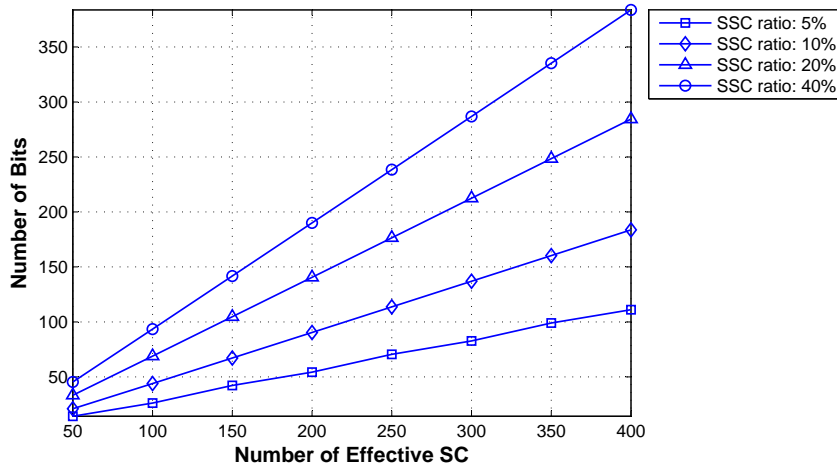


Figure 41: The number of bits can be encoded for different ratios of SSCs among effective sub-carriers

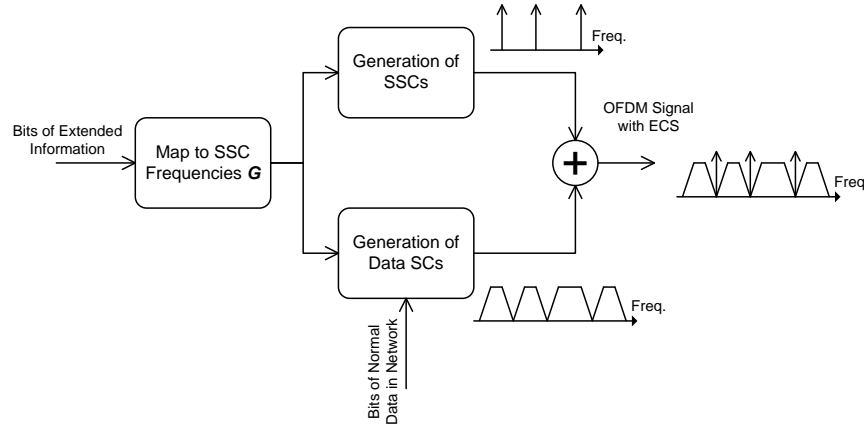


Figure 42: Generation of OFDM signal with extended information carried on ECS

5.4.2 Encoding and Decoding of Extended Information on ECS

5.4.2.1 Encoding

According to the *Scheme 2* illustrated in Section 5.2.1, the information is carried only on the frequency locations of SSCs. Recalling the notations from previous sections of this chapter, \mathbf{A} denotes the set of all the N_C effective sub-carriers, \mathbf{G} is the set of all the N_{SSC} fully correlated SSCs with sinusoids. The encoding of extended information on ECS using *Scheme 2* is depicted in Figure 42

An important issue which needs to be addressed in encoding is how to detect the hypothesis \mathcal{H}_0 when the interested signal is not presented and how to identify the situation when the decoded information is error. Hence, we define another set \mathbf{S} with size N_S for limiting the frequency locations of the SSCs and it should satisfy $\mathbf{G} \subset \mathbf{S} \subset \mathbf{A}$ and $N_C > N_S > N_{SSC}$. When the detected set of SSCs $\hat{\mathbf{G}}$ doesn't belong to \mathbf{S} , hypothesis \mathcal{H}_0 or wrong decoding is concluded and another sensing test may need to be conducted again.

Since there are N_S possible frequencies for the N_{SSC} SSCs, the amount of information can be carried becomes

$$N_{\text{bit}} = \left\lfloor \log_2 \binom{N_S}{N_{SSC}} \right\rfloor = \left\lfloor \log_2 \frac{N_S!}{N_{SSC}!(N_C - N_{SSC})!} \right\rfloor \quad (5.16)$$

bits. For example, assume an OFDM system has $N_C = 200$ effective SCs, $N_S = 100$ of them are allowed for placing SSCs, in which only $N_{SSC} = 20$ sub-carriers are actually SSCs. The overhead ratio is $20 \div 200 = 10\%$ and the number of bits can be denoted by the combinations of SSCs' frequencies is $\left\lfloor \binom{100}{20} \right\rfloor = 68$, which is large enough to accommodate some extended information described in Section 5.1. Some examples are listed as follows:

1. The BSSID (Basic Service Set Identity) of IEEE 802.11 WLAN is 48 bit.

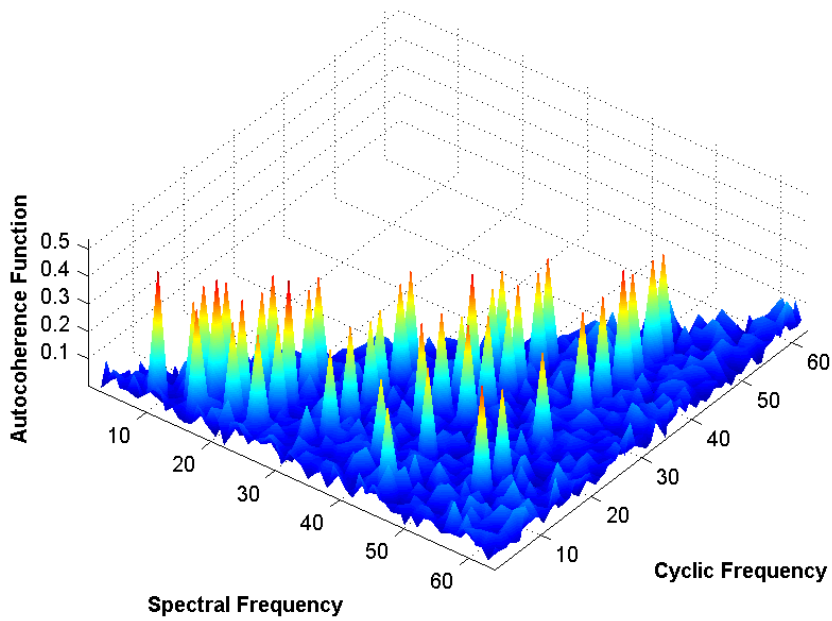


Figure 43: 3D view of the ACF for an OFDM signal with ECS, DFT size: 64, CP length: 16, effective SCs: 52, number of SSCs: 10

2. The metric of longitude or latitude which is accurate to 30.8 meters in distance can be denoted by $\lceil \log_2(360 \times 60 \times 60) \rceil = 21$ bits respectively.
3. The channel numbers in TV band, 2.4 GHz band and 5 GHz are less than 100. The status of each channel can be simply denoted by one bit for available or not unavailable.

A question arising here is how to map the binary information bits to the different combinations of SSCs' frequency set \mathbf{G} . In [85], an algorithm is proposed for generating a vector with certain combination from a lexicographical index and the programming implementation of this algorithm is contributed in [86]. The information bit word can be translated to the lexicographical index value using the binary to decimal conversion and mapped to the SSCs' frequency set \mathbf{G} using the algorithm. Then the multi-carrier signal with ECS can be generated following (5.7) and (5.6) in *Scheme 2*.

5.4.2.2 Decoding

At the receiver side, in order to decode the extended information carried on ECS, the ACF $C[n, m]$ which is essentially the normalized SCF should be estimated using the method presented in Section 5.2.3. In Figure 43, an example of the estimated ACF for an OFDM signal with embedded signatures is presented. It shows unique ECS pikes at some spectral-cyclic frequency pairs, which are generated by the coherence between the SSCs.

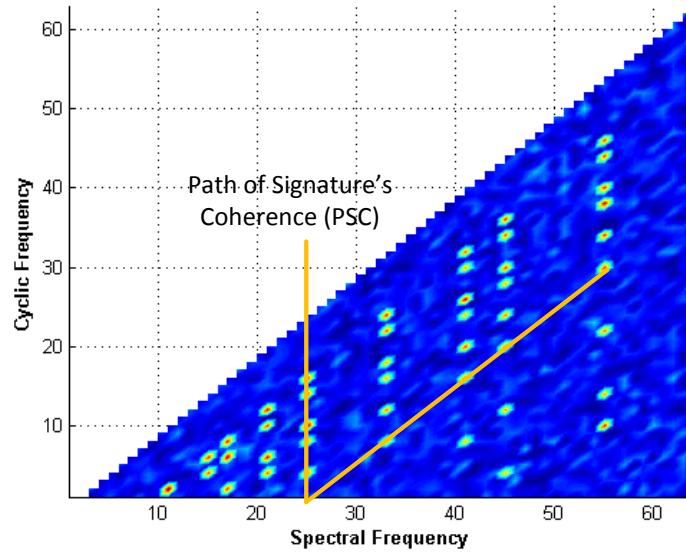


Figure 44: Top view of the ACF for an OFDM signal with ECS showing PSC of one SSC, DFT size: 64, CP length: 16, effective SCs: 52, number of SSCs: 10

A method is proposed in this thesis for translating the ECS pikes to the detected frequency set of SSCs $\hat{\mathbf{G}}$. Since every two SSCs can generate an ECS pike in ACF, a path showing the coherence of one SSC with all other SSCs can be found in the plain of spectral-cyclic frequencies, which is named the Path of Signature's Coherence (PSC) and depicted in Figure 44.

Assume $\mathbf{C}_m, m \in \mathbf{A}$ is the set of all the values along the PSC belonging to the SC with index m . The maximum value of \mathbf{C}_m 's elements are then found by:

$$\tilde{c}[m] = \max(\mathbf{C}_m). \quad (5.17)$$

Then the frequency set of SSCs $\hat{\mathbf{G}}$ can be detected by finding out the indexes of the N_{SSC} largest items among $\tilde{c}[m]$:

$$\hat{\mathbf{G}} = \left\{ m \mid \forall i : \tilde{c}[i] < \tilde{c}[m], i \notin \hat{\mathbf{G}} \right\}. \quad (5.18)$$

There are two situations when $\hat{\mathbf{G}}$ could be invalid and these situations should be discovered by the receiver:

- In hypothesis \mathcal{H}_0 when there is actually no interested signal in the channel, a random set $\hat{\mathbf{G}}$ is detected. This situation can be discovered by checking whether $\hat{\mathbf{G}} \subseteq \mathbf{S}$. The probability of failing to discover this situation, thus false alarm when there is no signal, can be calculated by

$$P_{FA} = \binom{N_S}{N_{SSC}} / \binom{N_C}{N_{SSC}} = \frac{N_S!(N_C - N_{SSC})!}{N_{SSC}!(N_S - N_{SSC})!}, \quad (5.19)$$

in which N_{SSC} , N_S and N_C are the numbers of elements in set \mathbf{G} , \mathbf{S} and \mathbf{A} respectively. Taking the example in Section 5.4.2.1, according to an OFDM signal with $N_{SSC} = 20$, $N_S = 100$ and $N_C = 200$, the PFA is as low as 3.32×10^{-7} .

- When the detected SSC set $\hat{\mathbf{G}}$ differs from the transmitted SSC set \mathbf{G} due to the destruction from noise or frequency-selective fading, this situation can be also discovered by checking whether $\hat{\mathbf{G}} \subseteq \mathbf{S}$. However, when the wrong frequencies in $\hat{\mathbf{G}}$ still fall into \mathbf{S} , they cannot be discovered. Assume there are L wrong SSCs in $\hat{\mathbf{G}}$, the Probability of Discovering the Wrong SSCs (PDW) can be calculated by

$$\begin{aligned} P_{DW} &= 1 - \frac{\binom{N_S - N_{SSC}}{L}}{\binom{N_C - N_{SSC}}{L}} \\ &= 1 - \frac{(N_S - N_{SSC})!(N_C - N_{SSC} - L)!}{(N_C - N_{SSC})!(N_S - N_{SSC} - L)!} \end{aligned} \quad (5.20)$$

It shows that the more the wrong SSCs, the more probable they can be discovered. Taking the above example, for one wrong SSC in $\hat{\mathbf{G}}$, $P_{DW} = 0.56$; for two, $P_{DW} = 0.80$.

After the frequencies of SSCs are detected and their correctness is validated using set \mathbf{S} , the bits of extended information can be decoded from $\hat{\mathbf{G}}$ using the algorithm proposed in [86]. The algorithm converts the combination vector $\hat{\mathbf{G}}$ back to lexicographical index, which is essentially the reverse algorithms of [85]. The binary form of lexicographical index value is actually the extended information bit word.

5.4.3 Simulation Performances

This section presents the simulation performances of decoding the extended information carried on ECS under practical conditions such as Carrier Frequency Offset (CFO) and frequency-selective channel fading.

Since the decoding relies on the locations of the ECS on the spectral-cyclic frequency plain, the frequency shift of SSCs caused by CFO can lead to some performance degradation. Fig.45 shows the destruction from CFO to the decoding performance. However, when the CFO is less than 0.2 sub-carrier spacing, the degradation is insignificant.

The multipath fading of wireless channel in time domain can be translated into the frequency selective fading which may greatly attenuates part of the SSCs and degrade the decoding performance. Fig.46 presents the impact of frequency-selective fading on decoding. The 3GPP typical urban (TUx) and rural area (RAx) channel models are applied, which features higher and lower frequency selectivity respectively. The results show that high frequency selectivity can lead to severe performance degradation.

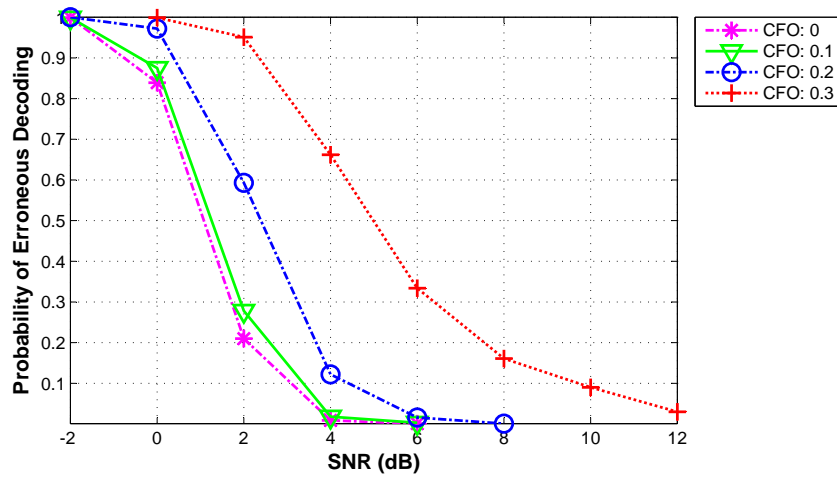


Figure 45: Probability of erroneous decoding of the extended information with CFO, DFT size: 256, CP length: 32, number of OFDM symbols: 30, effective SCs(size of \mathbf{A}): 200, size of \mathbf{S} : 50, number of SSC: 10

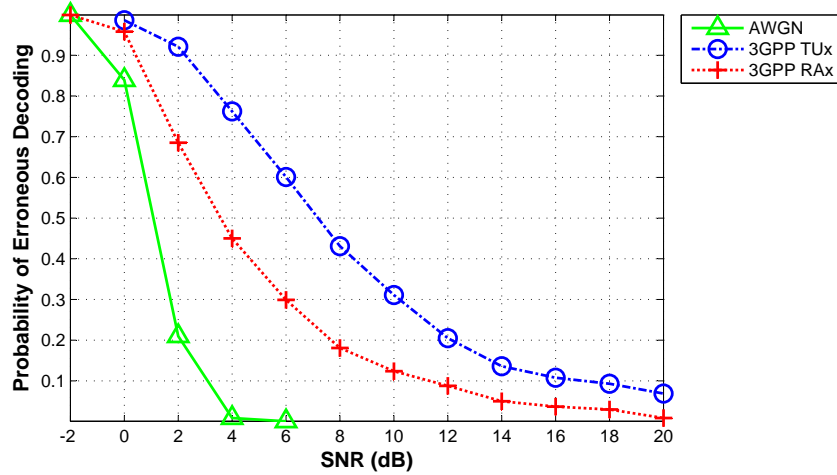


Figure 46: Probability of erroneous decoding of the extended information with frequency-selective fading channel, DFT size: 256, CP length: 32, number of OFDM symbols: 30, effective SCs(size of \mathbf{A}): 200, size of \mathbf{S} : 50, number of SSC(size of \mathbf{G}): 10

5.5 CONCLUDING REMARKS

This chapter presents two novel techniques of embedding cyclostationary signatures in multi-carrier signal for enhancing spectrum sensing. The first one presented in Section 5.2.3 is to utilize the different patterns of ECS for signal detection and classification, which is similar to the spectrum sensing techniques illustrated in Chapter 2 and Chapter 4. However, instead of using the inherent features in the signal, the ECS is intentionally created with flexible patterns, which can enable some new applications, such as the network identification and rendezvous in DSA.

The ECS-assisted signal detection and classification was originally proposed by P. D. Sutton and his colleagues in [18, 19, 20, 21]. Based on their work, in this thesis, a new scheme (*Scheme 2*) of using fully correlated sinusoids on SSCs for generating ECS is proposed, which can give improved classification performance over the reported original scheme (*Scheme 1*) in which the ECS is generated using correlated constellations on SSCs. Besides, the knowledge of CP length is not needed by the sensing receiver in the (*Scheme 2*), which is more favorable to the OFDM signal with multiple options of CP lengths.

Another novel technique proposed in this chapter is to use the ECS for carrying extended information, which can greatly enhance the knowledge gathered by spectrum sensing. The extended information can be device or network's identity and parameters, geo-location, spectrum allocation and spectrum sensing results etc. The encoding and decoding methods for the extended information are illustrated in Section 5.4.2. The simulated decoding performances considering practical constraints such as CFO and multipath fading are presented in Section 5.4.3, which shows its feasibility.

The two techniques using ECS are further implemented and validated using the sensing testbed with real-world signal transmissions, which will be presented in Chapter 6.

6.1 INTRODUCTION

In Chapter 3, the simulation performances of various signal detection methods for different types of signals are presented and compared considering some hardware imperfections. It is concluded by the simulations that the autocorrelation based detection methods, such as Feature Sequence Autocorrelation (FSA) based detections and Cyclic Prefix (CP) based detections, are more favorable due to their robustness against hardware imperfections and low complexities. Meanwhile, the autocorrelation based detections strongly rely on the unique features of different OFDM based standards and hence can be well applied to the classification of all these standards, which is illustrated in Chapter 4 with simulation performance presented. Chapter 5 presents the novel schemes of using ECS in multi-carrier signal for signal classification and delivering extended information.

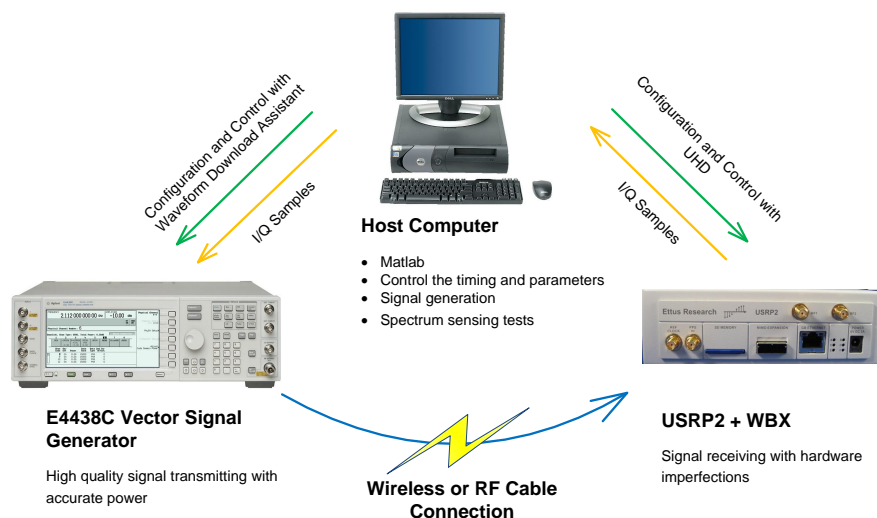


Figure 47: The structure of the spectrum sensing testbed

Computer simulations of these spectrum sensing techniques are performed, which effectively evaluate the sensing performance in idea situation or with part of the hardware effects modeled. However, not all of the real-world conditions can be taken into account in simulation. For example, the noise in simulations are often modeled as Additive White Gaussian Noise (AWGN) in reported literatures on spectrum sensing, but in practices, the noise is not perfectly white due to the filters' responses in receiver. Besides, spurs are often presented in the received signal which is harmful to sensing performances, especially for autocorrelation based signal detections.

The insufficiency of computer simulations draws the necessity of implementing the spectrum sensing scheme on real-world devices for experimental studies, which can further validate the feasibility and evaluate the performance in practical conditions. For this purpose, an experimental platform is built which consists of the following main components:

- *Host Computer* The host computer is a normal desktop PC with Windows operating system running on it. The digital waveform generators for signals of different standards or types as well as the various spectrum sensing algorithms are implemented in Matlab software on the host computer. Another task of the host computer is to configure the parameters and control the procedures and timing of spectrum sensing measurement.
- *Agilent E4438C Vector Signal Generator* [87]
The E4438C can generate and transmit arbitrary waveforms into the air. It support maximum bandwidth of 80 MS/s, carrier frequency range from 250kHz to 6GHz and adjustable transmit power range of -136 to +17dBm with level accuracy of ± 0.5 dB. The transmitted signal is downloaded from the host computer to the generator via Ethernet connection, which is supported by the Waveform Download Assistant software implemented in Matlab.
- *Ettus Research USRP2 + WBX RF Daughter-board SDR Platform* [88]
The Universal Software Radio Peripheral (USRP) is a series of cost-effective Software Defined Radio (SDR) platforms which enable the user to transmit and receive arbitrary signal within a wide frequency range. It provides the options of signal processing on host computer, onboard FPGA, DSP or embedded systems. In our configuration, the USRP2 motherboard performs analog-to-digital and digital-to-analog conversions (ADC/DAC) and is interfaced with the host computer by Gigabit Ethernet. The maximum supported sampling rate is 25MS/s which is enough to accommodate one TV channel. The WBX daughter-board is essentially a RF transceiver supporting the carrier frequency range of 50MHz to 2.2GHz which well covers the TVWS. Unlike the E4438C signal generator which has large internal memory for storing signal waveforms, the transmitted and received signal is streamed lively between USRP2 and the host computer. The USRP Hardware Driver (UHD) software is used for supporting the streaming of signal samples and configuring parameters, such as carrier frequency, sampling rate and amplifier gain.

Although the USRP2+WBX has the capability of signal transmission, we select the E4438C as the transmitter thanks to its high quality of signal generation and particularly the ability of adjusting the transmitting power accurately, which enable the measurement of spectrum sensing performances at deterministic SNR levels. The licence for signal transmission in the laboratory at 560 MHz, 625 MHz and 750 MHz is applied from the local spectrum regulator.

Using this platform, the key spectrum sensing methods studied in this thesis are validated with real-world signal transmissions and sensing receiver. This chapter first introduces the methodology for comprehensive evaluation of sensing performances. Then, the measurement of the noise power in the sensing receiver USRP2+WBX is presented which reveals notable Noise Uncertainty (NU) problem. The spectrum sensing tests start with the investigation of the FSA-2C introduced in Section 2.9.2.2 for detecting DVB-T signal at very low SNR levels. Then the experimental evaluation of the signal classifier introduced in Chapter 4 is given, which shows its effectiveness of classifying the major signals in TV band, they are DVB-T, LTE, IEEE 802.22, ECMA-392 and WM. Finally, the novel schemes of using ECS for assisting signal classification and delivering extended information are experimented on the platform showing their feasibility.

6.2 METHODOLOGY

Table 8: Methodologies of Performance Analysis

Methods	Signal Source	Noise	SNR Control
<i>Method 1</i>	simulated signal	simulated AWGN	scaling in simulation
<i>Method 2</i>	captured signal (high SNR)	captured receiver noise	scaling in simulation
<i>Method 3</i>	received signal with noise	the noise in received signal	adjust Tx power

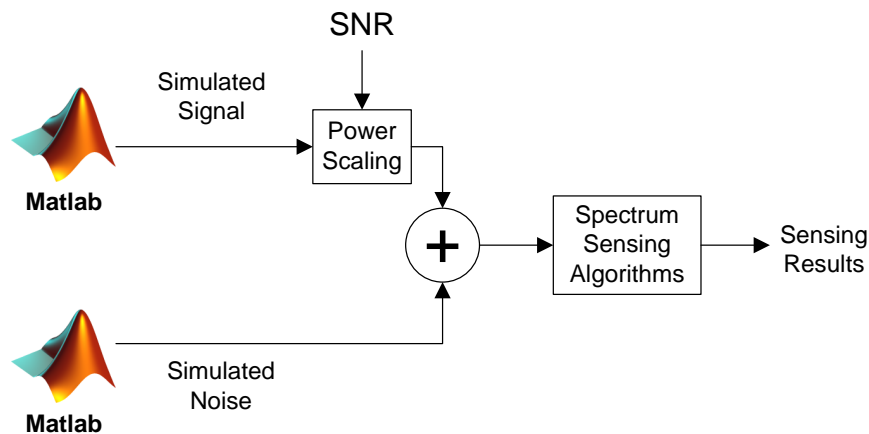


Figure 48: Method 1: sensing performance evaluation with simulated signal and noise

The evaluation of the spectrum sensing performances in this thesis are performed using three methods.

- In *Method 1*, the purely simulated signal and AWGN are used in sensing tests which was already presented in Chapter 3. In some of the simulations, the hardware imperfections such as spurs and nonwhite noise are taken into account.

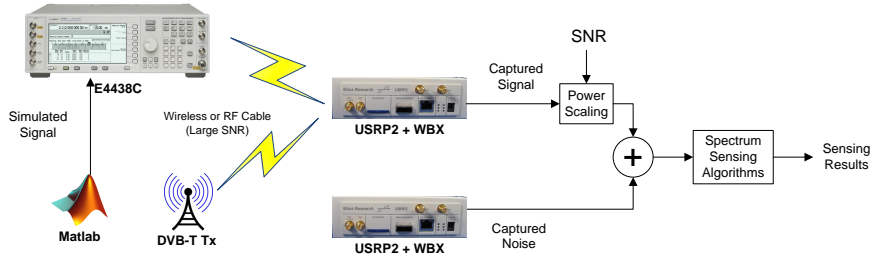


Figure 49: Method 2: sensing performance evaluation with separately captured signal and noise

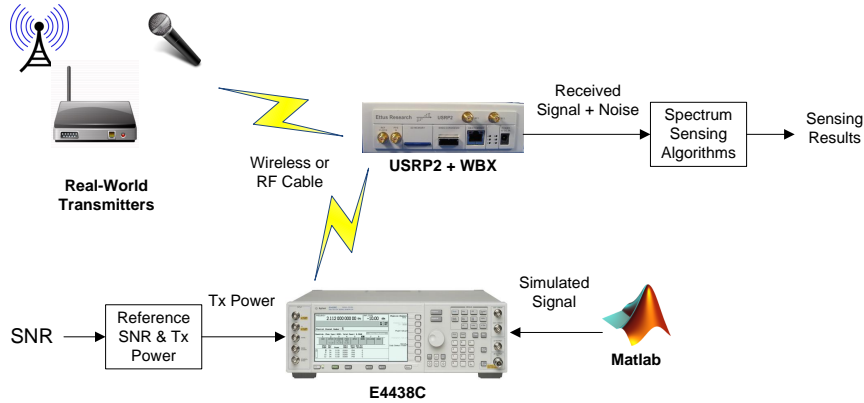


Figure 50: Method 3: sensing performance evaluation with received signal plus noise

- Going one step forward, in *Method 2*, the tested signal is directly captured by USRP2+WBX from the over-the-air transmission by E4338C or TV broadcast. The SNR of the captured signal is set to larger than 20 dB. In this way, when the signal is further scaled to very low power in sensing test, the influence of its inherent noise becomes ignorable. The noise used in *Method 2* is also directly captured from the USRP2+WBX sensing receiver with its RF input sealed by matched resistor and the transmitter turned off, which characterizes the hypothesis \mathcal{H}_0 . After a large amount of samples of the interested signals and the receiver noise are captured separately, the signal and noise are scaled according to the desired SNR levels. Then the summation of them is tested using the spectrum sensing algorithms.
- Finally, in *Method 3*, the performance of the real-world spectrum sensing device is measured, which takes only the received signal with inherent receiver noise as input. Unlike the method in *Method 2*, the artificial combination of the separated signal and noise is avoided in this method, thus, the SNR cannot be obtained by straightforward power scaling and summation. Therefore, the power estimation is utilized for achieving the desired SNR. First, the noise power $\hat{\sigma}_0^2$ is estimated in hypothesis \mathcal{H}_0 , thus with transmitter turned off and the receiver's RF input sealed by matched resistor. In hypothesis \mathcal{H}_1 , the

transmitter is turned on and set to a relative high transmitting power p_{ref} , resulting high SNR which is larger than 20 dB. The power of signal with noise is then estimated as $\hat{\sigma}_1^2$. The reason why a high SNR is required is because the error in estimated SNR can be significantly reduced as the SNR itself is sufficiently large[58]. Then the SNR for the transmitting power p_{ref} , can be accurately estimated by

$$\xi_{\text{ref.}} = 10 \log_{10} \left(\frac{\hat{\sigma}_1^2}{\hat{\sigma}_0^2} - 1 \right). \quad (6.1)$$

The transmitting power p_{ref} , and its corresponding SNR $\xi_{\text{ref.}}$, in receiver are taken as the reference for obtaining arbitrary SNR by further adjusting the transmitting power. For example, assuming $p_{\text{ref.}} = -50$ dBm can result the SNR of $\xi_{\text{ref.}} = 20$ dB, a desired SNR of -8 dB can then be achieved by simply changing the transmit power to -78 dB. Thanks to the high accuracy of E4438C in adjusting its transmitting power level, the obtained SNR levels of received signal are believed to be also accurate.

6.3 NOISE UNCERTAINTY MEASUREMENT

In Section 2.10.1, the NU problem in practical receivers and the solution to it using Dimension Cancellation (DIC) are introduced. The destruction of NU to the signal detection algorithms are also presented in the simulation results in Chapter 3. In this part, the measurements of NU in the signal from the sensing receiver USRP2+WBX are performed.

Since only the noise from the receiver is interested in this measurement, the two RF ports of the WBX daughter-board are sealed with matched filters. Besides, the frequency band of 750 MHz is selected, in which there is no interfering signal observed in our laboratory environment. There are some spurs generated by the receiver itself in the noise and their power ambiguity may affect the measured results. These spurs can be removed conveniently from the PSD $\hat{Y}[m]$ estimated by (2.32). Then the noise power can be estimated by

$$\hat{\sigma}^2 = \frac{1}{L_S} \sum_{m \in \mathbf{S}} \hat{Y}[m], \quad (6.2)$$

in which \mathbf{S} is the set of frequency components without spurs and L_S is the size of the set.

We performed two measurements with different observation times and sampling rates. In the first measurement, the sampling rate of the USRP2 is set to 12.5 MS/s which results about 10 MHz effective bandwidth considering the cut-off frequency of the anti-aliasing filter in the device. The observation time of 1 ms resulting 12.5 MS/s ms = 12500 samples are employed in measuring one noise power values. In the second measurement, the sampling rate is set to 25 MS/s and the observation time of 40 ms resulting 1 M samples are captured for calculating one noise power value. In

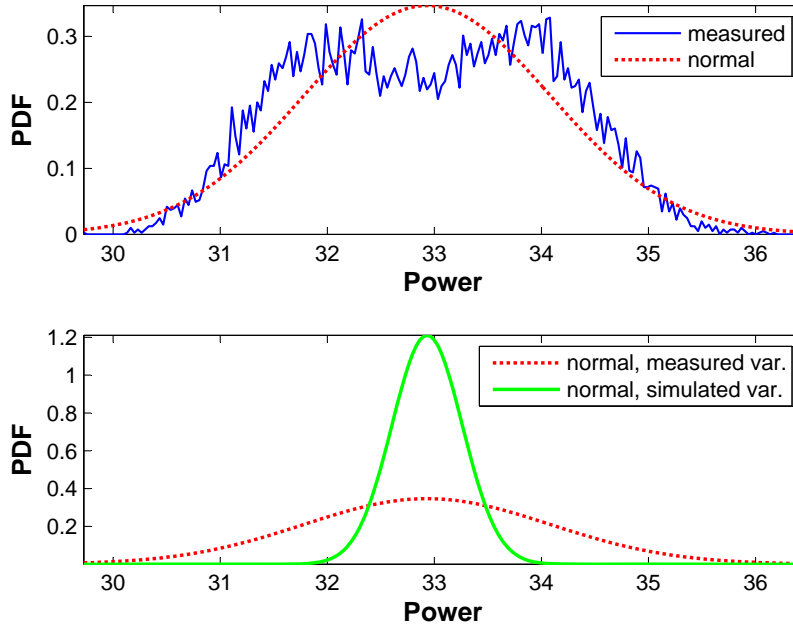


Figure 51: PDF of measured noise power from USRP2+WBX and simulated AWGN, sampling rate: 12.5 MS/s, observation time: 1 ms, carrier frequency: 750 MHz, number of measurements: 12000, duration: 12 hours

each measurement, totally 12000 measured noise power values are gathered within about 12 hours.

The Probability Density Function (PDF) of the estimated noise in both measurements are plotted in Figure 51 and Figure 52 respectively. In addition to the measured noise from the real receiver, the AWGN with the same mean power as the measured noise is simulated in computer, the PDF of which is also plotted in the two figures. Since all the simulated noise samples follows the same distribution, there is no uncertainty in it. The means and the standard variances of both measured and simulated noise's power values in the two measurements are listed in Table 9.

Interestingly, the standard variances of the measured noise power are much larger than that of the simulated AWGN powers. Besides, it is shown in Figure 51 and Figure 52 that the probability distribution of the measured noise's power values obviously differs from the normal distribution with the same mean and variance. Since the noise power values are obtained by averaging a large amount of samples (6.2), based on Central Limit Theorem (CLT), they should follow normal distribution with deterministic variance when there is no power uncertainty in the noise. The much larger variance and the non-normal distribution of the measured noise power can be only explained by the noise uncertainty problem in the sensing receiver.

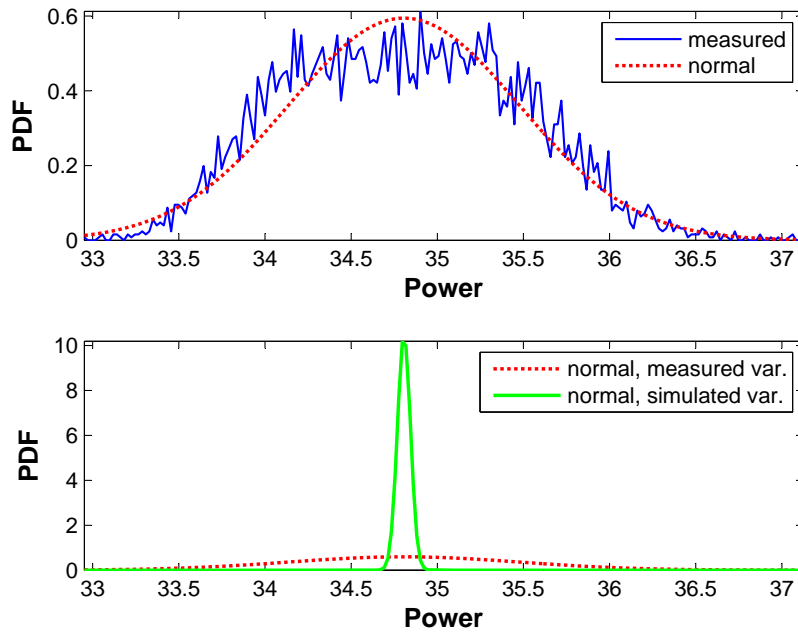


Figure 52: PDF of measured noise power from USRP2+WBX and simulated AWGN, sampling rate: 25 MS/s, observation time: 40 ms, carrier frequency: 750 MHz, number of measurements: 12000, duration: 12 hours

Table 9: Standard Variances of the Measured and Simulated Noise Power

Parameters	Measurement 1	Measurement 2
Sampling Rate	12.5 MS/s	25 MS/s
Observation Time	1 ms	40 ms
Mean	32.93	34.81
Std. Var. (measured)	1.151	0.6713
Std. Var. (simulated)	0.2950	0.0359
Maximum NU	0.445 dB	0.28 dB

6.4 SIGNAL DETECTION

The DVB-T signal is the Primary User (PU) in TV band, which brings about the challenges of detecting it at very low SNR regime for protection. Therefore, the effective detection of the DVB-T signal is the foundation of the signal classification proposed in this thesis. It is shown in the simulation results in Chapter 3 that the autocorrelation based FSA-2C can effectively detect the DVB-T signal of different modes. Besides, when the DIC is applied, the FSA-2C detection becomes immune to NU problem at nearly no cost of performance loss. These benefits makes the FSA-2C an attractive option for detecting DVB-T signal, which is validated in the detection and classification experiments introduced in this chapter.

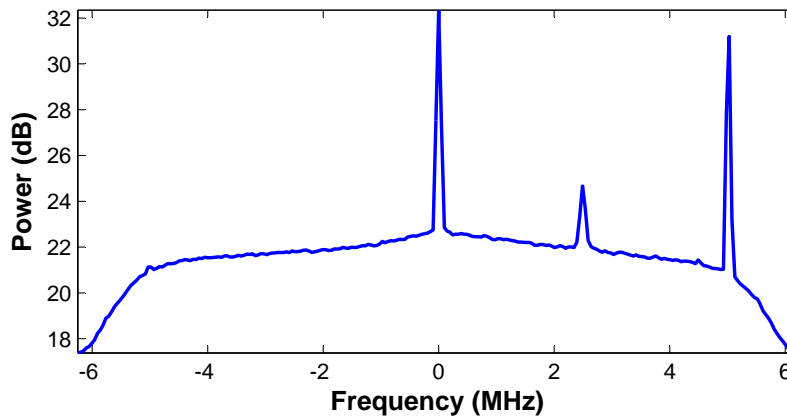


Figure 53: PSD of received signal of USRP2+WBX in hypothesis \mathcal{H}_0 , which shows nonwhite noise floor and spurs, carrier frequency: 560 MHz, sampling rate: 12.5 MS/s

All of the three methods introduced in Section 6.2 are applied in validating the FSA-2C detections. In *Method 2* and *Method 3* involving real-world signal transmitting and receiving, the sampling rate of USRP2 is set to 12.5 MS/s, which is achieved through a decimation ratio of 8 according the onboard ADC sampling at 100 MS/s. This sampling rate is enough to accommodate the signal in one TV channel of 8 MHz considering the signal loss at band edge due to the anti-aliasing filter.

In the 12.5 MHz band centered at the carrier frequency 560 MHz, three strong spurs can be observed, which is shown in Figure 53. These spurs generate strong component with non-zero mean in autocorrelation, which can degrade the detection performance significantly. Band-stop filters are used for eliminate the spurs in the signal before applying the detection algorithm.

The performances of using FSA-2C for detecting DVB-T signals in different modes are presented in Figure 54. It clearly shows that the results from the three evaluation methods agreed with each other very well. It is worth pointing out that in *Method 2*, the captured DVB-T signal with 8K DFT length is from the real TV broadcast in channel 28 centered at

530 MHz. Since the performance of detecting this real TV signal source is very coherence to the performances of detecting the modeled signal, both the effectiveness of the FSA-2C and the fidelity of the modeling of DVB-T are well validated.

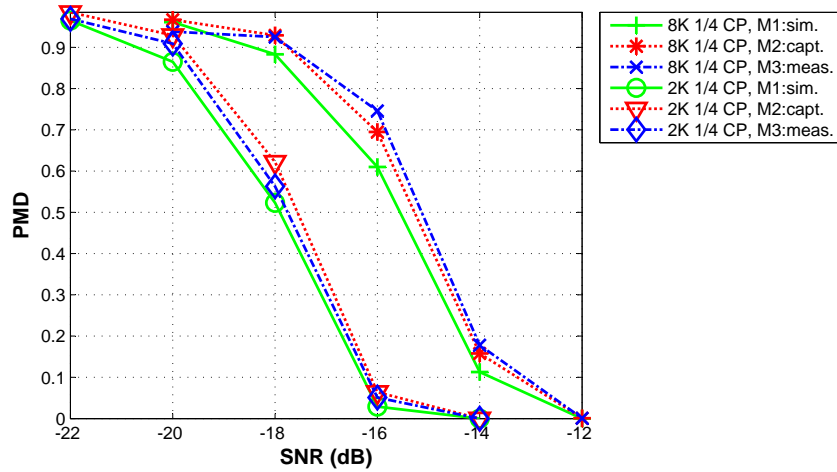


Figure 54: Performances of detecting DVB-T signals using FSA-2C with DIC, carrier frequency: 560 MHz, receiving sampling rate: 12.5 MS/s, observation time: 20 ms, PFA: 0.01

Particularly, the detection performances for DVB-T signal at low SNR using longer observation time of 100 ms is evaluated, which is presented in Figure 55. It shows that the signal can be reliably detected at SNR as low as -20 dB.

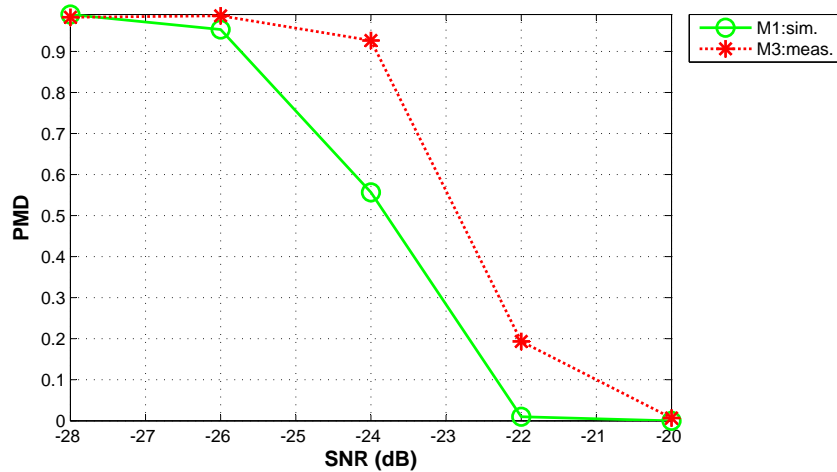


Figure 55: Performance of detecting DVB-T signal (2K, 1/32 CP mode) using FSA-2C with DIC at low SNR, carrier frequency: 560 MHz, receiving sampling rate: 12.5 MS/s, observation time: 20 ms, PFA: 0.01

The signal detection for WM signal using the PAR feature based method proposed in (4.8) is also validated using the three evaluation methods. The spurs are narrowband signals exhibiting also high PAR in the PSD of received wideband signal, which may be falsely detected as WM. An easy solution is to exclude the components around the frequencies of spurs in the estimated PSD before detection. The cost is, when the WM signal happens to appear at one of the spur's frequency, it may be ignored by the detector.

The performances of detecting WM signal based on the PAR of estimated PSD(4.8) are evaluated using the three methods, which is presented in Figure 56. The bandwidth of one TV channel, thus 8 MHz around the center 560 MHz is taken into account for detecting the WM signal. Besides, the frequency components with spurs in the interested band shown in Figure 53 should also be excluded from the detection algorithm. The PAR threshold is set to 3.6 which is larger than the PAR of all other OFDM signals in TV band. In this way, the false classification of the other OFDM signals to WM signal is avoided in the signal classification tests introduced later. Figure 56 shows that the performances evaluated using the three methods are closed to each other. The WM signal can be reliably detected at about -16 dB SNR with an observation time of 20 ms.

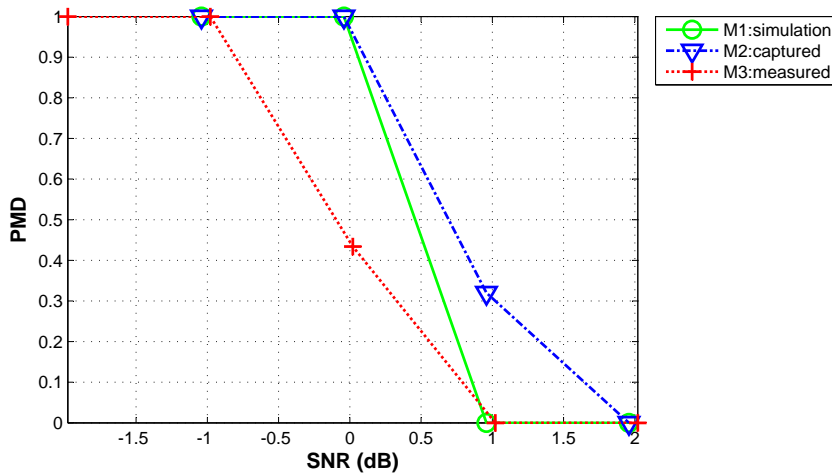


Figure 56: Performance of detecting WM signal by testing PAR of estimated PSD, carrier frequency: 558 MHz, receiving sampling rate: 12.5 MS/s, observation time: 20 ms, PAR threshold: 3.6

6.5 SIGNAL CLASSIFICATION FOR TVWS

In Chapter 5, the signal classifier for TV band White Space (TVWS) is presented, which is essentially the combination of several signal detection methods utilizing the unique features of different standards based on properly designed decision rule. In Section 6.4, the detection of DVB-T signal using FSA-2C and the detection of WM signal utilizing its high PAR prop-

erty in PSD are validated with real-world experiment using *Method 2* and *Method 3*, which show good agreement to the simulated result using *Method 1*. Based on the success of validating the signal detection algorithms, the signal classification framework for TVWS presented in Chapter 4 is also implemented on the spectrum sensing testbed and validated with experiments.

The selection of signal detection algorithms listed in Table 5 is also adopted in the experimental validations. Thus, the DVB-T signal is detected using FSA-2C method, the LTE signal is detected using CP-SW with pre-alignment, the CP-SUM is used to detect ECMA-392 and IEEE 802.22 signals while the WM signal is detected utilizing the high PAR property of its PSD. The procedure of signal classification is shown in Figure 57, which follows the decision rule in (4.11) and considers some practical issues in implementation, such as filtering, sampling rate conversion and spur removal.

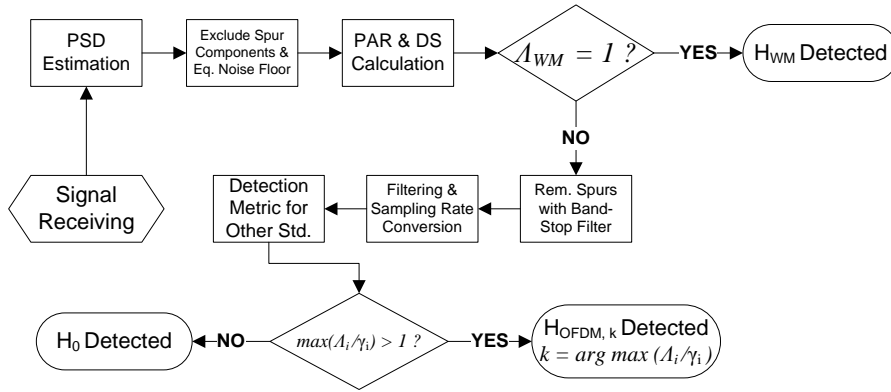


Figure 57: Signal classification procedures implemented on the spectrum sensing testbed

The target signal categories listed Table 6 are adopted here, which have the full coverage of the classifiable signals types and modes in the detection algorithm’s configuration in Table 5. During the classification tests, they are selected randomly with equal probability and tested by the classifier which then concludes which signal class is actually transmitted. In *Method 2*, the captured high-SNR signals samples by the testbed are first collected and combined with captured receiver noise according to the desired SNR in the simulation. In *Method 3*, all these signals with different modes are first downloaded into the internal memory of E4438C signal generator for speeding up the measurement procedures. The host computer sends commands to the E4438C for selecting the transmitted waveform, set the sampling rate according the standards and modes, as well as set the transmitting power according to the desired SNR using the reference power p_{ref} . and reference SNR ξ_{ref} . Then the host computer receive signal with sensing receiver USRP2+WBX and perform classification test lively.

The sensing receiver USRP2+WBX samples the signals at fixed rate of 12.5 MS/s resulting a higher effective bandwidth than the various OFDM

signals' standard-specified sampling rate and bandwidth which are listed in Table 4. The higher receiving bandwidth can involve some unwanted signal and noise from neighboring band and can degrade detection performance or even lead to false classification. Besides, the mismatch of the sampling rate can lead to the ambiguities in the time lags used in the autocorrelation based detections. In order to solve these two problems, the received signal is firstly low-pass filtered and re-sampled according to the standard-specified sampling rate before being processed by the signal detection algorithms for in the classifier.

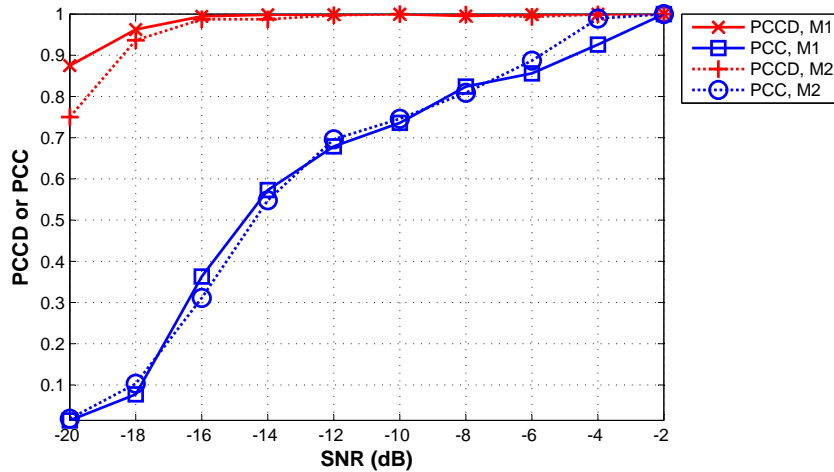


Figure 58: The overall signal classification performance, target signals in Table 6, detection algorithms in Table 5, carrier frequency: 560 MHz, receiving sampling rate: 12.5 MS/s, observation time: 20 ms, PFA: 0.01

As illustrated in Section 4.5, the different modes of DVB-T are combined into one class. Similarly, the TD-LTE signal in both normal CP mode and long CP mode are also combined into one class. Hence, there are totally five targeted classes of signals as is listed in Table 6.

The overall classification performance of all the signals are presented in Figure 58 showing good match of the results from *Method 1* using simulated ideal signal/noise and *Method 2* using real-world captured signal/noise. Besides, it confirms that the Probability of Correct Classification when Detected (PCCD) is close to one for most of the simulated SNRs. This is a favorable property that as long as the existence of the signal is successfully detected, it can be nearly always correctly classified, which can be also translated into a very small ambiguity in classification.

The Probability of Correct Classification (PCC) for the five specific signal classes are presented in Figure 59 to Figure 63 respectively. Generally, these results exhibit good agreement between the evaluation using *Method 1*, *Method 2* and the *Method 3* of real-world measurement. It should be noted that in the classification performances of ECMA-392 shown in Figure 62, the measured performance using *Method 3* differs obviously from the result

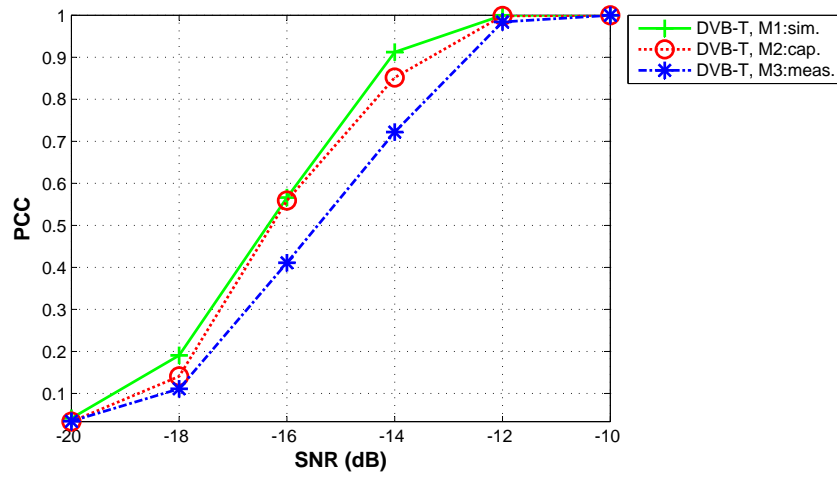


Figure 59: The PCC for DVB-T signal, target signals in Table 6, detection algorithms in Table 5, carrier frequency: 560 MHz, receiving sampling rate: 12.5 MS/s, observation time: 20 ms, PFA: 0.01

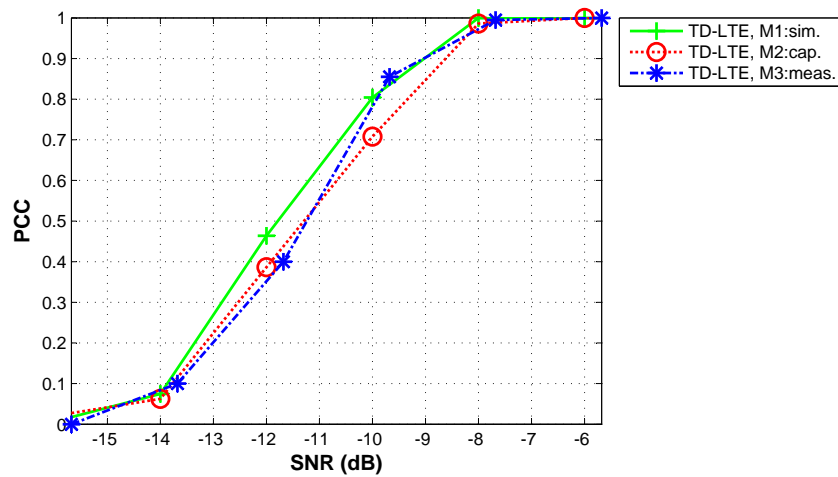


Figure 60: The PCC for DVB-T signal, target signals in Table 6, detection algorithms in Table 5, carrier frequency: 560 MHz, receiving sampling rate: 12.5 MS/s, observation time: 20 ms, PFA: 0.01

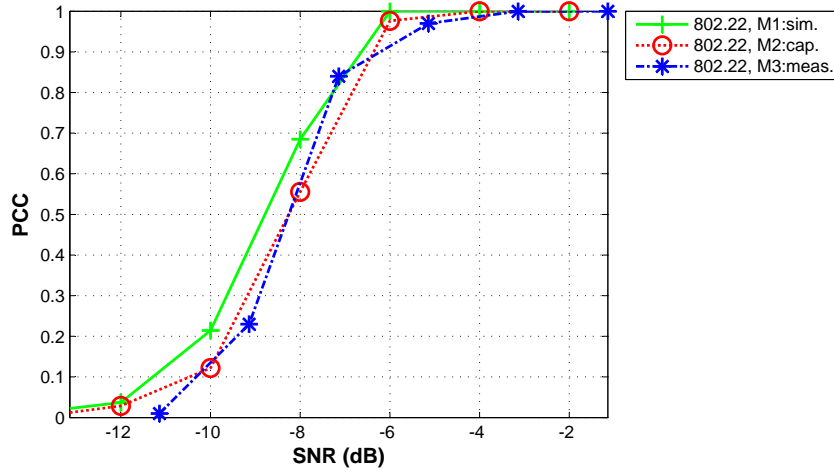


Figure 61: The PCC for DVB-T signal, target signals in Table 6, detection algorithms in Table 5, carrier frequency: 560 MHz, receiving sampling rate: 12.5 MS/s, observation time: 20 ms, PFA: 0.01

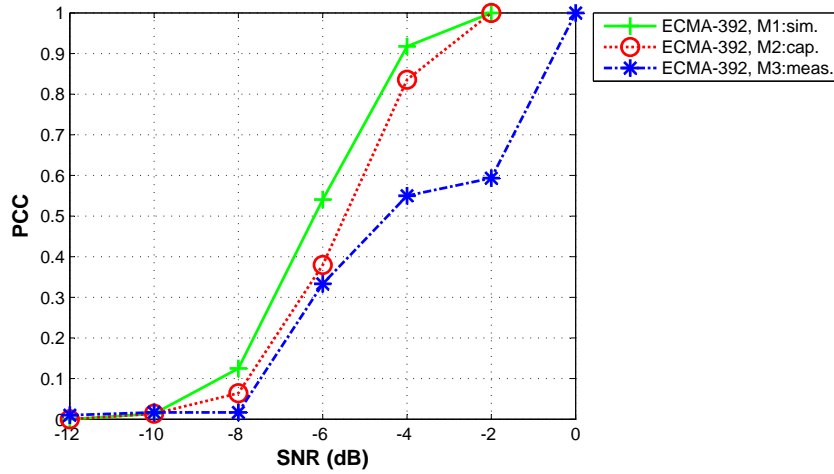


Figure 62: The PCC for DVB-T signal, target signals in Table 6, detection algorithms in Table 5, carrier frequency: 560 MHz, receiving sampling rate: 12.5 MS/s, observation time: 20 ms, PFA: 0.01

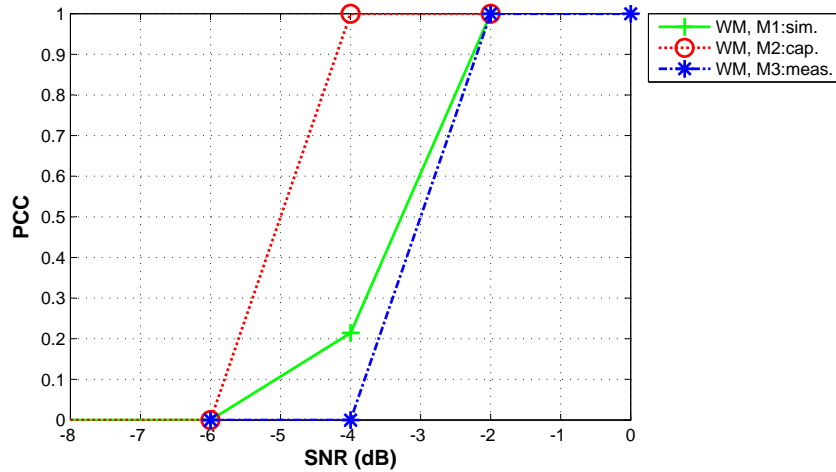


Figure 63: The PCC for DVB-T signal, target signals in Table 6, detection algorithms in Table 5, carrier frequency: 560 MHz, receiving sampling rate: 12.5 MS/s, observation time: 20 ms, PFA: 0.01

of *Method 1* and 2. This can be explained by the random bursty nature of ECMA-392 signal that in some observation windows, the actual duty cycles of the signal are less than the mean value 0.5 resulting lower PCC while in some other observation windows, the duty cycles become larger than 0.5 resulting higher PCC.

6.6 ECS FOR SIGNAL CLASSIFICATION

In Section 5.2.3, two schemes of using ECS for signal classification is presented. One scheme is to generate ECS with correlated constellations on SSCs which was widely adopted in the reported works on ECS for cognitive radio [18, 19, 20, 21]. The other scheme is to generate ECS with fully correlated sinusoids on SSCs. In the simulation results in Figure 39, it is shown that the signal classification performance can be improved using the *Scheme 2*, which is confirmed by both simulation and the real-world validation with the sensing testbed.

The experimented OFDM signal with ECS has the DFT length of 128 and CP length of 16 and 80 effective sub-carriers, among which 2, 6 or 10 sub-carriers are taken as SSCs. There are four signal classes with different ECS patterns for classification. The Auto-Coherence Function (ACF) showing these patterns are presented in Figure 64, which are generated from the signal received by USRP2+WBX. Since the USRP2+WBX has a strong spur near the DC which is harmful to the classification, the sub-carriers around the DC are excluded in the assignment of SSCs.

The classification performances with *Scheme 1* and *Scheme 2* are compared in Figure 65 which clearly shows the performance gain from the extra ECS generated in *Scheme 2* and confirms the result in Figure 39.

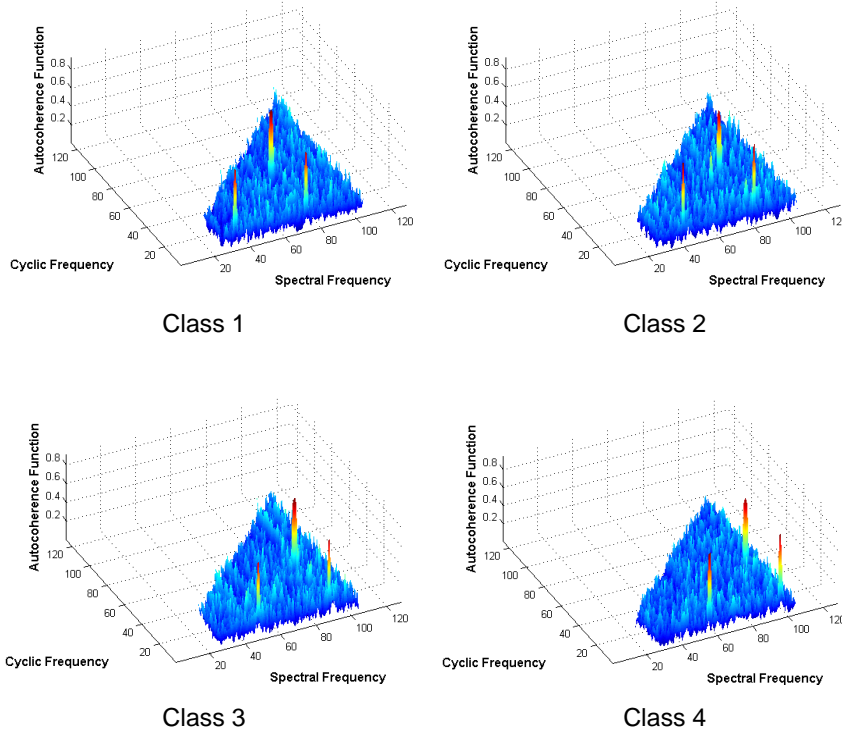


Figure 64: The ACFs of the OFDM signals with four ECS patterns, number of SSC: 6, number of effective SC: 80, DFT length: 128, CP length: 16, number of OFDM symbols: 30, carrier frequency: 750 MHz, receiving sampling rate: 12.5 MS/s

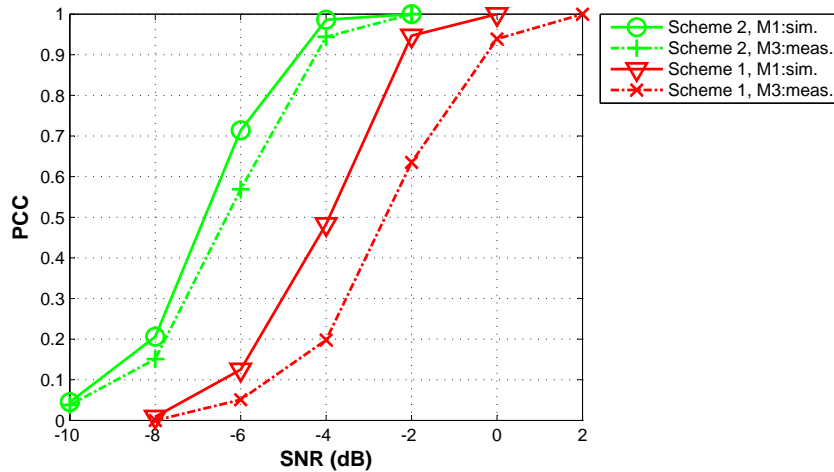


Figure 65: The performances of ECS based signal classifications using *Scheme 1* and *Scheme 2*, number of classes: 4, number of SSC: 6, number of effective SC: 80, DFT length: 128, CP length: 16, number of OFDM symbols: 30, carrier frequency: 750 MHz, receiving sampling rate: 12.5 MS/s, PFA: 0.01

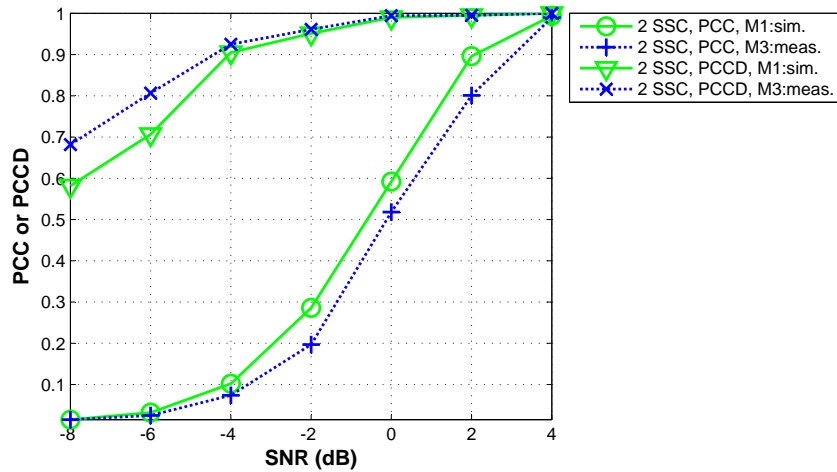


Figure 66: The performances of ECS based signal classifications, number of classes: 4, number of SSC: 2, number of effective SC: 80, DFT length: 128, CP length: 16, number of OFDM symbols: 30, carrier frequency: 750 MHz, receiving sampling rate: 12.5 MS/s, PFA: 0.01

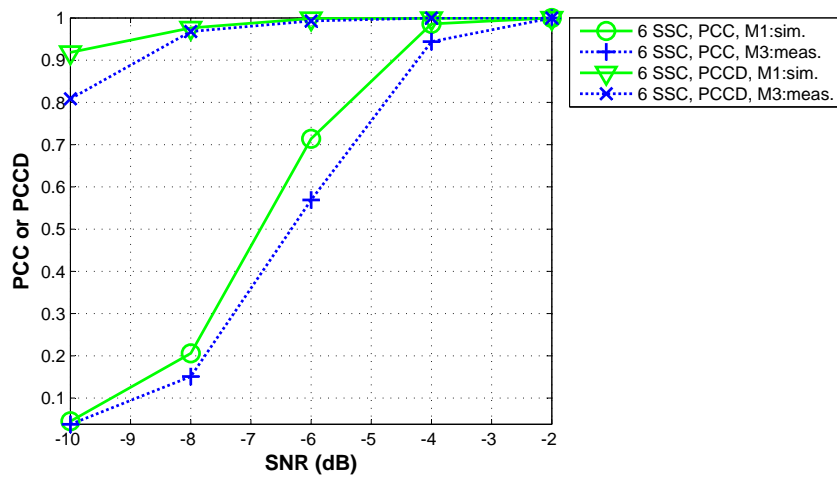


Figure 67: The performances of ECS based signal classifications, number of classes: 4, number of SSC: 6, number of effective SC: 80, DFT length: 128, CP length: 16, number of OFDM symbols: 30, carrier frequency: 750 MHz, receiving sampling rate: 12.5 MS/s, PFA: 0.01

The classification performances using *Scheme 2* with different numbers of SSCs are further examined with simulation (*Method 1*) and experiment (*Method 3*). The results of using two, six and ten SSCs are presented in Figure 66, Figure 67 and Figure 68 respectively. It shows that the PCC can be improved by increasing the number of SSCs, especially for increasing from two SSCs to six, remarkable gain of about 6 dB can be obtained. The results further shows that the PCCD can be also improved by increasing the number of SSCs. When 6 or 10 SSCs are used, the PCCD approaches one for most of the SNRs, which exhibits a favorable property that as long as the signal is detected, it can be correctly classified with high probability. It is also shown that the good agreement of the measured results in the experiment with the simulated results is achieved.

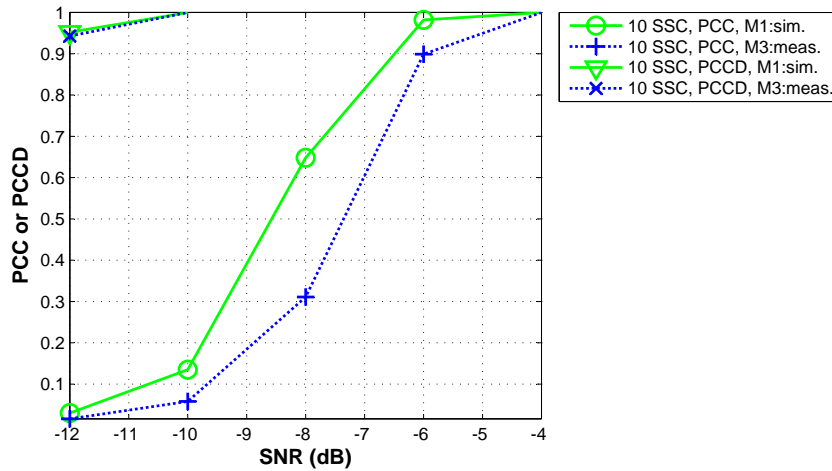


Figure 68: The performances of ECS based signal classifications, number of classes: 4, number of SSC: 10, number of effective SC: 80, DFT length: 128, CP length: 16, number of OFDM symbols: 30, carrier frequency: 750 MHz, receiving sampling rate: 12.5 MS/s, PFA: 0.01

6.7 ECS FOR CARRYING EXTENDED INFORMATION

The last experiment is for validating the feasibility of using ECS for delivering extended information. The experimented signal has the DFT length of 256, CP length of 64. The sizes of the effective SCs' set \mathbf{A} , the possible SSC locations' set \mathbf{S} and the SSCs' set \mathbf{G} are 160, 78 and 16 respectively, resulting an overhead ratio of $16 \div 160 = 10\%$. These sets are defined in Section 5.4.2.1. Based on the above configuration, there are totally $\lfloor \log_2 \binom{78}{16} \rfloor = 53$ information bits can be carried on the ECS. In the simulation and experiment, the ECS patterns are generated with random bits using the algorithm in [86]. The patterns are recognized using the method in Section 5.4.2.2 and can be later mapped to the information bits with the algorithm in [86]. Since the ECS pattern and the bit string have one-to-one correspondence,

the successful detection of the ECS pattern results directly to the correct decoding of the extended information carried on ECS.

The experimented Probability of Erroneous Detection (PED) performances presented in Figure 69 validates the the feasibility of carrying extended information on ECS successfully. It also shows that the experimented results using *Method 3* matches the simulated results well. The decoding performance can be improved by using more OFDM symbols, thus longer observation time.

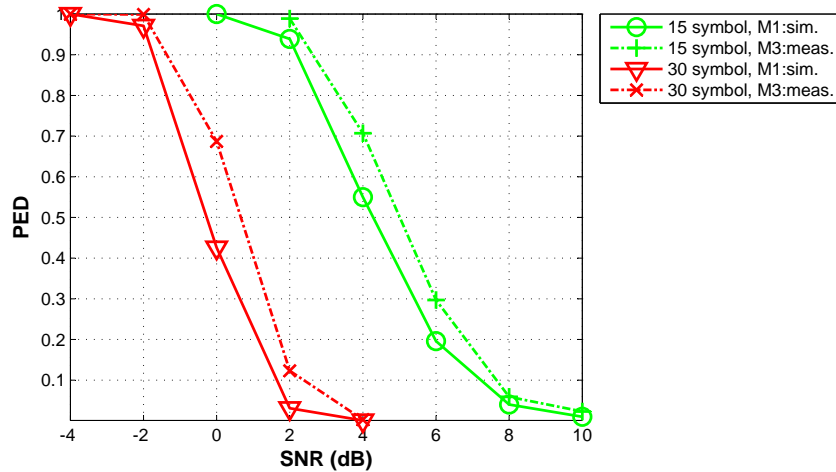


Figure 69: The probability of erroneous decoding (PED) for extended information carried on ECS, DFT length: 256, CP length: 64, effective SCs(size of \mathbf{A}): 160, size of \mathbf{S} : 78, number of SSC(size of \mathbf{G}): 16, carrier frequency: 750 MHz, receiving sampling rate: 12.5 MS/s

6.8 CONCLUDING REMARKS

This chapter presents the validation and performance evaluation of the spectrum sensing techniques with real-world experiments. In Section 6.1, the spectrum sensing testbed used for experiment is introduced. The testbed consists of three major components: a host computer with controlling software, waveform generator of different types/standards and various sensing algorithms implemented; the Agilent E4438C vector signal generator for transmitting target signals with accurately controlled power; the USRP2+WBX SDR frontend as a low-cost sensing receiver with practical hardware imperfections such as nonwhite noise floor and spurs. Based on the implementation of the sensing testbed, three methods for evaluating sensing performances are adopted and introduced in Section 6.2. They are the test of the simulated ideal signal with AWGN (*Method 1*), simulation test of the separately captured signal and receiver noise (*Method 2*) and the real-world spectrum sensing tests with SNR controlled by the transmitting power of the signal generator. Section 6.3 analyzes the noise power of the sensing receiver USRP2+WBX using two measurements with different ob-

servation time. By comparing the measured PDF to that of ideal AWGN, notable noise uncertainty in the sensing receiver is observed.

The spectrum sensing evaluation starts with the detection of DVB-T signal using the optimal FSA-2C algorithm and the detection of WM signal using the PAR feature in the estimated PSD, which are presented in Section 6.4. Since the spurs in the sensing receiver is harmful for both detections, they are removed by the band-stop filter or excluding the their frequency components in estimated PSD. The detection performances are successfully validated with both simulation and experimental measurement. It is worth mentioning that the reliable detection of DVB-T signal is achieved at SNR as low as -20 dB in the experiment using *Method 3*. The detection algorithms for both DVB-T and WM are further integrated in the signal classification framework previously proposed in Chapter 4 which is validated in Section 6.5 of this chapter. The signals of DVB-T, TD-LTE, IEEE 802.22, ECMA-392 and WM with different modes are targeted in the classifier implementation. The classification performances in both simulation and measurement agree with each other well and show very small ambiguity among different signal classes.

The novel scheme of using ECS for signal classification and carrying extended information is also validated with experiments, which are presented in Section 6.6 and Section 6.7 respectively. For signal classification using ECS, it is confirmed by both simulation and measurement that the proposed scheme of using sinusoid as SSCs with full correlations (Scheme 1) has better performance than the reported scheme of using SSCS with partially correlated constellations (Scheme 2). It also shows that the classification performance can be also improved by increasing the number of SSCs. The feasibility of decoding the extended information carried on ECS is also well validated by the experiment using the sensing testbed. It shows that the decoding performance at lower SNR can be improved by increasing the observation time.

The experimental validation and evaluation have greatly strengthened the feasibility and prospect of applying the the signal detection, classification and ECS schemes proposed in this thesis to real-world applications.

CONCLUSIONS AND FUTURE WORKS

7.1 CONCLUSIONS

In this thesis, spectrum sensing, the key functionality of the future cognitive radio systems is studied with special focus on the versatility and the robustness which are very important to its success.

The versatility here means that various kinds of information can be obtained via spectrum sensing according to the radio environment and user's requirement. Three types of spectrum sensing techniques for obtaining different information are discussed in this thesis, which are listed as follows.

- *Detection of Primary User (PU) Signal*
Detection of PU signal in order to find usable channels for Secondary User (SU) is the basic form of spectrum sensing, which is discussed most frequently. In Chapter 2, the key algorithms of the major reported signal detection algorithms and our proposed algorithms are summarized with concise formulation of their detection metrics and thresholds.
- *Signal Classification of Coexisting Wireless Systems*
Based on the investigation of signal detection methods, Chapter 4 proposes a robust signal classification framework and its implementation for classifying the existing and emerging signal standards in TV band. Another signal classification scheme utilizing Embedded Cyclostationary Signature (ECS) in multi-carrier modulation are also illustrated, which can lead to more flexible applications.
- *Delivering Extended Information using ECS*
A novel technique of carrying extended information on the ECS for multicarrier signal is proposed in this thesis, which enables the spectrum sensing device to obtain much richer information than using the conventional signal detection and classification techniques. Instead of using the standard-specific procedures of synchronization, channel estimation/equalization and demodulation/decoding in normal communication systems, the more general cyclostationary analysis technique can be used for decoding the extended information. This scheme is illustrated in Chapter 5.

In the study of the spectrum sensing techniques, the robustness in practical conditions is focused on in this thesis. The major imperfections of practical receiver which are harmful to the robustness of spectrum sensing are taken into account. They are Noise Uncertainty (NU), nonwhite

noise floor, spurs and clock mismatch. The Dimension Cancellation (DIC) method is proposed for completely mitigating the NU problem, which can be applied to nearly all the detection algorithms. A testbed is built and a series of experiments with real-world wireless signals are performed. The experimented performances and simulated performances agree with each other well, which strengthens the effectiveness and feasibility of applying the proposed spectrum sensing techniques to real-world applications.

The specific conclusions on various spectrum sensing techniques are drawn in the last sections of Chapter 2 to Chapter 6. Summarizing all the work in this thesis, it is concluded that the spectrum sensing has great potentials in exploiting the information versatily and robustly from the radio environment. At the current stage of the developing cognitive radio, the regulation bodies are more tend to use the approach of combining geo-location and spectrum database for giving strict protection to PU. However, the works presented in this thesis have strengthened the belief that the spectrum sensing techniques is promising and irreplaceable for solving many foreseeable challenges in future cognitive radio systems. Some examples are listed as follows.

- The schemes of signal classification and delivering extended information using ECS studied in this thesis can provide realtime and useful knowledge for optimizing the coordination and coexistence among different devices or networks, especially for heterogeneous systems.
- For the situations in emergency or public safety, the spectrum sensing is particularly helpful for avoiding interferences and maintaining the reliability of communications[89, 90].
- The spectrum sensing techniques can be used to monitor the radio spectrum and provide continuously updated information to the spectrum database.
- When the access to the database (e.g. via internet) is not available or the geo-location cannot be obtained, spectrum sensing can provide another mean of protecting the primary users and optimizing the coexistence of different wireless systems.

7.2 FUTURE WORKS

The works performed in this thesis open multiple directions of further research. Some of the most interesting unsolved issues are outlined as follows.

- The proposed classifier for signal in TV band focuses on recognizing the standard or type of signal in one channel. However, in a coexisting scenario, there may be multiple networks of different standards sharing the same channel. Hence, a classifier which is able to recognize multiple coexisting standards is desired. Besides, other knowledge such as the interference power and the duty cycle of the target system

are also important for optimizing the coexistence with them, which also need to be extracted.

- Cooperative spectrum sensing with multiple sensing receivers and multi-antenna sensing can effectively improve the overall sensing performance at low SNR, reduce the sensitivity requirement on single sensing node, mitigation channel fading, shadowing and noise uncertainty [54, 56, 17]. This issue is not comprehensively discussed in the thesis and can be further studied, especially considering the cooperative signal classification.
- The spectrum sensing techniques presented in this thesis consider only a single channel in one observation period. This approach may result in high consumption of time and power for sensing large amount of spectrum. The recently proposed compressed spectrum sensing [91, 92] can sense much wider bandwidth swiftly using sub-Nyquist sampling based on the sparse nature of the signals' distribution in radio spectrum. It would be an interesting topic that further combining the novel sensing techniques in this thesis with the compressed sensing for enhancing the agility of cognitive radio.

BIBLIOGRAPHY

- [1] S. Haykin, "Cognitive radio: brain-empowered wireless communications," *IEEE Journal on Selected Areas in Communications*, vol. 23, no. 2, pp. 201–220, Feb. 2005.
- [2] "Report of the Spectrum Efficiency Working Group," FCC spectrum policy task force, Tech. Rep., 2002.
- [3] "FCC 03-322, Notice of proposed rulemaking and order," FCC, Tech. Rep.
- [4] K. Patil, R. Prasad, and K. Skouby, "A Survey of Worldwide Spectrum Occupancy Measurement Campaigns for Cognitive Radio," in *2011 International Conference on Devices and Communications (ICDeCom)*. IEEE, Feb. 2011, pp. 1–5.
- [5] "FCC/OET 07-TR-1006: Initial Evaluation of the Performance of Prototype TV- Band White Space Devices," FCC office of engineering and technology, Tech. Rep., 2007.
- [6] "FCC/OET 08-TR-1005: Evaluation of the Performance of Prototype TV-Band White Space Devices Phase II," FCC office of engineering and technology, Tech. Rep.
- [7] "FCC 08-260: Second Report and Order and Memorandum Opinion and Order," FCC, Tech. Rep., 2008.
- [8] "FCC 10-174: Second memorandum opinion and order, in the matter of unlicensed operation in the TV broadcast bands and additional spectrum for unlicensed devices below 900 MHz and in the 3 GHz band," FCC, Tech. Rep., 2010.
- [9] "Implementing Geolocation: Summary of consultation responses and next steps," Ofcom, Tech. Rep., 2011.
- [10] "ECC Report 159: Technical and operational requirements for the operation of cognitive radio systems in the 'white spaces' of the frequency band 470-790 MHz," CEPT electronic communications committee, Tech. Rep., 2011.
- [11] J. Mitola and G. Maguire, "Cognitive Radio: Making Software Radios More Personal," *IEEE Personal Communications*, vol. 6, no. 4, pp. 13–18, 1999.
- [12] B. Fette, "Technical challenges and opportunities," in *Conference on Cognitive Radio*, Las Vegas, NV.
- [13] Q. Zhao and B. M. Sadler, "A Survey of Dynamic Spectrum Access," *Signal Processing Magazine, IEEE*, vol. 24, no. 3, pp. 79–89, May 2007.
- [14] I. F. Akyildiz, W.-Y. Lee, M. C. Vuran, and S. Mohanty, "NeXt generation/dynamic spectrum access/cognitive radio wireless networks: A survey," *Computer Networks*, vol. 50, no. 13, pp. 2127–2159, Sep. 2006.

- [15] T. Yucek and H. Arslan, "A survey of spectrum sensing algorithms for cognitive radio applications," *IEEE Communications Surveys & Tutorials*, vol. 11, no. 1, pp. 116–130, 2009.
- [16] E. Axell, G. Leus, and E. G. Larsson, "Overview of spectrum sensing for cognitive radio," in *2010 2nd International Workshop on Cognitive Information Processing*. IEEE, Jun. 2010, pp. 322–327.
- [17] I. Akyildiz, B. Lo, and R. Balakrishnan, "Cooperative spectrum sensing in cognitive radio networks: A survey," *Physical Communication*, vol. 4, pp. 40–62, 2011.
- [18] P. D. Sutton, "Rendezvous and Coordination in OFDM-based Dynamic Spectrum Access Networks," Ph.D. dissertation, University of Dublin, Trinity College, 2008.
- [19] P. D. Sutton, K. E. Nolan, and L. E. Doyle, "Cyclostationary Signatures in Practical Cognitive Radio Applications," vol. 26, no. 1, pp. 13–24, 2008.
- [20] P. D. Sutton, J. Lotze, K. E. Nolan, and L. E. Doyle, "Cyclostationary Signature Detection in Multipath Rayleigh Fading Environments," in *2007 2nd International Conference on Cognitive Radio Oriented Wireless Networks and Communications*. IEEE, Aug. 2007, pp. 408–413.
- [21] P. D. Sutton, K. E. Nolan, and L. E. Doyle, "Cyclostationary Signatures for Rendezvous in OFDM-Based Dynamic Spectrum Access Networks," in *2007 2nd IEEE International Symposium on New Frontiers in Dynamic Spectrum Access Networks*. IEEE, Apr. 2007, pp. 220–231.
- [22] H. Zhang, D. Le Ruyet, and M. Terre, "Signal detection for OFDM/OQAM system using cyclostationary signatures," in *2008 IEEE 19th International Symposium on Personal, Indoor and Mobile Radio Communications*. IEEE, Sep. 2008, pp. 1–5.
- [23] W. Gardner, A. Napolitano, and L. Paura, "Cyclostationarity: Half a century of research," *Signal Processing*, vol. 86, no. 4, pp. 639–697, 2006.
- [24] F. F. Digham, M.-S. Alouini, and M. K. Simon, "On the Energy Detection of Unknown Signals Over Fading Channels," *IEEE Transactions on Communications*, vol. 55, no. 1, pp. 21–24, Jan. 2007.
- [25] R. Tandra and A. Sahai, "Fundamental limits on detection in low SNR under noise uncertainty," in *2005 International Conference on Wireless Networks, Communications and Mobile Computing*, vol. 1. IEEE, pp. 464–469.
- [26] D. Cabric, S. Mishra, and R. Brodersen, "Implementation issues in spectrum sensing for cognitive radios," in *Conference Record of the Thirty-Eighth Asilomar Conference on Signals, Systems and Computers, 2004.*, vol. 1. IEEE, pp. 772–776.
- [27] H. Urkowitz, "Energy detection of unknown deterministic signals," *Proceedings of the IEEE*, vol. 55, no. 4, pp. 523–531, 1967.
- [28] T. J. Lim, R. Zhang, Y. C. Liang, and Y. Zeng, "GLRT-Based Spectrum Sensing for Cognitive Radio," in *IEEE GLOBECOM 2008 - 2008 IEEE Global Telecommunications Conference*. IEEE, 2008, pp. 1–5.

- [29] Y. Zeng, Y.-C. Liang, A. T. Hoang, and R. Zhang, "A Review on Spectrum Sensing for Cognitive Radio: Challenges and Solutions," *EURASIP Journal on Advances in Signal Processing*, vol. 2010, 2010.
- [30] Y. Zeng and Y.-C. Liang, "Maximum-Minimum Eigenvalue Detection for Cognitive Radio," in *2007 IEEE 18th International Symposium on Personal, Indoor and Mobile Radio Communications*. IEEE, 2007, pp. 1–5.
- [31] Z. Chen, N. Guo, and R. C. Qiu, "Demonstration of Real-Time Spectrum Sensing for Cognitive Radio," *IEEE Communications Letters*, vol. 14, no. 10, pp. 915–917, Oct. 2010.
- [32] P. Zhang, R. Qiu, and N. Guo, "Demonstration of Spectrum Sensing with Blindly Learned Features," *IEEE Communications Letters*, vol. 15, no. 5, pp. 548–550, May 2011.
- [33] S. W. Oh, W. Zhang, T. Le, Z. Yonghong, A. A. Phyu, and A. A. Syed, "TV white-space device prototype using covariance-based signal detection," in *IEEE Dyspan 2008 Demo paper*, 2008.
- [34] Z. Yonghong and L. Ying-chang, "Eigenvalue-based spectrum sensing algorithms for cognitive radio," *IEEE Transactions on Communications*, vol. 57, no. 6, pp. 1784–1793, Jun. 2009.
- [35] S. M. Kay, *Fundamentals of Statistical Signal Processing, Vol. 2: Detection Theory*. Prentice Hall, 1998.
- [36] Z. Quan, W. Zhang, S. J. Shellhammer, and A. H. Sayed, "Optimal Spectral Feature Detection for Spectrum Sensing at Very Low SNR," *IEEE Transactions on Communications*, vol. 59, no. 1, pp. 201–212, Jan. 2011.
- [37] P. Welch, "The use of fast Fourier transform for the estimation of power spectra: A method based on time averaging over short, modified periodograms," *IEEE Transactions on Audio and Electroacoustics*, vol. 15, no. 2, pp. 70–73, Jun. 1967.
- [38] W. A. Gardner, *Statistical Spectral Analysis A Nonprobabilistic Theory*. Prentice Hall, 1988.
- [39] —, *Introduction to Random Process with Applications to Signals and Systems*. MacMillan, 1986.
- [40] K. Kim, I. A. Akbar, K. K. Bae, J.-S. Um, C. M. Spooner, and J. H. Reed, "Cyclostationary Approaches to Signal Detection and Classification in Cognitive Radio," in *2007 2nd IEEE International Symposium on New Frontiers in Dynamic Spectrum Access Networks*. IEEE, Apr. 2007, pp. 212–215.
- [41] H. Cao, Q. Cai, J. P. Miranda, and T. Kaiser, "Cyclostationary beacon for assisting spectrum sensing in opportunistic spectrum access," *Majlesi Journal of Electrical Engineering (MJEE)*, vol. 5, 2011.
- [42] —, "Cyclostationary multitone beacon signal for opportunistic spectrum access," in *2009 4th International Conference on Cognitive Radio Oriented Wireless Networks and Communications (CROWNCOM 2009)*. Hannover, Germany: IEEE, Jun. 2009, pp. 1–6.

- [43] "IEEE 802.22-06/0127r0: Sensing Scheme for DVB-T," Huawei Technologies, UESTC, Tech. Rep., 2006.
- [44] E. Axell and E. G. Larsson, "Optimal and near-optimal spectrum sensing of OFDM signals in AWGN channels," in *Proc. 2nd Int Cognitive Information Processing (CIP) Workshop*, 2010, pp. 128–133.
- [45] —, "Optimal and Sub-Optimal Spectrum Sensing of OFDM Signals in Known and Unknown Noise Variance," vol. 29, no. 2, pp. 290–304, 2011.
- [46] H.-S. Chen, W. Gao, and D. Daut, "Spectrum Sensing for OFDM Systems Employing Pilot Tones," *IEEE Transactions on Wireless Communications*, vol. 8, no. 12, pp. 5862–5870, 2009.
- [47] Y. Chen and C. Tellambura, "Infinite Series Representations of the Trivariate and Quadrivariate Rayleigh Distribution and Their Applications," *IEEE Transactions on Communications*, vol. 53, no. 12, pp. 2092–2101, Dec. 2005.
- [48] S. Chaudhari, V. Koivunen, and H. Poor, "Autocorrelation-Based Decentralized Sequential Detection of OFDM Signals in Cognitive Radios," *IEEE Transactions on Signal Processing*, vol. 57, no. 7, pp. 2690–2700, Jul. 2009.
- [49] "ETSI EN 300 744: Digital Video Broadcasting (DVB); Framing structure, channel coding and modulation for digital terrestrial television," ETSI, Tech. Rep., 2009.
- [50] H.-S. Chen, W. Gao, and D. G. Daut, "Spectrum Sensing for OFDM Systems Employing Pilot Tones and Application to DVB-T OFDM," in *Proc. IEEE Int. Conf. Communications ICC '08*, 2008, pp. 3421–3426.
- [51] H. Cao, S. Daoud, A. Wilzeck, and T. Kaiser, "Practical issues in spectrum sensing for multi-carrier system employing pilot tones," in *3rd International Workshop on Cognitive Radio and Advanced Spectrum Management (CogArt 2010)*. Rome, Italy: IEEE, Nov. 2010, pp. 1–5.
- [52] S. Shellhammer and R. Tandra, "IEEE 802.22-06/0134r0: Performance of the Power Detector with Noise Uncertainty," Tech. Rep., 2006.
- [53] R. Tandra and A. Sahai, "Fundamental limits on detection in low SNR under noise uncertainty," in *2005 International Conference on Wireless Networks, Communications and Mobile Computing*, vol. 1. IEEE, pp. 464–469.
- [54] G. Ganesan, "Cooperative spectrum sensing in cognitive radio networks," in *First IEEE International Symposium on New Frontiers in Dynamic Spectrum Access Networks, 2005. DySPAN 2005*. IEEE, pp. 137–143.
- [55] S. Mishra, A. Sahai, and R. Brodersen, "Cooperative Sensing among Cognitive Radios," in *2006 IEEE International Conference on Communications*. IEEE, 2006, pp. 1658–1663.
- [56] D. Cabric, A. Tkachenko, and R. Brodersen, "Spectrum Sensing Measurements of Pilot, Energy, and Collaborative Detection," in *MILCOM 2006*. IEEE, Oct. 2006, pp. 1–7.
- [57] J. Neyman and E. S. Pearson, "On the problem of the most efficient tests of statistical hypotheses," *The Royal Society*, vol. 231, no. 1933, pp. 289–337, 1933.

- [58] H. Arslan and S. Reddy, "Noise power and SNR estimation for OFDM based wireless communication systems," in *IASTED International Conference on Wireless and Optical Communications (WOC)*, Banff, Alberta, Canada, 2003.
- [59] "3GPP TS 36.211(RP-54): Evolved Universal Terrestrial Radio Access (E-UTRA); Physical channels and modulation," 3GPP, Tech. Rep., 2011.
- [60] "IEEE Standard for Information Technology-Telecommunications and information exchange between systems Wireless Regional Area Networks (WRAN)-Specific requirements Part 22: Cognitive Wireless RAN Medium Access Control (MAC) and Physical Layer (PHY) Specification," IEEE, Tech. Rep., 2011.
- [61] "Standard ECMA-392: MAC and PHY for Operation in TV White Space," ECMA, Tech. Rep., 2009.
- [62] E. Reihl, "IEEE 802.22-06/0070r0: Wireless Microphone Characteristics," Tech. Rep., 2006.
- [63] ETSI EN 300 422-1 V1.3.2, "ETSI EN 300 422-1 V1.3.2: Electromagnetic compatibility and Radio spectrum Matters (ERM); Wireless microphones in the 25 MHz to 3 GHz frequency range; Part 1: Technical characteristics and methods of measurement," ETSI, Tech. Rep.
- [64] H.-S. Chen, W. Gao, and D. G. Daut, "Spectrum Sensing for Wireless Microphone Signals," in *Proc. 5th IEEE Annual Communications Society Conf. Sensor, Mesh and Ad Hoc Communications and Networks Workshops SECON Workshops '08*, 2008, pp. 1–5.
- [65] H.-S. Chen and W. Gao, "Spectrum Sensing for FM Wireless Microphone Signals," in *Proc. IEEE Symp. New Frontiers in Dynamic Spectrum*, 2010, pp. 1–5.
- [66] "ATSC Digital Television Standard (A/53) Revision E, with Amendments No. 1 and 2," Advanced Television Systems Committee, Tech. Rep., 2006.
- [67] S. Kuffner, "IEEE 802.22-07/0175r0: Channel Models with Non-Integer Delays," Tech. Rep., 2007.
- [68] "Digital Land Mobile Radio Communications - COST 207," Commission of the European Communities, Tech. Rep., 1988.
- [69] H.-S. Chen and G. Wen, "IEEE 802.11-10/0258r0: MAC and PHY Proposal for 802.11af," IEEE, Tech. Rep., 2010.
- [70] "C-PMSE Project." [Online]. Available: www.c-pmse.research-project.de
- [71] R. Hachemani, J. Palicot, and C. Moy, "A new standard recognition sensor for cognitive radio terminals," *EURASIP*, no. Eusipco, pp. 856–860, 2007.
- [72] M. Lopez-Benitez, F. Casadevall, A. Umbert, J. Perez-Romero, R. Hachemani, J. Palicot, and C. Moy, "Spectral occupation measurements and blind standard recognition sensor for cognitive radio networks," in *2009 4th International Conference on Cognitive Radio Oriented Wireless Networks and Communications*. IEEE, Jun. 2009, pp. 1–9.

- [73] H. Wang, W. Jouini, A. Nafkha, J. Palicot, L. Cardoso, and M. Debbah, "Blind standard identification with bandwidth shape and GI recognition using USRP platforms and SDR4all tools," *Cognitive Radio Oriented Wireless Networks & Communications (CROWNCOM), 2010 Proceedings of the Fifth International Conference on*, pp. 1–5.
- [74] N. Han, G. Zheng, S. H. Sohn, and J. M. Kim, "Cyclic Autocorrelation Based Blind OFDM Detection and Identification for Cognitive Radio," in *2008 4th International Conference on Wireless Communications, Networking and Mobile Computing*. IEEE, Oct. 2008, pp. 1–5.
- [75] M. Oner and F. Jondral, "On the extraction of the channel allocation information in spectrum pooling systems," *IEEE Journal on Selected Areas in Communications*, vol. 25, no. 3, pp. 558–565, Apr. 2007.
- [76] A. Punchihewa, Q. Zhang, O. A. Dobre, C. Spooner, S. Rajan, and R. Inkol, "On the Cyclostationarity of OFDM and Single Carrier Linearly Digitally Modulated Signals in Time Dispersive Channels: Theoretical Developments and Application," *IEEE Transactions on Wireless Communications*, vol. 9, no. 8, pp. 2588–2599, Aug. 2010.
- [77] A. Al-Habashna, O. A. Dobre, R. Venkatesan, and D. C. Popescu, "Second-Order Cyclostationarity of Mobile WiMAX and LTE OFDM Signals and Application to Spectrum Awareness in Cognitive Radio Systems," *IEEE Journal of Selected Topics in Signal Processing*, vol. 6, no. 1, pp. 26–42, Feb. 2012.
- [78] Z. Zhao, M. Schellmann, H. Boulaaba, and E. Schulz, "Interference study for cognitive LTE-femtocell in TV white spaces," in *Telecom World (ITU WT), 2011 Technical Symposium at ITU*, pp. 153–158.
- [79] J. Xiao, F. Ye, T. Tian, and R. Q. Hu, "CR Enabled TD-LTE within TV White Space: System Level Performance Analysis," in *2011 IEEE Global Telecommunications Conference - GLOBECOM 2011*. IEEE, Dec. 2011, pp. 1–6.
- [80] FCC, "Radio Broadcast Rules in Title 47 Codes of Federal Regulations (CFR), Part 74 (47cfr74)," Tech. Rep.
- [81] H. Cao, C. Konig, A. Wilzeck, and M.-D. Perez Guirao, "Cognitive Agile Networking testbed," in *2010 IEEE Radio and Wireless Symposium (RWS 2010)*. New Orleans, USA: IEEE, Jan. 2010, pp. 296–299.
- [82] W. Gardner, "Measurement of spectral correlation," *IEEE Transactions on Acoustics, Speech, and Signal Processing*, vol. 34, no. 5, pp. 1111–1123, Oct. 1986.
- [83] W. Gardner and W. Brown, "Spectral Correlation of Modulated Signals: Part II—Digital Modulation," *IEEE Transactions on Communications*, vol. 35, no. 6, pp. 595–601, Jun. 1987.
- [84] D. Gurney, G. Buchwald, L. Ecklund, S. L. Kuffner, and J. Grosspietsch, "Geo-Location Database Techniques for Incumbent Protection in the TV White Space," in *New Frontiers in Dynamic Spectrum Access Networks, 2008. DySPAN 2008. 3rd IEEE Symposium on*, 2008, pp. 1–9.
- [85] B. P. Buckles and M. Lybanon, "Algorithm 515: Generation of a Vector from the Lexicographical Index," *ACM Transactions on Mathematical Software (TOMS)*, vol. 3, 1977.

- [86] I. Saliu. Algorithms, Software to Calculate Combination Lexicographical Order, Rank, Index. [Online]. Available: <http://saliu.com/bbs/messages/348.html>
- [87] "Agilent E4438C Vector Signal Generator Data Sheet." [Online]. Available: cp.literature.agilent.com/litweb/pdf/5988-4039EN.pdf
- [88] "Ettus Research." [Online]. Available: www.ettus.com
- [89] A. Haniz, M. A. Rahman, M. Kim, and J.-i. Takada, "Spectrum sensing on emergency radio spectrum management system," in *10th International Symposium on Communications and Information Technologies*. IEEE, Oct. 2010, pp. 985–990.
- [90] "Tech Topic 8: Cognitive Radio for Public Safety." [Online]. Available: transition.fcc.gov/pshs/techttopics/techtopic8.html
- [91] Z. Tian and G. B. Giannakis, "Compressed Sensing for Wideband Cognitive Radios," in *2007 IEEE International Conference on Acoustics, Speech and Signal Processing - ICASSP '07*. IEEE, 2007, pp. IV-1357–IV-1360.
- [92] X. Wang, W. Guo, Y. Lu, and W. Wang, "Distributed compressed sensing for block-sparse signals," in *2011 IEEE 22nd International Symposium on Personal, Indoor and Mobile Radio Communications*. IEEE, Sep. 2011, pp. 695–699.